THE IMPACT OF microRNAs 96/ 183 AND NEUROPILIN-1 ON T CELL ACTIVATION AND AUTOIMMUNITY

Inaugural-Dissertation

zur

Erlangung des Doktorgrades

Dr. rer. nat.

der Fakultät für

Biologie

an der

Universität Duisburg-Essen

vorgelegt von

Jacqueline Thiel

aus Essen

August 2018

Die der vorliegenden Arbeit zugrunde liegenden Experimente wurden am Institut für Medizinische Mikrobiologie des Universitätsklinikums Essen durchgeführt.

1. Gutachter: Prof. Dr. Wiebke Hansen

2. Gutachter: Prof. Dr. Alexander Schramm

Vorsitzender des Prüfungsausschusses: Prof. Dr. Dirk Hermann

Tag der mündlichen Prüfung: 08.10.2018

Table of Contents

1 Introduction

1.1 The immune system

The immune system protects the body against a variety of external pathogens and stressed or diseased host cells. It can be divided into chemical and physical barriers, which prevent the infiltration of bacteria, viruses, fungi and parasites, and cellular components, which can actively identify and kill pathogens or hazardous cells. The cellular immune system combines different cell types that all origin from pluripotent hematopoietic stem cells in the bone marrow. Within an organism, these cells occupy different niches to protect against all kinds of threats. During a proper immune response, cells communicate through the release of cytokines and chemokines to activate, attract or inhibit each other. Moreover, the immune system is subdivided into innate and adaptive immune response (McComb et al., 2013).

1.1.1 The innate immune system

Innate immune cells originate from a common myeloid progenitor and express germ line encoded receptors that recognize conserved pathogen-associated molecular patterns (PAMPs) or damage-associated molecular patterns (DAMPs). Infections are first recognized by neutrophils and tissue resident macrophages, which phagocyte and eliminate pathogens and secrete pro-inflammatory cytokines, which render the blood vessels more permeable for other immune cells. Natural killer (NK) cells and granulocytes are attracted by chemokines from the blood into the tissue and support the immune response (Turvey and Broide, 2010). Additionally, dendritic cells (DCs) migrate to the side of inflammation, where they take up antigens and present them on major histocompatibility complex (MHC) class I and II molecules on their cell surface. Mature DCs migrate through the lymph system into lymph nodes, where they activate T cells and thereby induce the adaptive immune response (Iwasaki and Medzhitov, 2015).

1.1.2 The adaptive immune system

The adaptive immune system consists of T and B cells, which both origin from a common lymphoid progenitor. While B cells mature in the bone marrow, T cell maturation occurs in thymus. Both lymphocyte subsets develop a highly specific B/ T cell receptor through V(D)J-recombination that recognize a vast variety of epitopes. After activation by DCs, naïve T cells differentiate into $CD4^+$ T helper (Th) cells, which support the immune response by the production of cytokines and $CD8^+$ cytotoxic T

cells, which migrate into the tissue, where they identify and kill infected or transformed cells (Kumar et al., 2018). Furthermore, regulatory T cells (Tregs) with suppressive capacity maintain peripheral tolerance by preventing autoimmune and chronic inflammation (Vignali et al., 2008). B cells develop into antibody producing plasma cells after activation by cytokines (Nutt et al., 2015). T and B cells can both evolve into long live memory cells, which recognize new infections with the same pathogen immediately and thereby produce a faster and stronger immune response (Kumar et al., 2018; Kurosaki et al., 2015).

1.2 T cell development

T cells develop from multipotent hematopoietic stem cells that migrate from the bone marrow to the thymus. Within this central lymphoid tissue, the progenitors interact with stroma cells and continuous Notch signaling guides the thymocytes through different maturation steps. In the beginning, early thymocytes only express CD2 (Thy-1 in mice) on their cell surface and are termed double-negative (DN). This stage can be subdivided into four steps according to the expression of CD44, Kit and CD25. At first DN1 cells express the surface molecule CD44 and the stem cell factor receptor Kit. In the DN2 stage, the expression of CD44 and Kit is still high and CD25 (α-chain of interleukin [IL]-2 receptor) expression occurs. Furthermore, the rearrangement of the T cell receptor (TCR) β-chain locus takes place. Afterwards, DN3 cells reduce the expression of CD44 and Kit ($CD44^{low}Kit^{low}$). Those cells that fail appropriate β-chain rearrangement stay in the DN3 stage and undergo apoptosis. Cells with productive β-chain rearrangement also lose the expression of CD25. The β-chain pairs with a surrogate, invariant chain pTα to generate the pre-T cell receptor (pre-TCR) that associates with co-receptor protein CD3. The signaling through the lymphocyte-specific protein tyrosine kinase (Lck) leads to phosphorylation and degradation of the recombination activation gene 1 and 2 (Rag1, 2) proteins that stops β-chain rearrangement. Moreover, receptor signaling causes proliferation and expansion of the specific DN4 cell that triggers CD4 and CD8 co-receptor expression. After the proliferation phase, Rag1 and Rag2 expression occurs again and the double-positive (DP) thymocytes start to rearrange the α-chain locus. This specific chronological sequence of events enables one single β-chain to associate with many different α-chains and causes T cell variety. The rearrangement of the α-chain locus stops with positive selection (reviewed in (Murphy et al., 2012)).

The engagement of TCR, co-receptor and the MHC molecule initiates positive selection and leads to the upregulation of the cell surface molecule CD69 and the anti-apoptotic

protein B cell lymphoma 2 (Bcl-2) (Linette et al., 1994; Yasutomo et al., 2000b). Optimal positive selection of $CD4^+$ T cells is only maintained by thymic DCs and stroma cells that express the lysosomal protease cathepsin L. In addition, the expression of the protease β5t enables thymic stroma cells to positively select $CD8^+$ T cell (Nitta and Suzuki, 2016). Those TCRs that recognize self-peptide:self-MHC complexes with low affinity leave the thymic cortex, enter the medulla and mature. Stroma cell-expressed MHC class I molecules interact with CD8 while MHC class II molecules interact with CD4 co-receptor, respectively. Initiation of positive selection results in downregulation of CD4 and CD8 expression. Afterwards, the duration (Yasutomo et al., 2000a) and the intensity of the TCR signaling seem to determine the lineage fate of the single-positive (SP) T cell. Lck signaling downstream of the TCR is stronger when CD4 co-receptor is engaged in the complex. This leads to the expression of the transcription factor ThPOK that for his part represses the transcription factor Runx3 resulting in re-expression of CD4 co-receptor molecules. Weak TCR signaling is accompanied by constant expression of Runx3 that enables the silencing of CD4 and the re-expression of CD8 co-receptor molecules (Murphy et al., 2012; Singer et al., 2008).

During negative selection, T cells with high affinity TCR self-peptide:self-MHC interactions are recognized as potentially self-reactive and are eliminated from the T cell repertoire through apoptosis. To maintain tolerance medullary stroma cells and intrathymic DCs express ubiquitous self-antigens. Moreover, under the control of the nuclear protein Aire, those cells are able to express tissue-specific self-antigens. SP T cells reactive to these autoantigens are ejected from the T cell pool by apoptosis (Nitta and Suzuki, 2016).

SP thymocytes express only one of the two co-receptors and leave the thymus as either mature $CD4^+$ or $CD8^+$ T cells. For the egress of $CD4^+$ and $CD8^+$ T cells to the blood and the secondary lymphoid tissues like spleen and lymph nodes expression of sphingosine-1-phosphate (S1P) receptor, CD62L (L-selectin) and the chemokine receptor CCR7 is required (Murphy et al., 2012).

1.3 T cell activation

After development, naïve T cells circulate between the blood stream and the lymphoid tissue. Within lymphatic organs, T cells transiently bind to DCs by the interaction of lymphocyte function-associated antigen 1 (LFA-1) and CD2 with intercellular adhesion molecule 1 and 2 (ICAM-1/-2) and CD58. Thereby, T cells sample a large number of peptide:MHC complexes on the surface of the DCs. T cell activation occurs in response to a specific antigen presented by MHC class I and II molecules on DCs in the spleen

or lymph nodes. The initial encounter of a naïve T cell with its specific antigen resulting in T cell activation and clonal expansion is called priming. After recognition of a specific peptide:MHC complex, TCR-induced conformational changes in LFA-1 increase the binding to ICAM-1/-2 and stabilized the interaction of T cell and DC (Montoya et al., 2002). This interaction leads to the development of a highly specialized interface between T cell and DC called immunological synapse (IS) (Finetti and Baldari, 2018). Successful T cell activation is dependent on three signals. First, there is antigen-specific activation of the TCR. Furthermore, the interaction of co-stimulatory molecules (like CD80 and CD86) of antigen presenting cells (APCs) with co-stimulatory receptors on the T cell (e.g. CD28) as well as the secretion of specific cytokines are important for activation and differentiation of T cells (Murphy et al., 2012). Antigen-specific activation of the TCR in the absence of co-stimulatory signaling causes T cell anergy. Anergic T cells are functionally inactivated and unable to initiate a productive response (Macian et al., 2004).

1.3.1 T cell receptor signaling

The TCR is composed of the antigen-binding α:β heterodimer, the CD3 complex and one homodimer of ζ chains. Together, the intracellular region of the CD3 signaling and the ζ chains comprise ten immunoreceptor tyrosine-based activation motifs (ITAMs). Each ITAM contains two tyrosine residues that are phosphorylated by the initiation of TCR signaling. The binding of the CD4 or CD8 co-receptor to the MHC class II or I molecule respectively brings the co-receptor-associated kinase Lck in close proximity to the ITAMs and initiates phosphorylation. Afterwards, the zeta-chain-associated protein kinase 70 (ZAP-70) is recruited to the receptor complex and is phosphorylated and activated by Lck. Activated ZAP-70 phosphorylates the scaffold protein linker of activated T cells (LAT) and lymphocyte cytosolic protein 2 (LCP2). Additional stimulatory signals through the receptor CD28 activate the phosphoinositide 3-kinase (PI3K). PI3K phosphorylates phosphatidylinositol(4,5)-bisphosphate (PIP_2) to phosphatidylinositol(3,4,5)-triphosphate (PIP_3) which then recruits the membrane-associated IL-2-inducible T cell kinase (Itk) to the receptor complex where it is phosphorylated and activated by Lck. PIP_3 is also necessary to bring the phospholipase C-γ (PLC-γ) to the inner site of the membrane. Here, LAT and LCP2, together with the GRB2-related adaptor protein 2 (GRAP2), form a complex that favors the interaction of Itk and PLC-γ leading to the activation of the phospholipase. Thereafter, PLC-γ cleaves PIP_2 to generate diacylglycerol (DAG) and inositol trisphosphate (IP_3). DAG and IP_3 entering diverse signaling pathways leading to the activation of nuclear factor of activated T cell (NFAT), nuclear factor kappa-light-chain-

enhancer of activated B cells (NFκB) and activator protein-1 (AP-1). The major function of these three transcription factors is the induction of IL-2 expression. In proper activated T cells, IL-2 promotes proliferation and differentiation into effector cells (Marie-Cardine and Schraven, 1999; Murphy et al., 2012).

1.3.2 PI3K/Akt pathway

Co-stimulation through the CD28 receptor phosphorylates and activates PI3K which then produces PIP_3 by PIP_2 phosphorylation. Beside Itk and PLC-γ, PIP_3 also recruits the serine/threonine kinase Akt (Protein kinase B) to the inner face of the plasma membrane. Here, Akt is phosphorylated on threonine 308 by the phosphoinositide-dependent protein kinase-1 (PDK-1). Full activation of Akt is achieved through a second phosphorylation at serine 473 by the mammalian target of rapamycin complex 2 (mTORC2). Activated Akt regulates many downstream molecules through phosphorylation (Murphy et al., 2012). In T cells, the PI3K/Akt pathway promotes activation, clonal expansion, differentiation, survival of effector cells and suppresses the generation of Tregs (So and Croft, 2013).

The phosphatase and tensin homolog (PTEN), also described as a tumor suppressor gene (Steck et al., 1997), is the major negative regulator of the PI3K/Akt pathway. PTEN is able to dephosphorylate PIP_3 and thereby antagonizes the signals downstream of PI3K (Myers et al., 1998; Wu et al., 1998). On this account, PTEN is able to control $CD4^+$ T cell fate. Low expression levels of PTEN increase the signaling via the PI3K/Akt/mTor pathway favoring Th cell differentiation while increased PTEN expression counteracts the PI3K/Akt pathway resulting in the differentiation of Tregs (Hawse et al., 2015). Furthermore, PTEN maintains Treg cell stability and metabolic balance (Shrestha et al., 2015). Among others, PTEN expression is regulated by the transcription factor early growth response-1 (EGR-1). EGR-1 expression is induced in response to several growth factors, chemokines and injurious stimuli (Silverman and Collins, 1999). Several studies demonstrated that EGR-1-dependent upregulation of PTEN decreased Akt phosphorylation. This regulation of the PI3K/Akt pathway lead to impaired proliferation, migration and apoptosis in different cell types (Ferraro et al., 2005; Okamura et al., 2005; Tsugawa et al., 2003; Virolle et al., 2001; Yu et al., 2011).

1.4 T cell subtypes

After activation in response to different pathogens, $CD4^+$ T cells differentiate into various effector T cell populations. These Th cell subsets are defined by the expression of lineage-defining transcription factors, also called master regulators, and the

secretion of distinct cytokines. The major subtypes are the Th1, Th2, Th17 cells and Tregs (Zhu and Paul, 2010). Effector T cells are pivotal to mount a proper immune response. They provide help to B cells for antibody production and activate $CD8^+$ cytotoxic T cells and cells of the innate immune response (Keene and Forman, 1982).

Th1 cells polarize in the presence of DC-derived IL-12. They express the lineage specific transcription factor T-bet, which facilitates the production of the Th1 signature cytokine interferon γ (IFNγ) and the signal transducer and activator of transcription 4 (STAT4) (Zhu and Paul, 2010). Th1 cells are induced upon infection with intracellular pathogens and activate macrophages to destroy intracellular bacteria and viruses (Nauciel, 1995).

Th2 cells act against extracellular parasites like helminths. They are primed in the presence of the cytokine IL-4 and express the transcription factors GATA-3 and STAT5. GATA-3 induces the production of cytokines like IL-4, IL-5, IL-10 and IL-13. The Th1 and Th2 specific transcription factors T-bet and GATA3 respectively, inhibit the differentiation of the opposite lineage (Zhu and Paul, 2010).

In mice, Th17 cells are induced by IL-6 and transforming growth factor β (TGFβ) which inhibits Th1 differentiation. This cell subset is characterized by the expression of the transcription factors RORγt and STAT3 (Chen and O'Shea, 2008). Next to the specific cytokine IL-17, Th17 cells also produce IL-22, tumor necrosis factor α (TNFα) and the chemokine CXCL1. These cells promote immune response against extracellular bacteria and fungi through the recruitment of neutrophils and the production of antimicrobial proteins (Weaver et al., 2006).

$CD4^+CD25^+$ Tregs have a suppressive phenotype and play a pivotal role in maintaining peripheral tolerance. On the one hand they prevent autoimmune and limit chronic inflammatory disease, but on the other hand they limit antitumor immunity. There are two types of Tregs, the thymic-derived natural Tregs (nTregs) and peripheral naïve T cells that acquire immunosuppressive properties in the presence of TGFβ, and so called induced Tregs (iTregs). As a key transcription factor, Tregs express the forkhead box P3 (FoxP3). FoxP3 confers their suppressive function, since its loss lead to autoimmune-like lymphoproliferative disease (Fontenot et al., 2003). Four suppressive mechanisms in Tregs are described. Tregs suppress T effector cells by the secretion of inhibitory cytokines like IL-10, TGFβ and IL-35. Furthermore, they are able to induce cytolysis of target cells. Human Tregs express granzyme A, while murine Tregs express granzyme B. By granzyme release, Tregs facilitate target cell apoptosis either in a perforin-dependent or –independent manner. The suppression of target cells by

metabolic disruption involves the consumption of IL-2 by Tregs, cyclic adenosine monophosphate (cAMP)-mediated inhibition (Bopp et al., 2007) and CD39/ CD73-generated adenosine receptor 2A-mediated immunosuppression. Additionally, Tregs convey suppression by modulation of DC maturation or function (Vignali et al., 2008).

$CD8^+$ T cells are activated by DC to become cytotoxic T lymphocytes (CTLs) that recognize antigens presented by MHC class I molecules. CTLs play a major role in the host immune defense against intracellular pathogens like viruses and bacteria. Moreover, $CD8^+$ cytotoxic T cells are crucial for tumor surveillance. To execute their highly precise immune response, CTLs possess three mechanisms. Upon activation, CTLs express the first apoptosis signaling (FAS) ligand on their cell surface. The interaction with FAS receptor expressed on infected or malignant target cells results in caspase-induced apoptosis (Nagata, 1996). Furthermore, CTLs secrete cytokines like TNFα and IFNγ that inhibits viral replication and promotes macrophage activation (Gregory and Wing, 1993). The third mode of action is the release of cytotoxic granules into the IS. These granules contain perforin which penetrates the target cell membrane and facilitates the delivery of the second component granzyme into the cytosol of the target cell. Granzymes are serine proteases that are able to induce apoptosis in any type of cell (Russell and Ley, 2002).

1.5 Autoimmunity

Although several control mechanisms during T cell development have been evolved to convey central tolerance, autoreactive lymphocytes are able to enter the periphery. Under normal conditions, autoreactive lymphocytes are controlled by mechanisms of peripheral tolerance. Autoimmunity occurs due to failures in lymphocyte tolerance. Lymphocytes defective for inhibitory molecules such as cytotoxic T lymphocyte-associated protein 4 (CTLA-4), programed cell death protein 1 (PD-1) or lymphocyte-activation gene 3 (LAG-3) can become autoreactive. Inflammatory conditions are able to activate former anergic autoreactive lymphocytes. Furthermore, tissue damage caused by infection can lead to interactions between antigens and autoreactive lymphocytes that are normally separated. In addition, the loss of suppressive capacity by Tregs can also promote autoimmune disorders. In autoimmune diseases, the presence of autoantibodies and response of autoreactive lymphocytes to self-antigens cause tissue damage. Autoimmune diseases can be classified into organ-specific and systemic autoimmune disorders. Organ-specific autoimmunity is restricted to a specific tissue or organ and only autoantigens from this specific side of the body are targeted. Type I diabetes (T1D), multiple sclerosis (MS) and Graves' disease (GD) are examples

for organ-specific autoimmune disorders (Theofilopoulos et al., 2017). In systemic autoimmunity, like systemic lupus erythematosus (SLE) or rheumatoid arthritis (RA), several tissues are affected due to autoantibodies against ubiquitously expressed antigens (e.g. ribonucleoproteins) (Hardin and Mimori, 1985).

The organ-specific autoimmune disease T1D is caused by T cell-mediated destruction of pancreatic beta cells in the islets of Langerhans. The destruction causes insulin deficiency and hyperglycemia. Antigens from dying beta cells are presented by tissue-resident DCs to autoreactive $CD4^+$ T cells. The activated $CD4^+$ T cells promote macrophage-mediated killing of the beta cells. Moreover, $CD4^+$ T cells activate B cells to produce anti-beta cell antibodies and help to activate autoreactive $CD8^+$ T cells (Wang et al., 2017c).

GD is another organ-specific autoimmune disorder predominantly affecting the thyroid glands. It is characterized by lymphocytic infiltration and the presence of circulating autoantibodies against the thyroid-stimulating hormone receptor (TSHR). This causes an excessive thyroid hormone production resulting in hyperthyroidism (Weetman, 2000). Graves' orbitopathy (GO) or endocrine orbitopathy (EO) is a thyroid-associated orbitopathy closely related to GD (Bahn, 2010). In GO, the TSHR autoantibodies lead to T cell infiltration into orbital tissue. Here, fibroblasts are stimulated to present the autoantigens, which further activates autoreactive T cells and promotes proliferation of orbital fibroblast. This positive feedback loop favors remodeling of the orbital connective tissue, deposition of matrix glycosaminoglycans, intramuscular fibrosis and increased adipogenesis (Feldon et al., 2005).

1.6 MicroRNA development and function

In 1993, Lee et al. described the first microRNA (miRNA) *lin-4* in the nematode *Caenorhabditis elegans* (Lee et al., 1993). MiRNAs are endogenous, single-stranded, non-coding RNA molecules with a length of 21 to 25 nucleotides (nt) and are encoded in the genome of most eukaryotes. They are involved in the posttranscriptional gene regulation of eukaryotic cells. To generate mature miRNAs, the transcripts have to be sequentially processed by the two ribonuclease III (RNase III) enzymes Drosha and Dicer (Winter et al., 2009). The miRNA genes are transcribed by RNA polymerase II to form long (~500 – 3000 nt), primary miRNA transcripts (pri-miRNA) with stem-loop structures. Within the nucleus, the pri-miRNAs undergo the first step of miRNA maturation. They are cleaved by the microprocessor complex composed of the nuclear RNase III-type enzyme Drosha and its cofactor DiGeorge syndrome critical region gene 8 (DGCR8). This process creates short (~60 – 100 nt), hairpin structures called

precursor miRNAs (pre-miRNAs) (Lee et al., 2003). The shuttle of pre-miRNAs into the cytoplasm is mediated by the RanGTP-dependent nuclear transport receptor Exprotin-5 (Exp-5). The pre-miRNA-Exp-5 complex translocates through the nuclear pore complex and then RanGTP hydrolysis releases the pre-miRNA in the cytoplasm (Yi et al., 2003). Here, pre-miRNAs encounter the RNase III-type enzyme Dicer and its associated protein trans-activation response RNA-binding protein (TRBP). Dicer cleaves off the terminal hairpin loop, releasing short (~ 22 nt) miRNA duplexes (Lee et al., 2003).

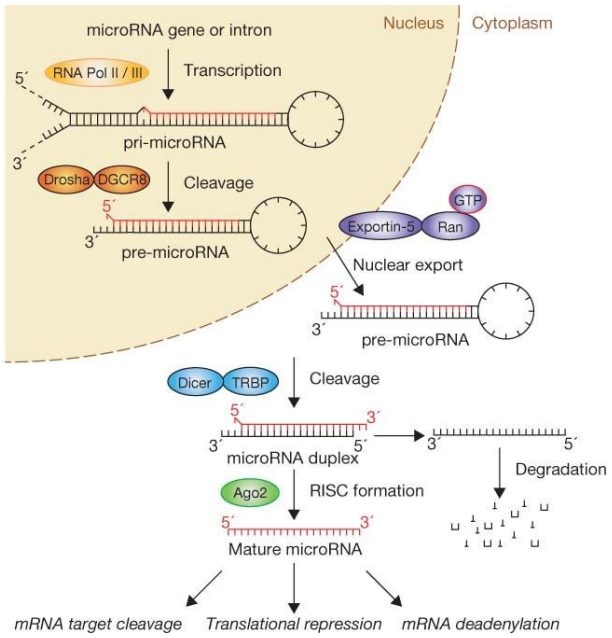

Figure 1: The mammalian miRNA biogenesis pathway. MiRNA genes are transcribed by RNA polymerase II (RNA Pol II) to generate pri-miRNA. The transcript is recognized by the microprocessor complex composed of the ribonuclease III-type (RNase III) enzyme Drosha and its cofactor DiGeorge syndrome critical region gene 8 (DGCR8). The complex produces the shorter hairpin-like structure pre-miRNA which is exported by the RanGTP-dependent nuclear transport receptor Exprotin-5 into the cytoplasm. The RNase III-type enzyme Dicer in association with the trans-activation response RNA-binding protein (TRBP, only in humans) mediates the second processing step that produces a miRNA duplex. The duplex binds to Argonaut (Ago) proteins. On strand of the duplex is degraded, while the other one is incorporated into the RNA-induced silencing complex (RISC) to facilitate mRNA target cleavage, translational repression of target mRNA or mRNA deadenylation (Graphic taken from (Winter et al., 2009))

After the generation of the approximately 22 nt long miRNA duplex, the duplex is incorporated into an Argonaute (Ago) protein complex. Subsequently Ago protein recruits other accessory proteins to form the RNA-induced silencing complex (RISC) (Hammond et al., 2001). One strand of the miRNA duplex is degraded, whereas the other strand remains bound to Ago as the mature miRNA (Khvorova et al., 2003). Within the RISC, the miRNA guides the complex to its target mRNA to silence it by messenger RNA (mRNA) degradation, translational repression or mRNA deadenylation (Zeng et al., 2003). The pathway of mammalian miRNA biogenesis is depicted in Figure 1.

MiRNAs facilitate posttranscriptional gene regulation by base-pairing between the 6-8 nt seed sequence at the 5' end of the miRNA and a complementary sequence usually in the 3' untranslated region (3'UTR) of the target mRNAs (Lee et al., 1993). The degree of miRNA-target mRNA complementarity seems to determine the gene silencing mechanism. An extensive base-pairing between the miRNA seed sequence and the 3'UTR of the mRNA leads to the endonuclease cleavage of the target mRNA by Ago protein (slicer-dependent silencing). Cleaved mRNA products subsequently undergo cellular mRNA degradation (Meister et al., 2004).

The slicer activity of Ago protein is inhibited by imperfect base-pairing at multiple complementary sites between the miRNA and its target mRNA, facilitating translational repression (slicer-independent silencing). The miRNA mediated repression can either affect translational initiation or elongation. Translation of target mRNA can also be influenced indirectly by special separation through accumulation of miRNA-bound mRNA in translational machinery-lacking processing bodies (P-bodies). MiRNA dependent deadenylation and decapping occur independently from slicer activity and effect translation and transcript stability (Valencia-Sanchez et al., 2006).

MiRNAs play pivotal roles in a wide range of cellular processes including development, differentiation, proliferation, homeostasis and apoptosis. Furthermore, miRNAs can be highly tissue specific, suggesting a critical role for dominant miRNAs in tissue specification and cell lineage decision (Lagos-Quintana et al., 2002). MiRNAs are fine tuners of protein expression levels and thereby confer cell robustness. They are elements of regulatory networks providing positive or negative feedback loops to determine cell fate, buffer protein expression noise or set thresholds for gene expression to commit cell fate. Within these networks multiple miRNAs can act either in a cooperative or antagonistic manner. Moreover, a single miRNA is able to regulate many different mRNA targets and many miRNAs can be involved in regulating a single target mRNA (Mehta and Baltimore, 2016).

1.7 Regulation of T cell development and function by microRNAs

For a vast amount of miRNAs it has been demonstrated that they play a pivotal role in the regulation of immunological processes comprising development, linage commitment, activation, function and ageing of innate and adaptive immune cells (Mehta and Baltimore, 2016). Furthermore, the expression of miRNAs is closely related to the degree of T cell development and differentiation. The relevance of miRNAs in T cell biology was well established using mice deficient for the RNase III-type enzyme Dicer. These mice exhibited an impaired T cell development. Conditional knockout of

Dicer in early T cell progenitors reduced the number and survival of mature α:β T cells (Cobb et al., 2005). In addition, $CD4^+$ T cells with conditional deletion of Dicer showed low proliferative response after stimulation *in vitro* (Muljo et al., 2005). Moreover, Dicer-deficient $CD4^+$ T cells failed to discriminate between activating and anergy-inducing stimuli and produced IL-2 also in the absence of co-stimulation (Marcais et al., 2014) Mice with a FoxP3 induced conditional knockout of the miRNA-processing enzyme spontaneously developed lethal autoimmune inflammatory disease accompanied by impaired development and function of Tregs (Liston et al., 2008; Zhou et al., 2008). These results demonstrate the requirement of miRNAs for appropriate T cell development and function.

During T cell development and maturation, the role of the two miRNAs, miR-181a and miR-150, is well established. MiR-181a is highly expressed in hematopoietic progenitors as well as in immature $CD4^+CD8^+$ DP T cells in the thymus. The expression level of miR-181a decreases in more differentiated T cell subsets in the periphery. MiR-181a plays a pivotal part in T cell differentiation in the thymus by regulating the expression of Bcl-2, CD69 and TCR which are important for positive selection. Furthermore, this miRNA increases the sensitivity of TCR signaling by direct targeting several phosphatases to enhance the efficiency of both positive and negative selection (Li et al., 2007). Besides miR-181a, miR-150 is strongly upregulated during T cell maturation. In immature T cells, miR-150 downregulates the transcription factor c-Myb to block thymic T cell development. In addition, this miRNA inhibits early T cell development by targeting NOTCH3 (Ghisi et al., 2011).

MiRNAs are not only involved in T cell development, they also play a role in T cell activation, proliferation and apoptosis. The miRNAs miR-155 and miR-181c have been shown to regulate the IL-2 signaling pathway. MiR-155 is increased upon T cell activation. By targeting the suppressor of cytokine signaling 1 (SOCS1) and CTLA-4, miR-155 enhances T cell proliferation (Dudda et al., 2013; Sonkoly et al., 2010). MiR-181c is able to modulate the activation state of T cells through direct targeting of IL-2 (Xue et al., 2011). MiR-214 represents another miRNA that is directly upregulated after TCR stimulation. It targets PTEN resulting in increased T cell proliferation (Jindra et al., 2010). PTEN and thereby mTOR are also regulated by the miR-17~92 cluster favoring the development of short-lived effector cells (Wu et al., 2012). For miR-17 and miR-20a it was also demonstrated that they are induced upon TCR signaling and later repress CD69 expression to tightly regulate T cell proliferation (Blevins et al., 2015). Another negative feedback loop involves miR-146a that is induced by NFκB in response to T cell activation. Upon induction, miR-146a represses the NFκB signaling transducers

interleukin-1 receptor-associated kinase 1 (IRAK1) and TNF receptor-associated factor 6 (TRAF6) (Yang et al., 2012). Furthermore, miR-146a inhibits T cell apoptosis by targeting the FAS-associated death domain (FADD) (Curtale et al., 2010). MiR-21 is also involved in the regulation of T cell proliferation, migration and apoptosis. In activated memory T cells, miR-21 acts anti-apoptotic, while it influences homing of activated naïve T cells through regulation of CCR-7 (Smigielska-Czepiel et al., 2013). In $CD8^+$ T cells, miR-130 and miR-301 are upregulated after activation and repress CD69 expression, like it is described for miR-17 and miR-20b in $CD4^+$ T cells (Zhang and Bevan, 2010).

Besides their role in T cell activation and survival, several miRNAs also influence the generation of different Th cell lineages and their specific function. Throughout the different T cells subsets, same miRNA can be expressed by different levels regulating different targets to facilitate lineages commitment. For instance, miR-19 and miR-17, members of the miR-17~92 cluster, promote Th1 response by targeting PTEN, cAMP-responsive element binding protein 1 (CREB1) and Ikarus zinc finger protein 4 (IKZF4) to prevent Th17 differentiation (Jiang et al., 2011; Liu et al., 2014). MiR-20b, also belonging to the miR-17~92 family, targets STAT3 and RORγt resulting in inhibition of Th17 differentiation (Zhu et al., 2014). Moreover, this specific cluster is involved in the expansion of $CD8^+$ T cells (Wu et al., 2012).

MiR-155 expression levels determine Th1 or Th2 differentiation by targeting the transcription factor c-Maf (Rodriguez et al., 2007). In addition, miR-155 affects Th17 cell differentiation by regulating the transcription factors ETS1 (Hu et al., 2013) and SOCS1 (Yao et al., 2012). In Tregs, miR-155 targets forkhead box O3 (FoxO3) regulating the Akt pathway (Yamamoto et al., 2011). The suppressive function of Tregs is regulated by miR-146a targeting STAT1 (Lu et al., 2010). Furthermore miR-146a regulates Th1/Th2 balance (Hou et al., 2018) and modulates autoreactive Th17 cell differentiation by blocking IL-6 and IL-21-induced pathways (Li et al., 2017). In $CD8^+$ T cells, miR-150 and miR-139 influence the expression of perforin, eomesodermin and IL-2 receptor α (IL2Rα) thus regulating CTL cell differentiation (Trifari et al., 2013).

All these studies demonstrate that miRNAs are essential for the regulation of T cell development and function. Nevertheless, the impact on T cell activation and survival of many miRNAs implicated in carcinogenesis and autoimmunity is still intensively studied.

1.8 The microRNA-183~96~182 cluster

The miRNA-183~96~182 cluster (miR-183 cluster) is a polycistronic, paralogous miRNA cluster comprising miR-183, miR-96 and miR-182 encoded on mouse chromosome 6qA3 or human chromosome 7q32.2. The three miRNAs have similar seed sequences, target genes and expression patterns, suggesting they may act in a coordinated fashion and are able to compensate for each other (Xu et al., 2007). In 2007, the miR-183 cluster was described by Xu et al. to be a sensory organ-specific miRNA cluster due to its high expression in murine photoreceptors, retinal bipolar and amacrine cells. For the whole cluster, they postulated a role in maturation and maintenance of normal retina function, since the abundance of the cluster members increased postnatally and peaked in the adult retina. Furthermore, they demonstrated miR-96 and miR-182 to be involved in the regulation of retinal circadian rhythm (Xu et al., 2007). A first loss of function study using miR-182 knockout mice showed no alterations in retinal structure suggesting a minor role of this miRNA in retinal development, maintenance and cell survival (Jin et al., 2009). However, in 2011 Zhu et al. used sponge transgenic mice for all three miRNAs of the miR-183 cluster to further elucidate their role in the retinal development. Under normal light conditions the retina of miR-183 cluster-blocked transgenic mice did not show any morphological or functional difference, while the exposure to 10,000 lux light led to a caspase-2-dependent retinal degradation linking the miR-183 cluster to apoptosis (Zhu et al., 2011). Using miR-96 and miR-183 double knockout mice, Xiang et al. demonstrated defective cone nuclear polarization and progressive retinal degeneration by the repression of the neuronal protectant Slc6a6 (Xiang et al., 2017).

Beside their expression in sensory organs, the three members of the miR-183 cluster are also found to be expressed in other cell types and to be differentially regulated in many different cancers and other diseases. In most non-sensory adult tissues, members of the miR-183 cluster are not expressed to a high extent. Nevertheless, high expression levels of miR-183 cluster members have been observed in pathologic conditions of neurons, autoimmunity and a wide variety of malignancies (Dambal et al., 2015).

The miR-183 cluster is highly expressed in hormonal cancers of the breast, ovary and the prostate compared to benign tissue. In breast cancer, the upregulation of miR-183 cluster members results in increased proliferation, migration and invasion by repressing diverse tumor suppressor genes (Cheng et al., 2016; Li et al., 2014; Lin et al., 2010; Zhang et al., 2015b). In this cancer type, miR-96 for example targets FoxO3 (Lin et al., 2010) or the reversion-inducing cysteine-rich protein with Kazal motifs RECK (Zhang et

al., 2015b). Furthermore, miR-183 is able to inhibit apoptosis by targeting programmed cell death 4 (PDCD4) (Cheng et al., 2016). PDCD4 is also targeted by miR-183 in esophageal cancer (Yang et al., 2014), while PDCD6 is repressed by miR-183 to enforce cell proliferation and to inhibit apoptosis in pediatric acute myeloid leukemia (Wang et al., 2017b). In ovarian cancer, miR-96 and miR-183 both repress FoxO3 which promotes cell proliferation and tumorigenicity (Xu et al., 2013).

In benign adult human prostate epithelial cells, the members of the miR-183 cluster are involved in zinc homeostasis by regulating zinc transporters. The increased expression of the miR-183 cluster leads to dysregulated zinc levels contributing to carcinogenesis (Mihelich et al., 2011). In addition, miR-96 targets the transcription factor FoxO1 (Fendler et al., 2013; Haflidadottir et al., 2013) and miR-183 the prostate-specific antigen (PSA) (Larne et al., 2015) resulting in increased proliferation and impaired apoptosis of prostate cancer cells. It was also shown, that TGFβ-dependent upregulation of miR-96 promotes bone metastasis in this specific cancer entity by targeting AKT1S1, a negative regulator of mTOR (Siu et al., 2015). Myocardial hypertrophy is also promoted by the miR-96-mediated inhibition of mTOR (Sun and Zhang, 2015) and in the neurodegenerative disorder spinal muscular atrophy (SMA) the direct binding of miR-183 to the 3'UTR of mTOR suppresses axon growth (Kye et al., 2014).

The members of the miR-183 cluster are also highly expressed in colorectal cancer and hepatocellular carcinoma (HCC) where they display the same oncogenic role as in the before mentioned cancer types. In colorectal cancer, miR-183 affects apoptosis and autophagy-mediated cell death by targeting the UV radiation resistance-associated gene (UVRAG) (Huangfu et al., 2016). Its family member miR-182 mediates tumorigenesis and invasion of colorectal cancer cells by regulating the PI3K/Akt pathway through the suppression of ST6GALNAC2 (Jia et al., 2017). Furthermore, miR-183 targets the tumor suppressor gene EGR-1. Thereby it regulates the downstream target and major negative regulator of the PI3K/ Akt pathway PTEN that affects cellular migration of colon cancer, synovial sarcoma and rhabdomyosarcoma cells (Sarver et al., 2010). In HCC, miR-96 and miR-182 regulate the tumor suppressor EphrinA5 (Wang et al., 2016) and the upregulation of the whole miR-183 cluster is used as prognostic factor for metastasis and tumor differentiation (Leung et al., 2015). MiR-96 was shown to promote the proliferation of human HCC cells (Baik et al., 2016).

Although most of the phenotypes are associated with high expression levels of the miR-183 cluster and an oncomiR-like behavior, there are some diseases where they show tumor suppressor activity. In T cell anaplastic large-cell lymphoma, non-small-cell

lung cancer and neuroblastoma miR-96 levels are decreased (Vishwamitra et al., 2012) and in gastric cancer the expression of miR-183 was lower than in normal tissue. This decreased expression of miR-183 inhibits cell proliferation and invasion (Cao et al., 2014; Xu et al., 2014). The bidirectional role of the miR-183 cluster either as oncomiR or tumor suppressor demonstrates a context and/ or cell type-specific phenotype for the cluster members in carcinogenesis.

Besides their role in carcinogenesis, the members of the miR-183 cluster also contribute to the pathogenesis of several autoimmune diseases. In the serum of patients suffering from the autoimmune disorder GD, miR-96 was highly expressed and correlated with a more sever outcome of the disease (Martinez-Hernandez et al., 2018). Moreover, miR-183 expression is upregulated in thyroid tissue from GD patients compared to healthy controls (Qin et al., 2015). The miR-183 cluster is also highly expressed in splenic lymphocytes from different mice models of SLE (Dai et al., 2013; Dai et al., 2010). Furthermore, a single nucleotide polymorphism of miR-182 was demonstrated to be associated with the two autoimmune syndromes Behçet's and Vogt-Koyanagi-Harada (Yu et al., 2014).

The altered expression of the miR-183 cluster is not only described systemically for several autoimmune disorders, the members also play part in the signaling pathways of different immune cells. The transcription of the miR-183 cluster was described to be regulated by TGFβ. In NK cells, TGFβ-induced miR-183 expression leads to the suppression of DAPI2, a signal adaptor for NK cell lytic function, resulting in immunosuppression (Donatelli et al., 2014). MiR-182 is highly expressed in B cells that undergo class switch recombination. Nevertheless, loss of miR-182 has only a minor impact on B cell development, class switch recombination and antigen-driven affinity maturation (Pucella et al., 2015). In $CD4^{+}FoxP3^{-}$ T cells, miR-182 plays a role in the clonal expansion of activated Th cells. MiR-182 expression is induced by STAT5 in an IL-2-dependent manner and suppresses the transcription factor FoxO1, a negative regulator of the cell cycle (Stittrich et al., 2010).

Although the role of miR-183 cluster in carcinogenesis is intensively studied and expanded to autoimmune disease, the impact, especially of miR-183 and miR-96, on $CD4^{+}$ T cell function still remains elusive.

1.9 Neuropilin-1 on CD4$^+$ T cells

Neuropilin-1 (Nrp-1) is a non-tyrosine kinase receptor and co-receptor for class III semaphorins and several members of the vascular endothelial growth factor (VEGF) family. Additionally, Nrp-1 is able to interact with other ligands like heparin-binding proteins, fibroblast growth factor 2, placental growth factor 2, transforming growth factor β1 (TGFβ1), hepatocyte growth factor (HGF), platelet derived growth factor (PDGF), integrins and extracellular miRNA. Through binding a wide variety of ligands, Nrp-1 has an important role in development, axonal guidance, angiogenesis, immunity and cancer (Ellis, 2006; Prud'homme and Glinka, 2012; Roy et al., 2017).

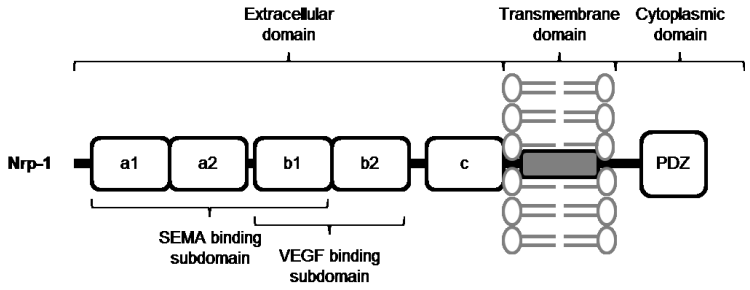

Figure 2: General structure of Neuropilin-1. Nrp-1 consists of three N-terminal extracellular domains (a1a2, b1b2 and c), a transmembrane domain, and a short cytoplasmic domain with a PDZ binding motif. Class III semaphorins bind Nrp-1 through the a1a2 domain in combination with the b1 subdomain. VEGF binding to Nrp-1 is facilitated by the b1b2 domain (adapted from (Prud'homme and Glinka, 2012)).

Nrp-1 is a type I transmembrane glycoprotein that consists of three N-terminal extracellular domains (a1a2, b1b2 and c), a transmembrane domain and a short cytoplasmic domain (Figure 2). Nrp-1 is thought to be unable to transduce intracellular signals on its own and forms co-receptor complexes. Within these ternary complexes, Nrp-1 enhances the cellular response to external signals. The class III semaphorin signaling requires Nrp-1 and a transmembrane protein of the plexin family. The interaction with semaphorins by Nrp-1 is facilitated by the a1a2 domain of Nrp-1, also known as complement binding (CUB-) domain, together with the b1 subdomain. In VEGF signaling, Nrp-1 also acts as a co-receptor and specifically binds VEGF-165. VEGF-165 forms a receptor complex with Nrp-1 and VEGF receptor-2 (VEGFR-2). The binding of VEGF to Nrp-1 involves the second extracellular domain, b1b2 or coagulation factor V/VIII of Nrp-1. The presence of Nrp-1 within the complex enhances the binding capacity of VEGF-165 and potentiates the VEGFR-2 signaling. In addition, the third extracellular domain of Nrp-1, the meprin domain is critical for homo- and heterodimerization. The intracellular domain of Nrp-1 possesses a PSD-95/Dig/ZO-1 (PDZ) binding motif that enables protein-protein recognition and signaling (Ellis, 2006).

Nrp-1 is expressed on endothelial cells, several other nonvascular cell types and by malignant tumor cells. Among immune cells, Nrp-1 is expressed by macrophages, DCs, T cells, B cells and mast cells (Roy et al., 2017). Nrp-1 is expressed in the murine thymus on $CD4^+CD8^+$ DP, $CD4^-CD8^-$ DN thymocytes and Tregs. During T cell development, the interaction of thymocytes and thymic epithelial cells was shown to enhance Nrp-1 expression upon TCR engagement. Nrp-1 has also been demonstrated to regulate the actin cytoskeleton reorganization modulating adhesion and migration within the thymus (Corbel et al., 2007).

The expression of Nrp-1 on human DCs and resting T cells was found to mediate the interaction between these two cell types. Upon cell contact, Nrp-1 polarization occurs on human T cells and blocking of Nrp-1 prevents DC-mediated T cell proliferation. Therefore, Nrp-1 seems to be essential for the induction of primary immune response (Tordjman et al., 2002). The interaction of class III semaphorin Sema3A and Nrp-1 leads to a downregulation of T cell activation (Lepelletier et al., 2006; Yamamoto et al., 2008). In 2004, Bruder et al. described Nrp-1 as a specific surface marker for murine $CD4^+CD25^+$ Tregs by using global gene expression studies. Moreover, they postulate that the constitutive expression of Nrp-1 on Tregs is independent of the activation status. A high expression of Nrp-1 correlates with the expression of Treg markers like FoxP3, PD-1, CD103, CTLA-4 and their suppressive phenotype (Bruder et al., 2004). Nrp-1 on Tregs was also shown to prolong the interaction with immature DCs. Therefore, Nrp-1 favors the formation of IS between DCs and Tregs, preventing Th cell interaction to establish tolerance under normal physiological conditions (Sarris et al., 2008). Besides Sema3A, Nrp-1 is a high affinity receptor for TGFβ1 promoting Treg activity (Glinka and Prud'homme, 2008). Nrp-1 is also discussed as a marker to distinguish between nTregs and iTregs. Compared to iTregs, nTregs express high levels of Nrp-1 (Yadav et al., 2012). However, iTregs from highly inflamed tissue were also shown to express Nrp-1 (Weiss et al., 2012). Furthermore, $Nrp\text{-}1^-$ Tregs, but not $Nrp\text{-}1^+$ Tregs are able to suppress autoreactive B cells by PD-L1/PD-1-induced apoptosis, controlling B cell tolerance against autoantigens (Gotot et al., 2018).

In humans the role of Nrp-1 as a Treg marker is controversially discussed, since its expression differs from murine Tregs. Battaglia et al. identified a small $Nrp\text{-}1^+CD4^+CD25^{high}$ T cell population in human lymph nodes that also displayed high FoxP3 expression accompanied with high suppressive capacity (Battaglia et al., 2008). Contrary to these results, Milpied et al. described a $Nrp\text{-}1^+FoxP3^-$ T cell population in human secondary lymphoid organs and claimed that Nrp-1 expression in not specific for human $FoxP3^+$ Tregs (Milpied et al., 2009).

In 2012, Hansen et al. showed that Nrp-1 acts a key mediator of FoxP3$^+$ Treg cell migration to the tumor microenvironment. In mice, ablation of Nrp-1 expression in CD4$^+$ T cells led to elevated antitumor immune responses in tumor bearing mice, demonstrated by increased CD8$^+$ and decreased Treg cell infiltration into the tumor site, reduced tumor burden and improved tumor free survival. This effect was reversed by adoptive transfer of Nrp-1$^+$ Tregs. Furthermore, the authors showed that Nrp-1 expression on FoxP3$^+$ Tregs do not directly promote their immunosuppressive function but confers migration along a tumor-derived VEGF gradient (Hansen et al., 2012). One year later, Delgoffe et al. demonstrated that the interaction of tumor infiltrating plasmacytoid DC-produced Sema4A and Nrp-1 potentiates Treg cell stability, function and survival. The interaction results in a PTEN-dependent decrease of Akt phosphorylation leading to increased nuclear localization of the transcription factor FoxO3. Therefore, Nrp-1 is indispensable for Tregs to limit anti-tumor immune response (Delgoffe et al., 2013). In the human system, Nrp-1 expression was shown to be increased on tumor-infiltrating lymphocytes in colorectal cancer liver metastases (Chaudhary and Elkord, 2015). Moreover, the loss of Nrp-1 on Tregs accompanied by an upregulation of Nrp-1 on effector T cells was described to cause allograft rejection (Campos-Mora et al., 2015).

Nrp-1 is essential for the suppressive capacity of Tregs especially in the tumor microenvironment. Nevertheless, the role of Nrp-1 under other inflammatory conditions like autoimmunity or its relevance for CD4$^+$ effector T cells is less understood.

2 Aim of the project

Autoimmune disorders are caused by tissue damage in the presence of autoantibodies and self-reactive lymphocytes. Inflammatory conditions let lymphocytes overcome the mechanisms of self-tolerance which highly contributes to the pathogenesis of the disease. A more extensive understanding in the regulation of T cell activation and function could help to discover molecules which might have an impact on the development of autoimmunity.

MicroRNAs (miRNAs) are described to play a fundamental role in the regulation of immune cell function. Aberrant miRNA expression patterns are observed in many immunological disorders including autoimmunity. Dysregulated miR-96 and miR-183 expression have been described in the context of autoimmune disease like Graves' disease, but little is known about their function in $CD4^+$ T cells. The aim of the first part of this thesis is to investigate the influence of both miRNAs on the phenotype and function of $CD4^+$ T cells *in vitro* and *in vivo* using gain- and loss-of-function experiments. After analyzing the miRNA expression pattern in naïve and activated murine and human $CD4^+CD25^-$ and $CD8^+$ T cells, the impact of miR-96 and miR-183 on T cell function should be investigated. MiRNA overexpressing as well as knockdown T cells will be characterized for their proliferative capacity *in vitro* and their ability to induce antigen-specific autoimmune diabetes *in vivo*. In addition, targets and downstream signaling pathways should be elucidated. Moreover, miR-96 and miR-183 expression patterns of human $CD4^+$ T cells from Graves' orbitopathy patients will be determined to investigate their relevance in the human system.

Neuropillin-1 (Nrp-1) was described as a cell surface maker for murine $CD4^+CD25^+$ Tregs. Moreover, Nrp-1 mediates VEGF-dependent infiltration of Tregs into tumor tissue. The second part of this thesis will investigate, whether the T cell-specific expression of Nrp-1 also influences the development of autoimmune diseases. To address this question, Nrp-1 knockout and wild type $CD4^+$ T cells will be analyzed for their ability to modulate the development of spontaneous autoimmune diabetes in Nrp-$1^{fl/fl}$ x CD4cre x TCR-HA x INS-HA mice. To get more insights in the role of Treg-specific Nrp-1 expression in the autoimmune setting, $HA^+CD4^+CD25^+$ Tregs from either T cell-specific Nrp-1 knockout or wild type mice will be co-transferred with HA-specific effector T cells into INS-HA x Rag2-KO mice. Mice will be monitored for diabetes development and T cell response.

This study will help to understand the effects of miR-96 and miR-183 as well as Nrp-1 expression on $CD4^+$ T cell activation and function in the context of autoimmune disease.

3 Materials

3.1 Chemicals

10 mM Magnesium chloride solution	Promega, Germany
2-Mercaptoethanol	Carl Roth GmbH, Germany
Agarose	Biozym, Germany
Albumin bovine fraction V pH 7.0	Serva, Germany
Ammonium acetate	Sigma Aldrich, USA
Ampicillin	Invitrogen, Germany
Brefeldin A	Sigma Aldrich, USA
Demethyl sulphoxide (DMSO)	Carl Roth GmbH, Germany
Deoxynucleoside Triphosphate (dNTPs)	Fermentas, Germany
Calcium chloride dehydrate	Carl Roth GmbH, Germany
Cell Proliferation Dye eFluor® 670	eBioscience, USA
Ethidium bromide	Carl Roth GmbH, Germany
Ethylenediaminetetraacetic acid (EDTA)	Carl Roth GmbH, Germany
Formaldehyde (37%)	Sigma Aldrich, USA
Geneticin (G418)	Biochrom/Merck KGaA, Germany
GeneRuler™ 100 bp DNA Ladder	Thermo Fisher Scientific, Germany
GeneRuler™ 1 kb DNA Ladder	Thermo Fisher Scientific, Germany
Fetal Bovine Serum (FCS/FBS)	Biochrom/Merck KGaA, Germany
Hepes Buffer	PAA, GE-Healthcare, UK
Ionomycin	Sigma Aldrich, USA
IGEPAL® CA-630 (NP-40)	Sigma Aldrich, USA
Linear Polyacrylamide	Ambion, USA
Lipofectamin® LTX & Plus Reagent	Invitrogen, Germany
PageRuler™ Prestained Protein Ladder	Thermo Fisher Scientific, Germany
Paraformaldehyde	Carl Roth GmbH, Germany
Penicillin / Streptomycin	Invitrogen, Germany
Phorbol 12-myristate 13-acetate (PMA)	Sigma Aldrich, USA
Polybrene (Hexadimethrine bromide)	Sigma Aldrich, USA
ReBlot Plus Strong Stripping Solution 10x	Merck, Germany
Reporter Lysis Buffer 5x	Promega, Germany
Sodium dodecyl sulfate	Carl Roth GmbH, Germany
Trypan Blue 0.4%	Invitrogen, Germany
Trypsin-EDTA solution 10x	Sigma Aldrich, USA
TurboFect™ *in vitro* Transfection Reagent	Fermentas, Germany
Tween 20	Sigma Aldrich, USA

3.2 Buffer

ACK buffer	155 mM NH_4Cl 9.98 mM $KHCO_3$ 0.5 M EDTA, pH 8 pH 7.4
PBS buffer	136 mM NaCl 2.68 mM KCl 8.09 mM Na_2PO_4 x 2 H_2O 1.47 mM KH_2PO_4 pH 7.4
FACS buffer	1x PBS-Buffer 2% (v/v) FCS 2 mM EDTA
HEBS 2x	280 mM NaCl 50 mM Hepes 1.5 mM Na_2HPO_4 x 2 H_2O
TBE	89 mM Tris 89 mM Boric acid 2.53 mM EDTA
Tail-lysis buffer	100 mM Tris HCL pH 8.5 200 mM NaCl 5 mM EDTA 0.2% (v/v) SDS
Protein lysis buffer	150 mM NaCl 1% (v/v) NP-40 50 mM Tris pH 8 Protease Inhibitor Cocktail
10x Running buffer	30 g/L Tris 144 g/L Glycine 1% (v/v) SDS
10X Tris glycine buffer	3.03 g/L Tris-Base 14.4 g/L Glycine
1X Blotting buffer	100 mL 10X Tris glycine buffer 200 mL Methanol Add 1 L H_2O
PBT buffer	PBS buffer 0.1% (v/v) Tween 20

3.3 Cell culture media

IMDM complete (IMDMc)	*Iscove`s Modified Dulbecco`s Medium* (IMDM) with GlutaMax® and 25 mM Hepes, Gibco Invitrogen, Germany 10% FCS, heat-inactivated 100 U/mL Penicillin/ Streptomycin 25 µM β-Mercaptoethanol
RPMI complete (RPMIc)	RPMI-1640 medium, Gibco Invitrogen, Germany 10% FCS, heat-inactivated 100 U/mL Penicillin/ Streptomycin 25 µM β-Mercaptoethanol
Opti-MEM	Opti-MEM™ Reduced Serum Medium, Gibco Invitrogen, Germany
Cell Freezing Medium	FCS + 5% DMSO
LB Medium	Lysogeny Broth, Carl Roth GmbH, Germany 50 µg/mL Ampicillin

3.4 Primer

Table 1: Primer for genotyping of transgenic mice

Transgene	Sequence (5`→ 3`)	Annealing temperature [°C]
Cre	ACGACCAAGTGACAGCAATG CTCGACCAGTTTAGTTACCC	60
Ins-HA	GGCTACCATGCGAACAATTCAACCG CTCCGTCAGCCATAGCAAATTTCTG	55
Neo	GCTATTCGGCTATGACTGGG GAAGGCGATAGAAGGCGATG	57
Nrp1KO	AGGCCAATCAAAGTCCTGAAAGACAGTCCC AAACCCCCTCAATTGATGTTAACACAGCCC	63
Rag2	ATGTCCCTGCAGATGGTAACA GCCTTTGTATGAGCAAGTAGC	57
TCR-HA	CCTGAACTGGGGATTCTACTCTTCC AGTCAGCTTATTATTGCCTCCACTC	58

Table 2: Primer for qRT PCR

Target gene	Sequence (5`→ 3`)	Annealing temperature [°C]
EGR1 5`	TTTTTGCCCGTCCCTTTGGTTTCA	58
EGR1 3`	GCCCTCTTCCTCGTTTTTGCTCTC	
PTEN 5`	AATGCGTACCTACCTTGCCC	58
PTEN 3`	TGTCTTGTTGTTAGCCCACCA	
RPS9 5`	CTGGACGAGGGCAAGATGAAGC	58
RPS9 3`	TGACGTTGGCGGATGAGCACA	
Mmu-miR-183-5p	UAUGGCACUGGUAGAAUUCACU	55
Mmu-miR-96-5p	UUUGGCACUAGCACAUUUUUGCU	55
Hs_RNU6B_13	- Not available -	55

Table 3: Primer for cloning

Designation	Sequence (5`→ 3`)	Annealing temperature [°C]
miR-96 BamH II 5`	GGATCCAGCTCCTCACCCCTTTCT	55
miR-96 Xho II 3`	CTCGAGTGTTGGCCCAGCTCGGATTG	

3.5 Enzymes & recombinant proteins

Ampli Taq Gold DNA Polymerase	Applied Biosystems, USA
BamH I	Fermentas, Germany
Bgl II	Fermentas, Germany
Bsu36 I	Fermentas, Germany
Calf Intestinal Alkaline Phosphatase	Invitrogen, Germany
Expand High Fidelity PCR System	La Roche, Switzerland
Go Taq Polymerase	Promega, Germany
Human rIL2	eBioscience, USA
M-MLV Reverse Transcriptase	Promega, Germany
Proteinase K (10 mg/mL)	Roche, Germany
Sac I	Fermentas, Germany
T4 DNA-Ligase	Invitrogen, Germany
Xho I	Fermentas, Germany

3.6 Plasmids

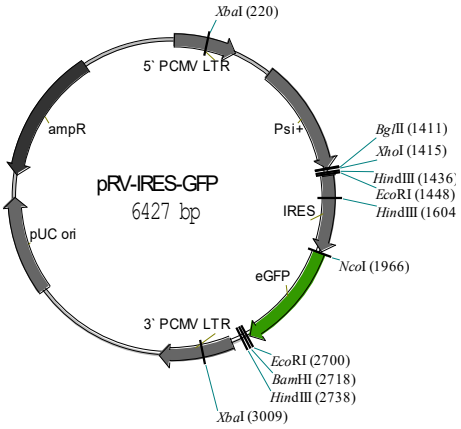

Figure 3: pRV-IRES-GFP. The retroviral vector, encoding a green fluorescent protein (GFP) reporter gene, was used as empty vector control.

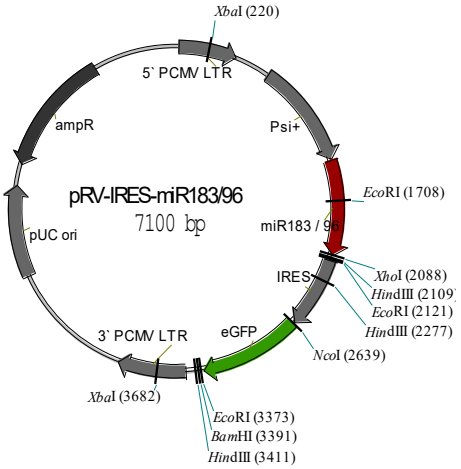

Figure 4: pRV-IRES-miR-183/-96. The retroviral vector derived from the pRV-IRES-GFP plasmid. The cDNA sequence encoding the mature miR-183 and miR-96 sequence was inserted via the restriction enzymes Bgl II und Xho I.

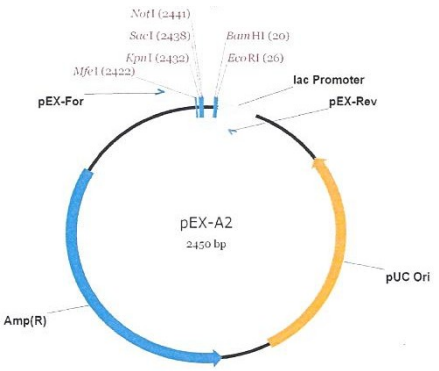

Figure 5: pEX-A2-miR183mut. The plasmid was purchased from Eurofins Genomics GmbH, Germany. It expresses the mature miR-183 and miR-96 sequence with six point mutations in the miR-183 seed sequence. The insert was used to generate the pRV-IRES-miR-183(mut)/-96 vector.

3.7 Antagomirs

Table 4: Antagomirs

Designation	Producer
miRIDIAN™ microRNA Mouse mmu-miR-96-5p hairpin inhibitor	Dharmacon™, USA
Custom miRIDIAN™ microRNA Mouse mmu-miR-96-5p hairpin inhibitor 5`Fluorescein	Dharmacon™, USA
miRIDIAN™ microRNA Mouse mmu-miR-183-5p hairpin inhibitor	Dharmacon™, USA
Custom miRIDIAN™ microRNA Mouse mmu-miR-183-5p hairpin inhibitor 5`Fluorescein	Dharmacon™, USA
miRIDIAN™ microRNA Hairpin Inhibitor Negative Control #1	Dharmacon™, USA
Custom miRIDIAN™ microRNA Hairpin Inhibitor Negative Control #1 5`Fluorescein	Dharmacon™, USA

3.8 Antibodies

Table 5: Antibodies for T cell isolation and activation

Epitope	Label	Clone	Producer
CD3	Purified	145-2C11	BD Bioscience, USA
CD25	Biotinylated	7D4	BD Bioscience, USA
CD28	Purified	37.51	BD Bioscience, USA

Table 6: Antibodies for flow cytometry

Epitope	Fluorochrome	Clone	Producer
Akt	R-Phycoerythrin	C67E7	Cell Signaling Technology, Germany
Akt-P-Ser-473	Alexa Fluor 647	C31E5E	Cell Signaling Technology, Germany
Akt-P-Thr-308	Alexa Fluor 647	D9E	Cell Signaling Technology, Germany
CD4	Allophycocyanin	RM4-5	BD Bioscience, USA
	Pacific Blue	H129.19	BD Bioscience, USA
	R-Phycoerythrin Cyanine7	RM4-5	BioLegend, USA

CD8	Allophycocyanin	53-6.7	BD Bioscience, USA
CD25	R-Phycoerythrin Cyanine7	PC61	BD Bioscience, USA
CD62L	R-Phycoerythrin	MEL-14	eBioscience, USA
CD69	Allophycocyanin	H1.2F3	BioLegend, USA
	Fluorescein isothiocyanate	H1.2F3	eBioscience, USA
EGR-1	unconjugated	15F7	Cell Signaling Technology, Germany
FoxP3	Allophycocyanin	FJK-16s	eBioscience, USA
	Fluorescein isothiocyanate	FJK-16s	eBioscience, USA
HA-specific TCR	AlexaFluor 647	6.5	Kirberg *et al*., 1994
Ki-67	R-Phycoerythrin Cyanine7	SolA15	eBioscience, USA
Nrp-1	R-Phycoerythrin	3E12	R&D Systems, USA
	Brilliant Violet 421	3E12	BioLegend, USA
PTEN	Allophycocyanin	REA270	Miltenyi Biotec, Germany
Thy1.1	Fluorescein isothiocyanate	OX-7	BD Bioscience, USA
	R-Phycoerythrin	OX-7	BD Bioscience, USA

Table 7: Antibodies for Western Blotting

Epitope	**Isotype**	**Clone**	**Producer**
Akt (pan)	Rabbit IgG	C67E7	Cell Signaling Technology, Germany
Phospho-Akt (Ser473)	Rabbit IgG	193H12	Cell Signaling Technology, Germany
Phospho-Akt (Thr308)	Rabbit IgG	244F9	Cell Signaling Technology, Germany
GAPDH	Rabbit IgG	14C10	Cell Signaling Technology, Germany
Anti-Rabbit IgG HRP-linked	Goat IgG		Cell Signaling Technology, Germany

3.9 Commercially available kits

$CD4^+$ T Cell Isolation Kit, human	Miltenyi Biotec, Germany
$CD4^+$ T Cell Isolation Kit, mouse	Miltenyi Biotec, Geramny
$CD8^+$ T Cell Isolation Kit, human	Miltenyi Biotec, Germany
$CD8^+$ T Cell Isolation Kii, mouse	Miltenyi Biotec, Germany
Criterion™ TGX™ Precast Gels 4 – 20%	Bio-Rad Laboratories, USA
Cytofix/Cytoperm Kit	BD Bioscience, USA
Firefly Luciferase Beetle Juice Kit	PJK, Germany
FoxP3 Staining Buffer Kit	eBioscience, USA
miScript Primer Assays	Qiagen, Germany
miScript Reverse Transcription Kit	Qiagen, Germany
miScript SYBR Green PCR Kit	Qiagen, Germany
NucleoBond PC 500	Machery-Nagel, Germany
NucleoSpin Plasmid	Machery-Nagel, Germany
Luc-Pair miR Luciferase Assay Kit	GeneCopoeia, USA
PCR-Purification Kit	Qiagen, Germany
PE Annexin V Apoptosis Detection Kit I	BD Bioscience, USA
Pierce™ BCA Protein Assay Kit	Thermo Fisher Scientific, Germany
Power Maxima SYBR Green qPCR Master Mix	Fermentas, Germany
QIAquick Gel Extraction Kit	Qiagen, Germany
Renilla-Juice Kit	PJK, Germany
RNeasy MinElute Clean up Kit	Qiagen, Germany
RNeasy Mini Kit	Qiagen, Germany
RNeasy Plus Mini Kit	Qiagen, Germany
SuperSignal™ Western Blot Enhancer	Thermo Fisher Scientific, Germany
TOPO TA Cloning Kit	Qiagen, Germany
Western Lightning® Plus-ECL	Perkin Elmer, USA

3.10 Equipment

Blood glucose meter	Xpress-i, Nova Biomedical, UK
Cell Sorter	Aria II, BD Bioscience, USA
Flow Cytometer	LSR II, BD Bioscience, USA
Luminometer	Orion II, Titertek Berthold, Germany
Magnetic Activated Cell Sorter	AutoMACS Pro, Miltenyi Biotech, Germany
Microplate reader	Epoch, BioTek Instruments, USA
Neubauer Counting chamber	Assistant, Germany
NanoDrop spectrophotometer	Thermo Fisher Scientific, Germany
qRT-PCR Cycler	7500 Fast Real Time PCR System, ABI, Germany

3.11 Cell lines

NIH-3T3 Cells	Murine fibroblast cells (purchased by ATCC, CRL-165P)
GPE86 Cells	NIH3T3 cells transfected with Gag, Pol and Env of the Moloney murine leukemia virus (MMLV) (Markowitz et al., 1990)
GPE86-eGFP	GPE86 cells transfected with pRV-IRES-eGFP
GPE86-miR-183/-96	GPE86 cells transfected with pRV-IRES-miR-183/96
GPE86-miR-183(mut)/-96	GPE86 cells transfected with pRV-IRES-miR-183(mut)/96

3.12 Bacteria

One Shot Top10 chemically competent *E. coli*, Invitrogen, Germany

3.13 Mice

The utilized mice were housed and bred in a specific pathogen-free (SPF) facility at the University Hospital Essen. Cages were individually ventilated. To exclude microbial contamination, histological, serological and parasitological samples of sentinel mice were analyzed by an external laboratory every three month. All used mice were on the genetic background of BALB/c mice and either heterozygous or homozygous for the specific transgene. All experiments were performed when animals were at least six to eight weeks of age and in accordance with institutional, state and federal guidelines.

3.13.1 BALB/c mice

The used BALB/c mice were purchased from Envigo RMS GmbH, Germany.

3.13.2 Thy 1.1 mice

The Thy 1.1 mice express the allele one of Thy1 (CD90.1) and were kindly provided by Jochen Hühn (Braunschweig, Germany).

3.13.3 Thy 1.1 x TCR-HA mice

In these transgenic mice around 30% of the $CD4^+$ T cells express a TCR specific for the MHC class II $H2E^d$:$HA_{110-120}$-restricting epitope of the Influenza hemagglutinin (HA) (Kirberg et al., 1994).

3.13.4 INS-HA x Rag2-KO mice

The double transgenic INS-HA x Rag2-KO mice express the model antigen HA of the Influenza A virus under the control of the rat insulin promoter (INS-HA, (Lo et al., 1992)) on pancreatic beta cells. Furthermore, a mutation in the *rag2* gene leads to total inability to initiate V(D)J rearrangement resulting in a lack of mature B and T cell (Shinkai et al., 1992).

3.13.5 Nrp-$1^{fl/fl}$ x CD4cre x TCR-HA mice

In this mouse strain the exon 2 of *nrp-1* gene is flanked by loxP sites (Gu et al., 2003). The concurrent expression of cre recombinase under the control of the CD4 enhancer, promoter and silencer sequence (Lee et al., 2001) leads to a depletion of Nrp-1 in T cells. Furthermore, 15 – 20% of the T cells of these mice express a TCR specific for the MHC class II $H2E^d$:$HA_{110-120}$-restricting epitope of the Influenza HA.

3.13.6 Nrp-$1^{fl/fl}$ x CD4cre x TCR-HA x INS-HA mice

These transgenic mice have an insertion of loxP sites up and downstream of exon 2 of the *nrp-1* gene. They express the cre recombinase under the control of the CD4 enhancer, promoter and silencer sequence which leads to a depletion of Nrp-1 in T cells. 15 – 20% of these $CD4^+$ T cells express a TCR specific for the MHC class II $H2E^d$:$HA_{110-120}$-restricting epitope of the Influenza HA. In addition, the model antigen HA of the Influenza A virus is expressed under the control of the rat insulin promoter on pancreatic beta cells (INS-HA). In approximately 30 – 40% of the mice, the concurrent expression of the transgenic TCR and the HA antigen on the beta cells result in the development of autoimmune diabetes (Sarukhan et al., 1998).

3.14 Patients

Blood samples were obtained from patients suffering from severe GO (in the following called EO) at the department of Ophthalmology and age- and sex-matched healthy donors. All patients gave their written informed consent. The study was approved by the medical ethical committee of the University Hospital Essen, Germany.

3.15 Software

7500 Fast System v1.4.0	Thermo Fisher Scientific, Germany
BD FACSDiva™ Software 8.0	BD Bioscience, USA
Fusion 15.18	Vilber Lourmat GmbH, Germany
FlowJo 7.2.5	FlowJo, USA
Gen5 1.09	BioTek Instruments, USA
GraphPad Prism 7.04	STATCON GmbH, Germany
ImageJ 1.51j8	open source
Simplicity 4.2	Titertek Berthold, Germany

4 Methods

4.1 Cell biological methods

4.1.1 Preparation of single cell suspension

Lymphocytes were harvested from spleen, mesenteric lymph nodes and pancreas using different protocols. Centrifugation steps were performed with a Multifuge 3SR+ (Thermo Fisher Scientific, Germany) at 300 x g for 10 minutes at 4°C.

4.1.1.1 Spleen

Spleens were rinsed with 10 mL erythrocyte lysis buffer (ACK buffer) using a catheter and syringe by simultaneously squeezing of the organ using tweezers. Afterwards cells were filtered through a 100 µm cell strainer, centrifuged and resuspended in FACS buffer or IMDMc cell culture medium.

4.1.1.2 Mesenteric lymph nodes

Mesenteric lymph nodes were grinded through a 70 µm cell strainer in FACS buffer. After centrifugation, cells were resuspended in IMDMc cell culture medium.

4.1.1.3 Pancreas

First pancreas was minced using scissors. Then the tissue was grinded and filtered through a 70 µm cell strainer in IMDMc cell culture medium. After centrifugation, cells were resuspended in IMDMc cell culture medium.

4.1.2 Isolation of peripheral blood mononuclear cells from whole blood

To analyze the miRNA expression in human T cells, whole blood samples were obtained from healthy donors and patients suffering from severe endocrine orbitopathy. Blood samples were collected in NH_4-Heparin Monovette tubes (Sarstedt). Prior to T cell isolation, peripheral blood mononuclear cells (PBMCs) were isolated from blood by Bicoll density gradient (Biochrom GmbH, Germany). Therefore, 15 mL Bicoll were filled carefully into a Falcon tube and centrifuged for one minute at 1700 x g to allow sedimentation. The blood of two NH_4-Heparin Monovette tubes was poured carefully onto the filter and filled up to 40 mL with PBS. After 10 minutes of centrifugation at 1700 x g the supernatant was transferred into a new 50 mL Falcon tube and subsequently centrifuged at 1200 x g for seven minutes. Isolated cells were washed

twice with 40 mL PBS and stored in fetal calf serum and 10% DMSO (Carl Roth GmbH, Germany) in liquid nitrogen.

4.1.3 Isolation of T lymphocytes by MACS technology

The isolation of $CD4^+$ and $CD8^+$ T cell from murine erythrocyte depleted splenocytes or human PBMCs was performed using the autoMACS® Pro Separator (Miltenyi Biotec, Germany) and the $CD4^+$ and the $CD8^+$ T cell isolation kit (Miltenyi Biotec, Germany), respectively according to the manufacturer's recommendations. To isolate murine $CD4^+CD25^-$ T cells 1 µL biotinylated anti-CD25 antibody was added to the antibody cocktail per sample.

4.1.4 Cell counting

The Neubauer counting chamber was used to determine the amount of cells within a single cell suspension. Therefore, cell suspension was diluted with Trypan Blue and 10 µL were applied to the counting chamber. White and round-shaped cells within four squares were counted and average was calculated. Then the cell number per milliliter was calculated by multiplying the average with the diluent factor and 10^4.

4.1.5 T lymphocyte activation *in vitro*

For flow cytometric analysis, gene expression analysis and retroviral infection $CD4^+CD25^-$ T cells were needed to be activated *in vitro*. Therefore, human and murine $CD4^+CD25^-$ T cells either isolated by MACS Technology or by Fluorescence Activated Cell Sorting (see 4.1.7) were resuspended in an appropriate cell culture medium containing 1 µg/mL anti-CD28 antibody. Then the cells were transferred to a multiwell flat bottom cell culture plate preincubated with 0.75 µg/mL anti-CD3 for 90 minutes.

4.1.6 Flow cytometry

The expression of surface and intracellular proteins was analyzed by flow cytometry. The measurements were performed on the LSR II flow cytometer using FACS DIVA software (BD Bioscience, USA). The utilized antibodies are listed in Table 6. They were titrated for optimal concentration of use. Cells were stained in 96 round-bottom plates.

4.1.6.1 Staining of surface proteins

For surface staining cells were transferred into a 96 well round-bottom plate and centrifuged at 300 x g for 5 minutes. Antibodies were diluted in FACS buffer. To distinguish viable from dead cells, the fixable viability dye eFluor780 (eBioscience,

USA) was used. Cells were resuspended in 100 µL antibody solutions and incubated for 10 minutes at 4°C in the dark. For Neuropilin-1 staining incubation time was extended to 30 minutes. Afterwards cells were washed with 100 µL FACS buffer and centrifuged for another five minutes. Then supernatant was discarded and cells were resuspended in 200 µL FACS buffer for analysis.

4.1.6.2 Intracellular staining

Intracellular staining often followed surface staining. In this case cells were washed with 100 µL PBS instead of FACS buffer.

FoxP3 staining was performed using the FoxP3 Staining buffer kit (eBioscience, USA) according to the manufacturer's recommendations and anti-FoxP3 antibody.

The intracellular staining of Akt and phospho-Akt was initiated after stimulation of cells with 1 µg/mL anti-CD3 antibody for 30 minutes at 37°C. Then the cells were fixed for 30 minutes using the Cytofix/Cytoperm kit (BD Biosciences, USA). After two rounds of washing with permeabilization buffer, proteins were stained with anti-Akt, anti-Akt-P-S473 and anti-Akt-P-T308 antibodies diluted in permeabilization buffer for one hour at 4°C in the dark.

For intracellular staining of EGR-1 cells were resuspended in 200 µL formaldehyde (2%) and incubated for one hour at 4°C in the dark. Then the cells were washed twice with permeabilization buffer from FoxP3 Staining buffer kit (eBioscience, USA). Anti-EGR-1 unconjugated antibody was diluted in permeabilization buffer and added to the cells for 30 minutes at 4 °C in the dark. Afterwards cells were washed with permeabilization buffer and stained with an anti-rabbit secondary antibody for another 30 minutes at 4°C in the dark.

The intracellular staining of PTEN was performed using the Cell signaling buffer set A (Miltenyi Biotec, Germany) according to the manufacturer's recommendations. Following surface staining cells were fixed in 200 µL Inside Fix buffer for 10 minutes at room temperature in the dark. For permeabilization cells were resuspended in 50 µL -20°C cold permeabilization buffer A and incubated for 30 minutes at 4°C in the dark. Intracellular staining of PTEN was performed with an anti-PTEN antibody diluted in FACS buffer for another 30 minutes at 4°C in the dark.

4.1.7 Fluorescence Activated Cell Sorting

Fluorescence activated cell sorting (FACS) was applied on the one hand to isolate $CD4^+CD25^-$ T cells for proliferation assays and Western Blot. On the other hand it was used to purify 6.5^+eGFP^+ or $6.5^+CD4^+CD25^-$ T cells for adoptive transfer experiments. Cell sorting was performed on the ARIA II cell sorter using FACS DIVA software (BD Bioscience, USA). Prior cell sorting $CD4^+$ T cells were enriched from splenocytes using the $CD4^+$ T cell isolation kit (Miltenyi Biotec, Germany, see 4.1.2).

Surface staining for $CD4^+CD25^-$ T cells was performed with anti-CD4 and anti-CD25 as Pacific Blue (PB) and R-Phycoerythrin-Cyanine7 (PE-Cy7) conjugates. For 6.5^+eGFP^+ T cell sorting staining was done with anti-HA-specific TCR(6.5) antibody conjugated to Alexa Fluor 647 (AF647) and Fixable viability dye. Anti-CD4, anti-CD25 and anti-6.5-specific TCR as PB, Fluorescein isothiocyanate (FITC) and AF647 conjugates were used to stain for $6.5^+CD4^+CD25^-$ T cells. Cells were either collected in IMDMc or RPMIc cell culture medium.

4.1.8 Proliferation assay

Proliferation assays were performed either with miRNA over-expressing retroviral transduced $CD4^+CD25^-GFP^+$ (see 4.3) or with antagomir-treated $CD4^+CD25^-$ (see 0) T cells. 48 hours after retroviral transduction $eGFP^+$ T cells were isolated by FACS. 1 x 10^5 cells were stained with the cell proliferation dye eFluor®670 (eBioscience, USA) according to the manufacturer's recommendations and stimulated with 1 µg/mL anti-CD3 in the presence of 4 x 10^5 $CD4^+$-depleted irradiated splenocytes for 72 hours. Antagomir-treated $CD4^+CD25^-$ T cells were stained after three days of initial activation and were also stimulated for another 72 hours. The dilution of the proliferation dye reflects the cell proliferation and was measured by flow cytometry.

4.1.9 Apoptosis assay

Annexin-V staining was performed with the Annexin-V-PE Detection Kit (BD Bioscience, USA) according to the manufacturer's recommendations. After surface staining, cells were washed with PBS twice. Then the cell were resuspended in Annexin-V binding buffer and stained with anti-Annexin-V-PE and anti-7-AAD antibodies for 15 minutes at room temperature in the dark. At the end, cells were resuspended in Annexin-V binding buffer and immediately analyzed by flow cytometry.

4.1.10 SDS Page

For the cell lysates, 2 x 10^6 antagomir-treated cells (see 0) were harvested with or without re-stimulation with 1 µg/mL anti-CD3 for 30 minutes. After centrifugation at 300 x g and 4°C for 10 minutes, cells were suspended in 20 µL lysis buffer and incubated on ice for 15 minutes. Then, the cell suspension was centrifuged again at 20,000 x g and 4°C for 10 minutes. Supernatant was transferred into a new 1.5 mL Eppendorf tube and stored on ice.

Protein concentration was determined using the Pierce™ BCA Protein Assay Kit (Thermo Fisher Scientific, Germany) according to the manufacturer's recommendations. In brief, samples were diluted 1:5 with water and were used as duplicates. A 1:5 dilution of the lysis buffer was used as blank. 10 µL of the sample was mixed with 200 µL working solution (1:50 Solution A: Solution B) and incubated in the dark at 37°C on a horizontal shaker for 30 minutes. Afterwards, the protein concentration was calculated using a microplate reader and the program Gen5 (both BioTek Instruments, USA).

A protein concentration of 50 µg per sample was diluted with 5 x reducing sample buffer and heated to 95°C for five minutes. Afterwards, the samples were separated on a Criterion™ TGX™ 4-20% Precast SDS-Gel (Bio-Rad Laboratories, USA) at 200 V for one hour.

4.1.11 Western Blot

A nitrocellulose blotting membrane (Amersham™Protran™0.2 µM, GE Healthcare, UK) was placed on the SDS gel and inserted with six chromatography papers (Whatman® , GE Healthcare, UK) and two sponges into Western Blot cassette. The cassette was placed in a tank-blot system (Bio-Rad Laboratories, USA), filled with transfer buffer and the blotting was performed at 100 V for 43 minutes.

Thereafter, the membrane was incubated in SuperSignal™ Western Blot Enhancer Antigen Pretreatment Solution (Thermo Fisher Scientific, Germany) for 10 minutes and then washed five times with water before it was blocked with 5% non-fat milk powder in PBT for one hour at room temperature. Then, the blocking solution was removed and the primary antibodies (see Table 7), diluted in SuperSignal™ Western Blot Enhancer Primary Antibody Solution (Thermo Fisher Scientific, Germany) were added for incubation at 4°C with gentle agitation overnight. The Akt antibodies were always applied in combination with a glyceraldehyde 3-phosphate dehydrogenase (GAPDH) antibody. The unbound antibody was washed off with PBT and the membrane was

incubated with the secondary, horseradish peroxidase-linked antibody (anti-rabbit), diluted in milk powder, at room temperature for one hour.

Then, the membrane was washed three times with PBT and two times with PBS and analyzed with the Western Lightning® Plus ECL solution (PerkinElmer, USA) to detect the horseradish peroxidase enzyme activity. Before the ReBlot Plus strong antibody stripping solution (Merck, Germany) was applied to the membrane, it was washed two times with PBT and five times with water. Stripping was performed at room temperature for five minutes. After five times washing with PBT, the membrane was blocked again and the procedure continued until the blot was incubated with phospho-Akt (Ser473), phospho-Akt (Thr308) and Akt (pan) antibodies.

4.2 Molecular biological methods

4.2.1 Genotyping of transgenic mice

To analyze the genotype of transgenic mice, tail biopsies were digested at 55°C overnight in 90 µL tail-lysis buffer and 10 µL proteinase K (10 mg/mL), followed by 10 minutes at 94°C. After centrifugation at 10,000 x g for 15 minutes the supernatant containing the chromosomal DNA was diluted 1:50 in MilliQ water and stored at 4°C. Genotyping was performed by polymerase chain reaction (PCR) followed by gel electrophoresis on 1% agarose gels stained with ethidium bromide. Primers were ordered from eurofins Genomics (Germany) and listed in Table 1. Table 8 shows the composition of the PCR master mix and Table 9 displays the PCR cycler settings.

Table 8: PCR master mix composition for genotyping

Volume or concentration	Components
1 µL	genomic DNA
1x	reaction buffer
1.5 mM	$MgCl_2$
1 mM	dNTPs
5 µM	forward primer
5 µM	reverse primer
0.5 U	GoTaq Hot Start polymerase
ad 20 µL	MilliQ H_2O

Table 9: PCR cycler program for genotyping

		10 cycles			27 cycles		
Temperature [°C]	95	95	T^A	72	95	T^A	72
Time [mm:ss]	10:00	00:30	01:30	01:30	00:15	00:45	00:45

T^A: Annealing temperature

4.2.2 Isolation of RNA & microRNA purification

RNA and miRNA were isolated from naïve or activated $CD4^+CD25^-$ T cells to analyze gene expression by quantitative real-time PCR (see 4.2.5). For gene expression analysis RNA and miRNA were isolated from 5 x 10^5 cells using the RNeasy Plus Mini Kit and the RNeasy MinElute Clean up Kit (both Qiagen, Germany) according to the manufacturer's recommendations. The RNeasy Plus Mini Kit separates the total RNA into a mRNA fraction with a size >200 bp and a miRNA fraction with a size <200 bp. The isolated mRNA fraction was precipitated with linear polyacrylamide and 7.5 M ammonium acetate diluted in absolute ethanol at -80°C overnight. After two rounds of washing with ice-cold ethanol (80%) the RNA was resuspended in 14 µL of RNAse-free water. The miRNA fraction is further purified with the RNeasy MinElute Clean up Kit (Qiagen, Germany).

4.2.3 Synthesis of complementary DNA

After isolation of mRNA the concentration was determined using a NanoDrop spectrophotometer (Thermo Fisher Scientific, Germany) and 1 µg total RNA was used for complementary DNA (cDNA) synthesis. Therefore, 13 µL total RNA was incubated with 0.5 µL Oligo(dT) and 0.5 µL Random Primer (both Invitrogen, USA) at 70°C for 10 minutes. Afterwards reverse transcription was performed by adding of 1 µL M-MLV (H-) point mutant reverse transcriptase, 4 µL 5x M-MLV RT-Buffer (both Promega, USA) and 1 µL 10 mM dNTPs (Fermentas, USA) at 42°C for 60 minutes. The synthesis was completed by inactivation of the enzyme at 95°C for five minutes.

The cDNA synthesis of miRNA was done using the miScript Reverse Transcription Kit (Qiagen, Germany) according to the manufacturer's recommendations. The miRNA underwent reverse transcription at 37°C for 60 minutes followed by five minutes at 95°C. Samples were stored at -20°C until further use.

4.2.4 Semi-quantitative PCR

Before analyzing the relative amount of mRNA by quantitative real-time PCR it was necessary to determine if the cDNA concentration is equal throughout the different

samples. Therefore, the cDNA amount of the house keeping gene ribosomal protein S9 (RPS9) was analyzed through semi-quantitative PCR. The PCR reaction mix was used as described in Table 8 using RPS9 primer pair (see Table 2). The PCR cycler settings are depicted in Table 10. Samples were diluted to ensure the same amount of cDNA within every sample.

Table 10: PCR cycler program for RPS9

		30 circles			
Temperature [°C]	94	94	58	72	72
Time [mm:ss]	10:00	00:45	00:58	01:00	10:00

4.2.5 Quantitative real-time PCR

To determine the relative amount of EGR-1 and PTEN mRNA quantitative real-time PCR (qRT-PCR) was performed using the Power Maxima SYBR Green qPCR Master Mix (Fermentas, Germany) and appropriate primers (see Table 2) according to the manufacturer's recommendations with a 7500 Fast Real-Time PCR system (ABI, Germany). The composition of the master mix is shown in Table 11.

Table 11: qRT-PCR master mix composition for mRNA expression analysis

Volume or concentration	Components
~ 20 ng	cDNA template
1x	Power Maxima SYBR Green qPCR Master Mix
50-900 nM	forward primer
50-900 nM	reverse primer
ad 20 µL	MilliQ H_2O

The relative expression of miR-183 and miR-96 was also analyzed by qRT-PCR using the miScript SYBR Green PCR Kit and miScript Primer Assay (both Qiagen, Germany see Table 2) according to the manufacturer's recommendation. Besides the miRNA specific primer, the system uses an unspecific primer directed against the universal tag sequence added to the 5' end of the cDNA during reverse transcription. Table 12 depicts the master mix composition.

Table 12: qRT-PCR master mix composition for miRNA expression analysis

Volume [µL]	Components
1	cDNA template
10	QuantiTect SYBR Green PCR Master Mix
2	unspecific primer
2	specific primer
ad 20	MilliQ H_2O

In both qRT-PCRs the relative mRNA or miRNA levels were calculated with included standard curves for each individual gene. Furthermore, RPS9 was used as a housekeeping gene to normalize the expression of the mRNA while RNU6B was used to normalize the expression of the miRNAs. The quotient of the mean quantity of the target gene and the housekeeping gene reflected the relative gene expression.

4.3 Generation of miR-183(mut)/-96 expressing packaging cell line GPE86

4.3.1 Cloning of miR-183(mut)/-96 sequence into pRV-IRES-eGFP

The pRV-IRES-miR-183(mut)/-96-eGFP vector derives from the pRV-IRES-eGFP vector (see 3.6). This vector was digested and linearized using the restriction enzymes Bgl II and Xho I (Fermentas, Germany) at 37°C for two hours (see Table 13). The miRNA sequence for miR-183(mut)/-96 was purchased from eurofins Genomics (Germany) and delivered as pexA2-miR-183(mut). To isolate the microRNA coding sequence, the plasmid was digested using the enzymes BamH I and Xho I (Fermentas, Germany) at 37°C for two hours (see Table 14).

Table 13: Restriction of pRV-IRES-eGFP

Volume or concentration	Components
2 µg	Plasmid DNA
1 x	Buffer Orange
2 µL	Bgl II
2 µL	Xho I
ad 50 µL	MilliQ H_2O

After digestion both plasmids were dephosphorylated to prevent subsequent self-ligation. Therefore, calf intestinal alkaline phosphatase (CIAP) and 10 x CIAP buffer (Invitrogen, Germany) were added to the digestion mix and incubated at 37°C for one hour. The reaction was terminated by adding 6 x DNA loading dye (Thermo Fisher Scientific, Germany). The DNA fragments were separated by gel electrophoresis. The linearized pRV-IRES-eGFP vector and the insert were extracted and purified using the QIAquick gel extraction kit (Qiagen, Germany) according to the manufacturer's recommendation. Afterwards the digested plasmid and the insert were ligated at 16°C overnight using T4 DNA ligase (Invitrogen, Germany).

Table 14: Restriction of pexA2-miR-183(mut)

Volume or concentration	Components
10 µg	Plasmid DNA
1 x	Buffer Red
2 µL	BamH I
2 µL	Xho I
ad 50 µL	MilliQ H_2O

The ligation mix was used to transform chemically competent *E. coli* TOP 10 (Invitrogen, Germany) according to the manufacturer's recommendation. The bacteria were seeded on LB agar plates containing 50 mg/mL ampicillin and incubated at 37°C overnight.

Different colony forming units were picked to inoculate LB medium at 37°C overnight. The plasmids were purified using the NucleoSpin Plasmid kit (Macherey-Nagel, Germany). To test the successful ligation of pRV-IRES-miR-183(mut)/-96 the plasmid was digested with the restriction enzyme Sac I (Fermentas, Germany) for one hour at 37°C. Gel electrophoresis of positive clones showed three bands (3638 bp, 1928 bp and 1534 bp) on a 1% agarose gel. To gain higher amounts of DNA for further applications, the plasmid was extracted from 400 mL bacteria culture via the NucleoBond PC 500 kit (Macherey-Nagel, Germany). The plasmid map of the pRV-IRES-miR-183(mut)/-96 vector is depicted in Figure 6.

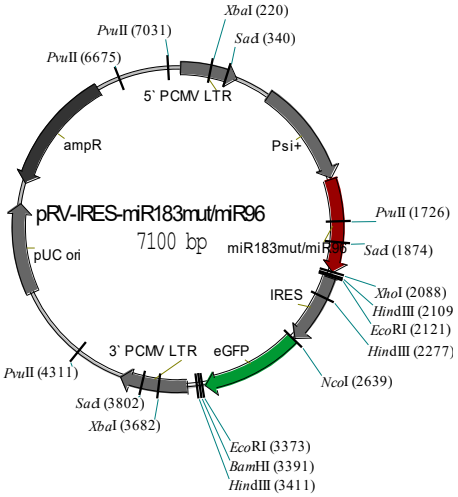

Figure 6: pRV-IRES-miR-183(mut)/-96. The vector expresses the mature miR-183 and miR-96 sequence containing six point mutations in the miR-183 seed sequence.

4.3.2 Stable transfection of GPE86 cells

The retroviral vector pRV-IRES-miR-183(mut)/-96-eGFP was used to stably transfect the ectopic packaging cell line GPE86+. This cell line consists of murine embryonic fibroblast cells (NIH-3T3) which were transfected with the Gag-, Pol- and Env-encoding sequence of the Moloney murine leukemia virus (MMLV). Retroviral particles produced from this cell line are able to infect T cells via the MMLV Env leading in this case to a stable over-expression of miRNAs.

3 x 10^5 GPE86+ cells were transfected with 5 µg pRV-IRES-miR-183(mut)/-96-eGFP, 0.5 µg pcDNA3.1(-) and 4.5 µg high molecular genomic DNA from NIH-3T3 cells using calcium phosphate transfection. After 24 hours the cells were cultivated in the presence of 800 µg/mL of the selection antibiotic Geneticin (G418) for several days or weeks. G418 inhibits the elongation step resulting in the block of protein synthesis. The presence of the Neomycin resistance gene within the co-transfected pcDNA3.1(-) vector mediates the resistance against G418. Stably transfected, GFP^+ cells were sorted with the ARIA II cell sorter (BD Bioscience, USA, see 4.1.7) and subsequently used for retrovirus generation (see 4.4.1).

4.4 Retroviral overexpression of microRNAs in primary $CD4^+CD25^-$ T lymphocytes

4.4.1 Generation of retroviral particles

Retrovirus was produced from stably transfected ectopic packaging cell line GPE86+. Cell lines were incubated in a humidified incubator at 37°C and 5% CO_2. Cells were maintained in IMDMc cell culture medium and split every two to three days. Cells were slowly frozen in cell freezing medium at -80°C and long-term stored in liquid nitrogen. Virus producing cells were cultivated in 175 cm^2 cell culture flasks in 25 mL IMDMc cell culture medium. For the production of retrovirus the cell culture supernatant was filtrated and concentrated at 10,000 x g and 4°C for four hours. After centrifugation the concentrated retrovirus-containing pellet was resuspended in 1 mL IMDMc and stored at -80°C until further use.

4.4.2 Transduction of $CD4^+CD25^-$ T lymphocytes

Stimulated $CD4^+CD25^-$ T cells were transduced with the concentrated retrovirus-containing cell culture supernatants supplemented with 20 mM Hepes and 8 µg/mL Polybrene by spinfection at 500 x g for two hours at 23°C. Subsequently 50 U/mL IL-2 were added and cells were cultivated at 37°C.

4.4.3 Luciferase reporter assay for biological activity

The luciferase reporter assay was used to determine the biological activity of the retrovirally over-expressed miRNAs. Therefore, 3 x 10^4 GPE86 cells expressing the retroviral plasmids pRV-IRES-eGFP, pRV-IRES-miR-183/-96 and pRV-IRES-miR-183(mut)/-96 were transfected with pLightSwitch_3UTR183 or pLightSwitch_3UTR96 (both Switchgear Genomics, USA) and/ or pmiR-Luc-146a (Signosis, USA) using the Lipofectamin® LTX & Plus Reagent (Invitrogen, Germany) according to the manufacturer's recommendations.

In brief, per one well of a 96 wellplate 0.5 µL Lipofectamin were mixed with 25 µL Opti-MEM cell culture medium and incubated for five minutes at room temperature. Meanwhile three different vector combinations were diluted in 25 µL Opti-MEM in the presence of 2.5 µL Plus Reagent (❶ 0.4 µg pLightSwitch_3UTR183 and 0.25 µg pmiR-Luc-146a, ❷ 0.4 µg pLightSwitch_3UTR96 and 0.25 µg pmiR-Luc-146a, ❸ 0.25 µg pmiR-Luc-146a). Afterwards the Lipofectamin solution was added to the DNA dilution and incubated for 15 minutes at room temperature. Then, the 50 µL of the Lipo-DNA-Opti-MEM solution were mixed with 50 µL cell suspension (3 x 10^4 cells), transferred

into one well of a 96 flat bottom plate and incubated at 37°C. Six hours later medium was changed to IMDMc.

The plasmids pLightSwitch_3UTR183 and pLightSwitch_3UTR96 encode a *Renilla* luciferase mRNA with a 3'UTR containing the binding sequence for miR-183 and miR-96, respectively. pmiR-Luc-146a encodes a *Firefly* luciferase mRNA containing the binding sequence for miR-146a in the 3'UTR. Since the expression of miR-146a is not altered in the transduced GPE86 cells, the *Firefly* signal was used to normalize the *Renilla* signal. 24 hours after transfection the medium was replaced by 40 µL 1 x Reporter Lysisbuffer (Promega, USA) and cells were lysed at room temperature by horizontal shaking. Then, 20 µL were transferred into one well of a white 96 well plate and analyzed for their luciferase activity in the presence of *Renilla* and *Firefly* substrate using the Orion II Luminometer (Berthold, Germany). The ratio of luminescence from the *Renilla* luciferase to the *Firefly* luciferase was calculated as Luciferase activity.

4.4.4 EGR-1 Luc-Pair™ miR luciferase assay

The Luc-Pair™ miR luciferase assay (GeneCopoeia Inc., USA) was used to analyze the potential interaction of miR-183 and miR-96 with the 3'UTR of the EGR-1 mRNA. To conduct the assay, 4 x 10^4 of GPE86 cells expressing the retroviral plasmids pRV-IRES-eGFP, pRV-IRES-miR-183/-96 and pRV-IRES-miR-183(mut)/ -96 were seeded in 1 mL IMDMc in one well of a 24 wellplate and incubated at 37°C for 24 hours. Then, 1 µg pEZXMT-01 vector encoding for a *Firefly* luciferase fused to the 3'UTR of EGR-1 or 1 µg of a control plasmid (both GeneCopoeia Inc., USA) were diluted in 100 µL serum-free IMDM and 2 µL of TurboFect™ reagent (Fermentas, Germany) was added. 20 minutes after incubation at room temperature, the TurboFect™/ DNA mixture was added drop-wise to each well. After another 24 hours of incubation at 37°C the growth medium was replaced by 250 µL of solution I and cells were incubated horizontally shaking for 45 minutes at room temperature. 80 µL of the cell suspension were transferred into one well of a white 96 wellplate (in triplets). The luciferase activity was measured in the presence of *Firefly* (5 x working solution I) and *Renilla* substrate (working solution II) using the Orion II Luminometer (Berthold, Germany). The ratio of luminescence from the *Firefly* luciferase to the *Renilla* luciferase was calculated as the luciferase activity.

4.5 Knockdown of microRNAs in primary $CD4^+CD25^-$ T lymphocytes

To analyze the impact of miRNA knockdown, $CD4^+CD25^-$ T cells were incubated with antagomirs. Antagomirs are single stranded, chemically-enhanced RNA oligonucleotides which bind and sequester the complimentary, mature miRNA strand. The antagomirs used in this study were directed against miR-183 (antagomir-183) and miR-96 (antagomir-96). The miRIDIAN™ microRNA Hairpin Inhibitor Negative Control #1 was used as an antagomir scrambled control (antagomir-Scr). All antagomirs were purchased from Dharmacon (USA, see Table 4)

The transfection of $CD4^+CD25^-$ T cells was performed as described by Haftmann et al. (Haftmann et al., 2015). Therefore, cells were either sorted by magnetic or fluorescence activated cell sorting and washed with ice cold PBS. After 10 minutes of centrifugation at 4°C cells were resuspended in serum-free RPMI cell culture medium and subsequently counted. Then, cells were seeded in 0.25 volumes of final culture volume and transfected with 1 µM antagomir. After 90 minutes of incubation at 37°C, cells were transferred to anti-CD3 coated wells and 0.75 volumes of serum-containing RPMI supplemented with anti-CD28 were added. Cells were cultured for 24 up to 72 or 96 hours at 37°C, respectively. The utilized cell amounts and medium volumes are summarized in Table 15.

Table 15: Cell amount and medium volume for miRNA knock-down experiments

Wells per plate	Cell number/ well	Serum-free medium [µL]	Serum-containing medium [µL]
96	5×10^5	50	150
12	2×10^6	500	1500

4.6 Animal experiments

4.6.1 INS-HA x Rag2-KO model for antigen specific induction of diabetes

In this mouse model HA-specific (6.5^+) $CD4^+CD25^-$ T cells were transferred intravenously (i.v.) into INS-HA x Rag2-KO mice. The HA-specific TCR of the donor T cells interacts with the HA-antigen expressed by the pancreatic beta cells of the recipient mice leading to an antigen-specific induction of diabetes.

To analyze the impact of miRNA-183 and miR-96 overexpression on the development of autoimmune diabetes, $CD4^+CD25^-$ T cells from Thy1.1 x TCR-HA mice were sorted by magnetic activated cell sorting. After 48 hours of activation with anti-CD3/ anti-CD28 cells were spinfected with retroviral vectors resulting in overexpression of miR-183/-96-eGFP, miR-183(mut)/-96-eGFP or eGFP alone. Two days after infection cells were sorted via FACS for 6.5^+GFP^+ donor cells. 10^5 cells per 150 µL PBS were immediately i.v. injected into INS-HA x Rag2-KO mice.

For miRNA knockdown experiments, $6.5^+CD4^+CD25^-$ T cells were directly sorted by FACS from Thy1.1 x TCR-HA mice. Then, the cells were transfected with 1 µM antagmir-183-Fluorescein/ antgomir-96-Fluorescein and 1 µM antagomir-Scr-Fluorescein and activated at 37°C for 72 hours. On day three the transfection rate was determined by the percentage of $Fluorescein^+$ cells using flow cytometry. As described above 10^5 cells were transferred i.v. into INS-HA x Rag2-KO mice.

The development of diabetes was monitored by blood glucose level from tail vein. Mice with a blood glucose level over 200 mg/dL were considered diabetic and subsequently sacrificed and analyzed by flow cytometry.

4.6.2 Breeding of Nrp-$1^{fl/fl}$ x CD4cre x TCR-HA x INS-HA mice

In this mouse model INS-HA x TCR-HA mice were crossed to $Nrp1^{fl/fl}$ x CD4cre mice. One third of INS-HA x TCR-HA double transgenic mice has been described to develop diabetes (Sarukhan et al., 1998). HA transgenic mice harbor $CD4^+$ T cells expressing a TCR specific for the MHC class II $H2E^d$:$HA_{110-120}$-restricting epitope of the Influenza HA. Furthermore, those mice which are transgenic for INS-HA express the HA-antigen on the pancreatic beta cells. In Nrp-$1^{fl/fl}$ x CD4cre mice, the insertion of loxP sites up and down stream of exon 2 of the *nrp-1* gene in combination with the expression of the cre recombinase under the control of the CD4 enhancer, promoter and silencer sequence leads to depletion of Nrp-1 expression in $CD4^+$ cells.

In this setup the blood glucose level of T cell-specific Nrp-1 wildtype and knockout, TCR-HA and INS-HA double transgenic mice were monitored over a period of eight weeks, starting from week five after birth. Mice with a blood glucose level over 200 mg/dL were considered diabetic and subsequently sacrificed and analyzed by flow cytometry. Mice which were double transgenic for TCR-HA and INS-HA and did not develop diabetes within 12 weeks of age were sacrificed after week 12 and handled as non-diabetic control groups.

4.6.3 Adoptive transfer of HA-specific T effector and either Nrp-1 wildtype or knockout regulatory T cells into INS-HA x Rag2-KO mice

In this mouse model $6.5^{+}CD4^{+}CD25^{-}$ effector T cells where co-transferred with $6.5^{+}CD4^{+}CD25^{+}$ regulatory T cells from either T cell-specific Nrp-1 knockout ($Nrp\text{-}1^{fl/fl}$ x CD4cre x TCR-HA) or wildtype mice into INS-HA x Rag2-KO mice.

$6.5^{+}CD4^{+}CD25^{-}$ effector T cells were sorted from Thy1.1 x TCR-HA mice splenocytes using the MACS technology. The percentage of 6.5^{+} cells was determined by surface staining via flow cytometry. $6.5^{+}CD4^{+}CD25^{+}$ regulatory T cells were sorted from either Nrp-1 wildtype or knockout $Nrp\text{-}1^{fl/fl}$ x CD4cre x TCR-HA mice by FACS. 10^{5} $6.5^{+}CD4^{+}CD25^{-}$ effector T cells and 10^{5} $6.5^{+}CD4^{+}CD25^{+}$ regulatory T cells from either T cell-specific Nrp-1 knockout or wildtype mice were transferred i.v. into the recipient INS-HA x Rag2-KO mice. The control group only received 10^{5} $6.5^{+}CD4^{+}CD25^{-}$ effector T cells.

As described above, the interaction of the HA-specific donor cells with the HA-expressing pancreatic beta cells of the recipient leads to an antigen-specific induction of diabetes. The development of diabetes was monitored by blood glucose level. Mice with a blood glucose level over 200 mg/dL were considered diabetic and subsequently sacrificed and analyzed by flow cytometry.

4.7 Statistical analysis

Statistical analyses were performed with One-Way ANOVA, Students-t test or Mann-Whitney test with significance set as levels $*p < 0.05$, $**p < 0.01$, $***p < 0.001$ and $****p < 0.0001$. Calculation was done using GraphPad Prism 7.04 software (STATCON GmbH, Germany).

5 Results

5.1 Part I

5.1.1 Enhanced microRNA-96 and microRNA-183 expression in murine CD4$^+$CD25$^-$ and CD8$^+$ T cells after activation

To address the question if miRNA-96 (miR-96) and miRNA-183 (miR-183) play a role in T cell biology the expression patterns of both miRNAs were analyzed in naïve and activated CD4$^+$CD25$^-$ and CD8$^+$ T cells by qRT-PCR. Therefore, T cells were isolated from spleen of naïve BALB/c mice by magnetic associated cell sorting and left either unstimulated (0 days) or activated with 0.75 µg/mL anti-CD3 and 1 µg/mL anti-CD28 for up to four days.

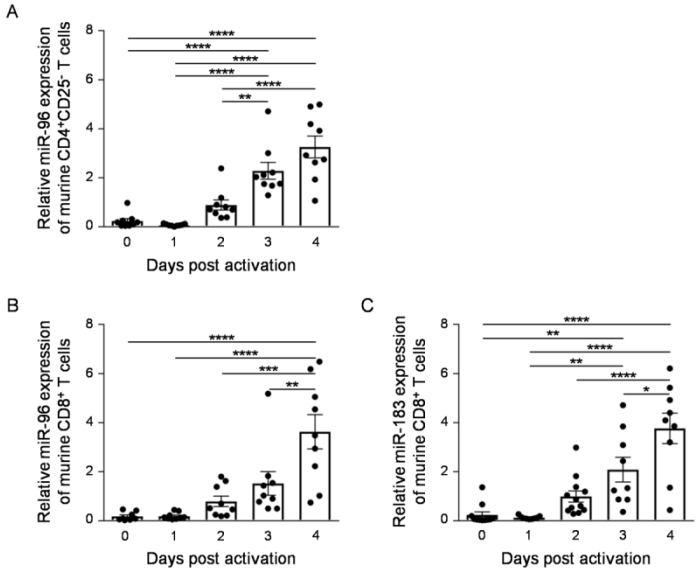

Figure 7: MiR-96 and miR-183 expression profile in naïve and activated murine CD4$^+$CD25$^-$ and CD8$^+$ T cells. (**A**) CD4$^+$CD25$^-$ and (**B**, **C**) CD8$^+$ T cells were isolated from spleen of BALB/c mice by magnetic-associated cell sorting, left un-stimulated or activated for indicated time points with anti-CD3 and anti-CD28. MiRNAs were isolated, reverse transcribed and analyzed for (**A**, **B**) miR-96, (**C**) miR-183 and RNU6B (housekeeping control) expression by qRT-PCR. Results from three independent experiments were summarized as mean ± SEM. One-way ANOVA followed by Bonferroni's post-hoc comparisons test was used for statistical analysis. *p < 0.05, **p < 0.01, ***p < 0.001, ****p < 0.0001

Upon activation miR-96 expression increased in CD4$^+$CD25$^-$ T cells and was significantly elevated with a twofold increase after three days compared to unstimulated T cells. This increase further expanded after three and four days of activation (Figure 7 A). The expression of both miRNAs was also elevated in CD8$^+$ T cells after activation. Four days post activation, miR-96 expression in CD8$^+$ T cells was fourfold higher compared to the expression of unstimulated cells. MiR-183 expression was significantly

higher after three days of activation in $CD8^+$ T cells and increased to fourfold higher extent four days post activation (Figure 7 B, C). These results suggest a role for both miRNAs in the course of T cell activation.

5.1.2 Retroviral overexpression of biologically active microRNAs

To get deeper insights into the particular role of miR-96 and miR-183 in $CD4^+$ T cell activation, pri-miR-96 and pri-miR-183 were overexpressed by retroviral gene transfer in $CD4^+CD25^-$ T cells. In this study, three different retroviral vectors were used (Figure 8 A).

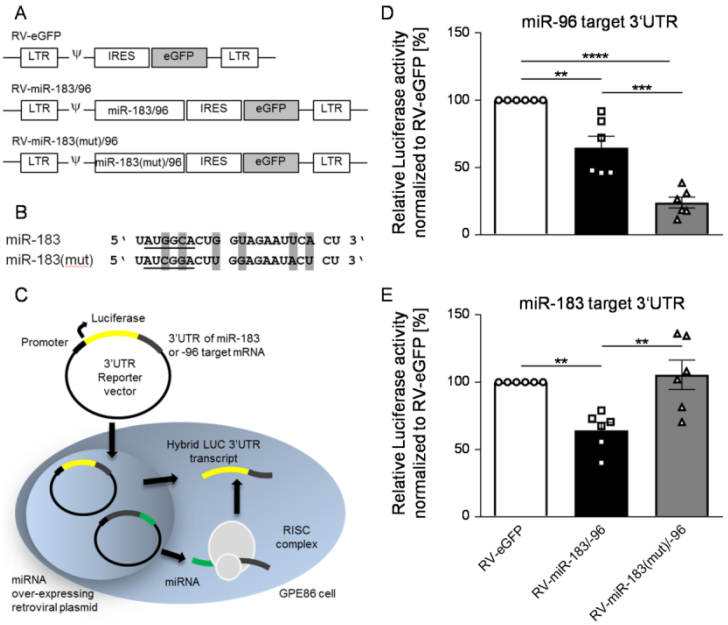

Figure 8: Overexpression of miR-96 and miR-183 by retroviral gene transfer. (**A**) Schematic drawing of retroviral vector constructs RV-eGFP, RV-miR-183/-96 and RV-miR-183(mut)/-96. The vectors consist of long terminal repeats (LTR), the packaging signal ψ, an internal ribosomal entry side (IRES) and enhanced green fluorescent protein (eGFP). RV-miR-183/-96 and RV-miR-183(mut)/-96 encoding a genomic DNA fragment compromising the mature miR-96 and miR-183 sequence with additional up- and downstream sequences. (**B**) Furthermore, RV-miR-183(mut)/-96 has six point mutations within the seed sequence of miR-183, highlighted in grey. (**C**) Schematic overview of the luciferase reporter gene assay. GPE86+ cells stably transfected with RV-eGFP, RV-miR-183/-96 or RV-miR-183(mut)/-96 were co-transfected with a plasmid encoding for a *Renilla* luciferase either fused to a 3'UTR containing a (**D**) miR-96 or (**E**) miR-183 target sequence and a control plasmid encoding a *Firefly* luciferase fused to the 3'UTR of miR-146a (not depicted). Luciferase activity was determined in lysed cell 24 hours post transfection. Data from six independent experiments done in triplicates were summarized as mean ± SEM. One-way ANOVA followed by Bonferroni's post-hoc comparisons test was used for statistical analysis. **p < 0.01, ***p < 0.001, ****p < 0.0001

The RV-IRES-eGFP (RV-eGFP) vector encodes a green fluorescent protein (GFP) reporter gene under the control of an internal ribosomal entry site (IRES) and was used as an empty vector control. Furthermore, it represents the backbone of the two other plasmids. The vector RV-miR-183/-96 has a 671 bp genomic DNA fragment insertion encoding the pri-mature miR-96 and miR-183 sequence. The third retroviral vector also

encodes the pri-mature miR-96 and miR-183 sequence but with six point mutations in the miR-183 seed sequence (Figure 8 B, highlighted in grey). To verify that both miRNAs were processed correctly and biologically active, a luciferase reporter gene assay was conducted (Figure 8 C). GPE86+ cells stably transfected with one of each retroviral vector were co-transfected with a plasmid encoding for the *Renilla* luciferase. This luciferase was either fused to a 3'UTR containing a miR-96 or miR-183 target sequence. In addition, cells were also transfected with a control plasmid encoding a *Firefly* luciferase fused to the 3'UTR of miR-146a. The expression of retroviral vectors RV-miR-183/-96 and RV-miR-183(mut)/-96 led to a significant reduction of the luciferase activity in the presence of the plasmid encoding the luciferase fused to the miR-96 target 3'UTR (Figure 8 D). The second luciferase assay with the plasmid encoding the luciferase fused to the miR-183 target 3'UTR, only co-transfection of the miR-183/-96 encoding retroviral vector resulted in significantly reduced luciferase activity (Figure 8 E). These data indicate that miR-96 and miR-183 encoded by RV-miR-183/-96 and miR-96 encoded by RV-miR-183(mut)/-96 were able to interfere with the luciferase expression and are thereby correctly processed from the constructs. Furthermore, it shows that the inserted point mutations in the seed sequence of miR-183 impaired the activity of this miRNA.

5.1.3 Increased microRNA expression in murine $CD4^+CD25^-$ T cells after retroviral transduction

In the next step, activated $CD4^+CD25^-$ T cells were transduced with the three different retroviral vectors.

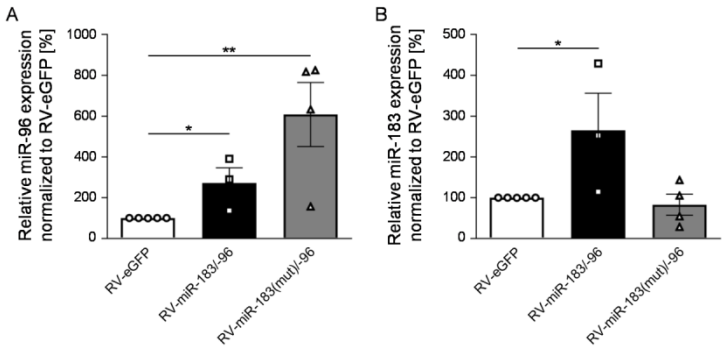

Figure 9: MiR-96 and miR-183 expression profile in retroviral transduced $CD4^+CD25^-$ T cells. (**A**) miR-96 and (**B**) miR-183 expression were analyzed in $CD4^{+-}eGFP^+$ sorted miR-183/-96 (RV-miR-183/-96), miR-183(mut)/-96 (RV-miR-183(mut)/-96) or control vector (RV-eGFP) transduced $CD4^+CD25^-$ T cells 48 hours after transduction. MiRNAs were isolated, reverse transcribed and analyzed by qRT-PCR. Results from three to five independent experiments were summarized as mean ± SEM. Student`s t-test was used for statistical analysis. *$p < 0.05$, **$p < 0.01$

The transduction of $CD4^+CD25^-$ T cells with the RV-miR-183/-96 vector resulted in a 2.7-fold higher miR-96 and a 2.6-fold higher miR-183 expression compared to T cells transduced with the control vector (RV-eGFP) 48 hours after transduction (Figure 9). Activated $CD4^+CD25^-$ T cells transduced with the retroviral vector RV-miR-183(mut)/-96 exhibited a six fold higher miR-96 expression while the expression of miR-183 was not altered in comparison to control vector transduced T cells (Figure 9).

5.1.4 Elevated proliferation of microRNA-96 and -183 as well as microRNA-96 overexpressing $CD4^+CD25^-$ T cells *in vitro*

Since both miRNAs were upregulated in $CD4^+CD25^-$ T cells during the course of activation, the influence of miRNA overexpression on the proliferative capacity was analyzed.

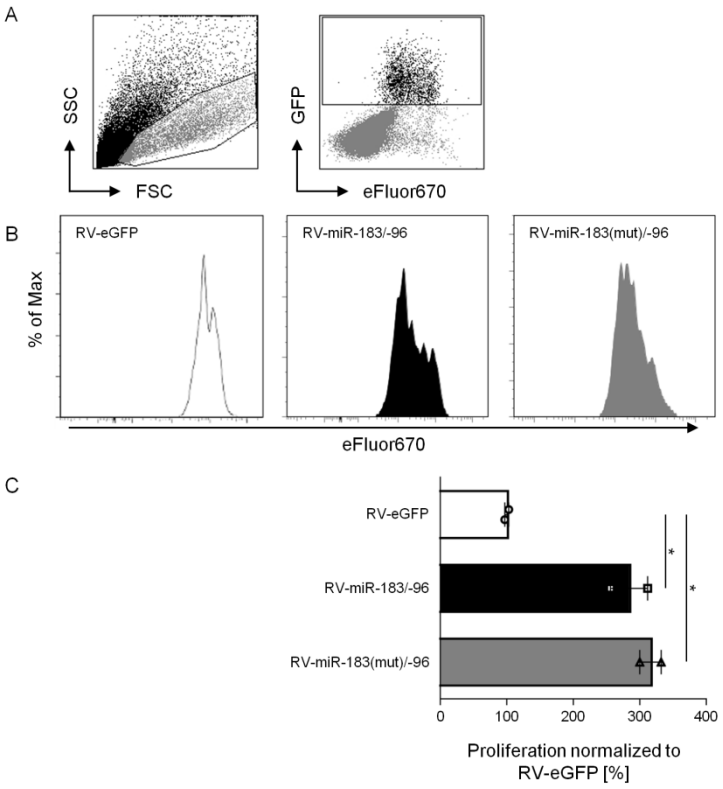

Figure 10: Proliferative activity of miR-96 and miR-183 overexpressing $CD4^+eGFP^+$ T cells. $CD4^+CD25^-$ T cells were transduced with miR-183/-96 (RV-miR-183/-96), miR-183(mut)/-96 (RV-miR-183(mut)/-96) or control vector (RV-eGFP). 96 hours after transduction $CD4^+eGFP^+$ T cells were isolated by FACS. Sorted miRNA and control vector overexpressing cells were labeled with cell proliferation dye eFlour®670 and stimulated with anti-CD3 in the presence of $CD4^+$-depleted irradiated splenocytes for 72 hours. Proliferation was assessed as loss of eFluor®670 dye by flow cytometry. (**A**) $GFP^+eFluor670^+$ cells were gated among lymphocytes. (**B**) Representative histogram of $eFlour670^+$ cells from all three differently transduced samples. (**C**) Proliferation of RV-miR-183/-96 and RV-miR-183(mut)/-96-transduced T cells was normalized to RV-eGFP-transduced cells (set to 100%). Data from two independent experiments done in triplicates are summarized as mean ± SEM. One-way ANOVA followed by Bonferroni's post-hoc comparisons test was used for statistical analysis. *$p < 0.05$

eGFP$^+$ cells were isolated from retrovirally transduced CD4$^+$CD25$^-$ T cells by FACS 96 hours post transduction and labeled with the cell proliferation dye eFluor®670. Afterwards, cells were stimulated with 1 µg/mL anti-CD3 in the presence of CD4$^+$-depleted irradiated splenocytes. 72 hours later, the proliferation was assessed as loss of eFluor®670 dye by flow cytometry (Figure 10 A, B). RV-miR-183/-96 and RV-miR-183(mut)/-96-transduced CD4$^+$CD25$^-$ T cells showed a significant increase in proliferative activity, which was threefold higher than control vector-transduced cells (Figure 10 C). Interestingly, not only the combined overexpression of miR-96 and miR-183 led to an elevated proliferation but also the overexpression of miR-96 alone increased the proliferative capacity.

5.1.5 MicroRNA-96 and microRNA-183 transduced CD4$^+$CD25$^-$ T cells accelerate the development of autoimmune diabetes *in vivo*

Next, the INS-HA x Rag2-KO mouse model was used, to investigate if the overexpression of miR-96 and miR-183 in effector T cells modulates their activity also in a more complex *in vivo* situation.

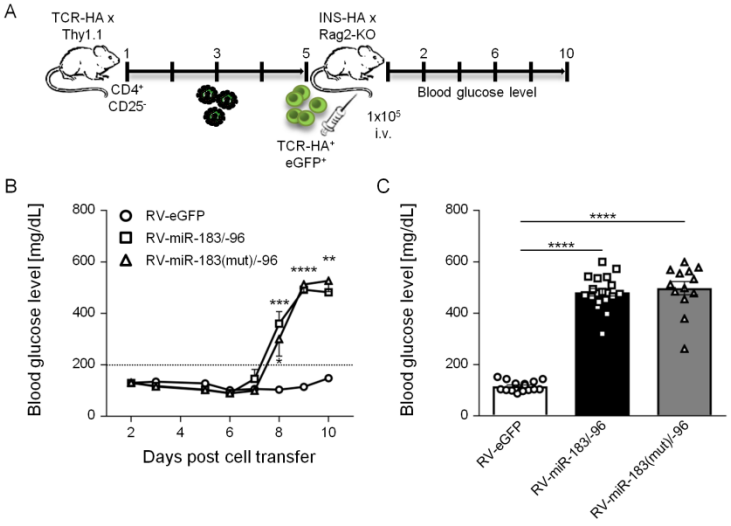

Figure 11: Adoptive transfer of miR-96, miR-183 and control vector overexpressing HA-specific T cells to INS-HA x Rag2-KO mice. (**A**) CD4$^+$CD25$^-$ T cells from TCR-HA x Thy1.1 mice were retrovirally transduced with RV-miR-183/-96, RV-miR-183(mut)/-96 or RV-eGFP. 48 hours after transduction 6.5$^+$eGFP$^+$ T cells were isolated by FACS and adoptively transferred to INS-HA x Rag2-KO mice. (**B**) The development of diabetes was monitored by blood glucose level from tail vein at indicated time points. Mice with a blood glucose level > 200 mg/dL were considered as diabetic. (**C**) Endpoint blood glucose level. Data from n = 13 – 19 mice analyzed in five independent experiments are summarized as mean ± SEM. Each data point represents one animal. One-way ANOVA followed by Bonferroni's post-hoc comparisons test was used for statistical analysis. **p < 0.01, ***p < 0.001, ****p < 0.0001

For this purpose, retrovirally transduced (eGFP$^+$) HA-specific (6.5$^+$) CD4$^+$CD25$^-$ T cells from TCR-HA x Thy1.1 mice were adoptively transferred into INS-HA x Rag2-KO mice.

The interaction of HA-specific donor T cells with the HA model antigen expressed by the pancreatic beta cell of the recipient mice led to diabetes upon transfer measurable by increasing blood glucose level (Figure 11 A). Those mice that received miR-96 and miR-183 as well as miR-96 overexpressing HA-specific T cells developed diabetes much faster than mice that received control vector-transduced T cells. While the transfer of miRNA overexpressing HA-specific T cell led to an onset of diabetes (blood glucose level ≥ 200 mg/dL) eight days post adoptive transfer, transfer of the control vector-transduced HA-specific T cells did not cause diabetes by day ten (Figure 11 B).

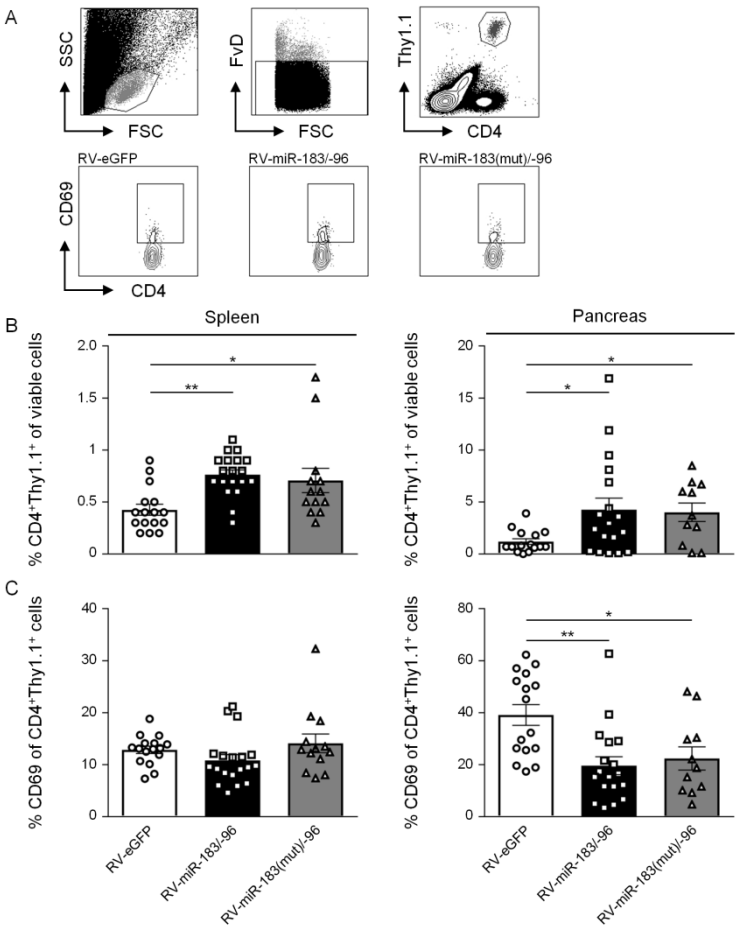

Figure 12: Analysis of transferred miR-96, miR-183 and control vector overexpressing HA-specific T cells in INS-HA x Rag2-KO mice. After the adoptive transfer of retrovirally transduced HA-specific T cells in INS-HA x Rag2-KO mice, blood glucose level was monitored up to 10 days. Diabetic mice and non-diabetic controls were sacrificed and cells from spleen and pancreas of INS-HA x Rag2-KO mice were analyzed by flow cytometry. (**A**) $Thy1.1^+CD4^+$ cells were gated from living (fixable viability dye, FvD^-) lymphocytes. CD69 expression was analyzed on $Thy1.1^+CD4^+$ cells. (**B**) Percentage of transferred $CD4^+Thy1.1^+$ T cells and (**C**) frequency of CD69 expressing $CD4^+Thy1.1^+$ T cells from spleen and pancreas of INS-HA x Rag2-KO mice analyzed by flow cytometry. Data from n = 13 – 19 mice analyzed in five independent experiments are summarized as mean ± SEM. Each data point represents one animal. One-way ANOVA followed by Bonferroni's post-hoc comparisons test was used for statistical analysis. *p < 0.05, **p < 0.01

Furthermore, glycaemia was significantly increased in those mice that received miRNA overexpressing T cells compared to mice that were transferred with control vector-

transduced T cells (Figure 11 C). Within the spleen and pancreas of the diabetic mice, significant elevated frequencies of $CD4^+Thy1.1^+$ donor cells were detected in comparison to the healthy controls (Figure 12 B). In addition, $CD4^+Thy1.1^+$ cells within the pancreas expressed significant lower levels of the surface protein CD69 in INS-HA x Rag2-KO mice transferred with miRNA overexpressing HA-specific T cells (Figure 12 C). These results demonstrate that overexpression of miR-96 and miR-183 as well as miR-96 alone increases the proliferation of $CD4^+$ T cells not only *in vitro* but also *in vivo*.

5.1.6 EGR-1 and PTEN expression negatively correlate with microRNA expression of activated $CD4^+CD25^-$ T cells

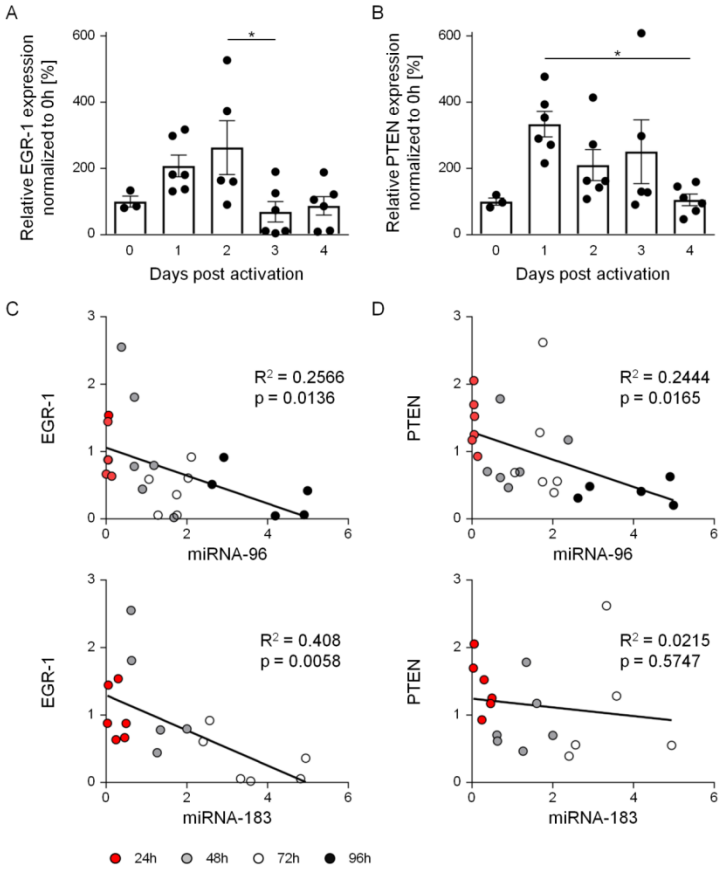

Figure 13: EGR-1 and PTEN expression profile in naïve and activated $CD4^+CD25^-$ T cells and correlation with miRNA expression. $CD4^+CD25^-$ T cells were isolated from BALB/c mice by magnetic-associated cell sorting, left unstimulated or activated for indicated time points in the presence of anti-CD3 and anti-CD28. RNA were isolated, reverse transcribed and analyzed for the expression of (**A**) EGR-1 (**B**) PTEN and RPS9 as housekeeping control by qRT-PCR. Results from two independent experiments with n = 3 - 6 were summarized as mean ± SEM. One-way ANOVA followed by Bonferroni's post-hoc comparisons test was used for statistical analysis. (**C**) Pearson correlation with linear regression for relative miR-96 and miR-183 and EGR-1 expression in $CD4^+CD25^-$ T cells activated for 72 and 96 hours (**D**) Pearson correlation with linear regression for relative miR-96 and miR-183 and PTEN expression in $CD4^+CD25^-$ T cells stimulated for 72 and 96 hours. *p < 0.05, **p < 0.01

To get further insights into the intracellular signaling leading to increased proliferation of miR-96 and miR-183 overexpressing $CD4^+CD25^-$ T cells, the expression profile of the transcription factor EGR-1 and the lipid phosphatase PTEN was analyzed in activated $CD4^+CD25^-$ T cells by qRT-PCR (Figure 13 A, B). EGR-1 was already described as a target molecule for miR-183 in tumor cells (Sarver et al., 2010). The transcription factor is able to induce the expression of PTEN (Sukhatme et al., 1988), which is a major negative regulator of the PI3K/Akt pathway (Wu et al., 1998). This pathway is involved in various cellular processes including cell proliferation (Tsugawa et al., 2003). qRT-PCR data revealed an increased relative EGR-1 expression upon two days after initial activation of $CD4^+CD25^-$ T cells followed by a significant decrease three days post activation (Figure 13 A). The relative PTEN expression of activated $CD4^+CD25^-$ T cells was upregulated over three days of activation. At day four post activation the relative PTEN expression decreased significantly compared to day one after initial activation (Figure 13 B). To analyze if there is a direct link between the EGR-1 and PTEN expression and the expression of miR-96 and miR-183, a correlation analysis was performed. The relative EGR-1 and PTEN expression was correlated with the relative expression of miR-96 (see Figure 7 A) and miR-183 (unpublished data) in activated $CD4^+CD25^-$ T cells (see Figure 13 A, B). The analysis revealed a significant negative correlation between the expression of both miRNAs and the expression of EGR-1 (Figure 13 C). Furthermore, there was also a significant negative correlation for the miR-96 and the PTEN expression but not for the miR-183 and PTEN expression (Figure 13 D). This data suggests an interaction of miR-183 and also of miR-96 with the transcription factor EGR-1 in $CD4^+$ effector T cells resulting in PTEN regulation.

5.1.7 MicroRNA-96 and microRNA-183 target EGR-1 mRNA resulting in decreased EGR-1 und PTEN expression and increased Akt phosphorylation

Based on the miRNA and EGR-1 expression analysis (Figure 13), the interaction between both miRNAs and the transcription factor EGR-1 was analyzed in more detail using a luciferase reporter gene assay. Therefore, GPE86+ cells stably transfected with one of each retroviral vector were co-transfected with a plasmid encoding a *Firefly* luciferase fused to the 3'UTR of EGR-1. 24 hours post transfection the luciferase activity was analyzed. Cells expressing the miRNA overexpressing vectors RV-miR-183/-96 and RV-miR-183(mut)/-96 in combination with the luciferase fused to the EGR-1 3'UTR showed a significant decrease in luciferase activity compared to control vector (RV-eGFP)-transduced cells (Figure 14 A). This result identifies the 3'UTR of EGR-1 as direct target of miR-183 in T cells as already described for tumor cells in the literature

(Sarver et al., 2010). Moreover, the data also demonstrates an interaction between miR-96 seed sequence and the EGR-1 3'UTR, due to the decreased luciferase activity in those cells overexpressing the mutated miR-183 and the mature miR-96. To investigate the impact of miR-96 and miR-183 overexpression on EGR-1 expression in $CD4^+CD25^-$ T cells, transduced cells were further analyzed by flow cytometry (Figure 14 B).

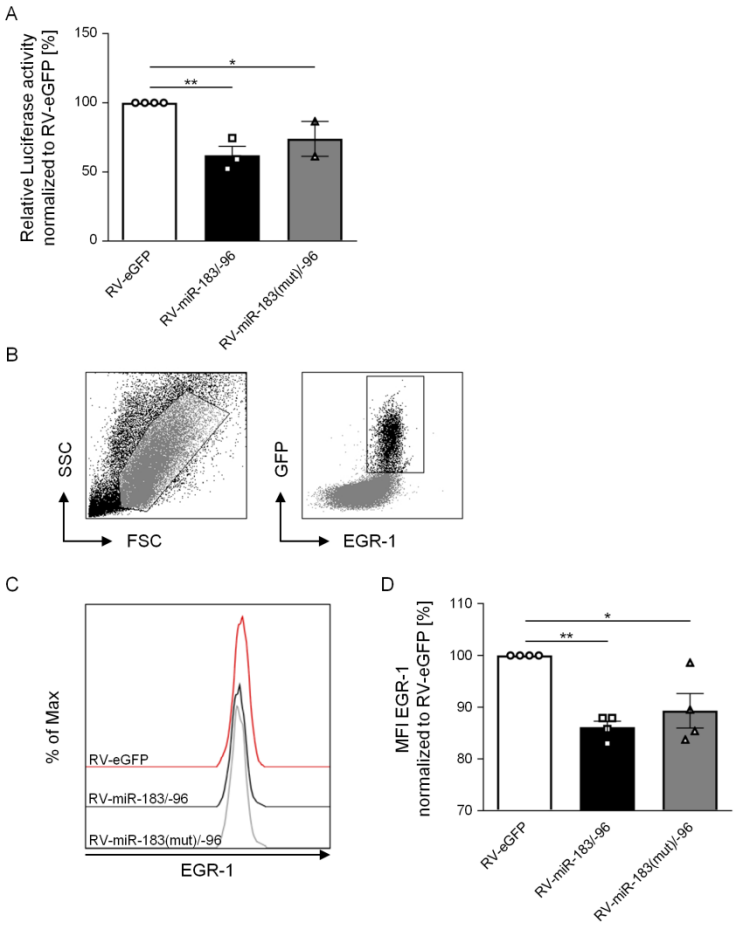

Figure 14: MiR-96 and miR-183 targets EGR-1. (**A**) Luciferase reporter gene assay. GPE86+ cells were transfected with RV-eGFP, RV-miR-183/-96 or RV-miR-183(mut)/-96 and a plasmid encoding a *Firefly* luciferase fused to the 3'UTR of EGR-1. Luciferase activity was determined in lysed cell 24 hours post transfection. EGR-1 expression of miRNA and control vector-transduced $CD4^+CD25^-$ T cells were analyzed by flow cytometry 48 hours post transduction. Data from four individual experiments (n = 2 – 4) done in triplicates were summarized as mean ± SEM. One-way ANOVA followed by Bonferroni's post-hoc comparisons test was used for statistical analysis. *$p < 0.05$, **$p < 0.01$ (**B**) $EGR\text{-}1^+GFP^+$ cells were gated from lymphocytes. (**C**) Representative overlayed histograms, showing EGR-1 expression of gated GFP^+ cells from all three differently transduced samples. (**D**) Mean fluorescent intensity (MFI) of control vector-transduced cells was set to 100 percent and MFI of miRNA-transduced cells (GFP^+) was normalized to RV-eGFP. Data from four individual experiments were summarized as mean ± SEM. One-way ANOVA followed by Bonferroni's post-hoc comparisons test was used for statistical analysis. *$p < 0.05$, **$p < 0.01$

Two days after retroviral transduction $CD4^+CD25^-$ T cells were stained intracellularly for EGR-1 protein. As depicted in Figure 14 C, the frequency of $EGR\text{-}1^+GFP^+$ cells was not altered between the differently transduced cells. However, the mean fluorescence

intensity (MFI) of EGR-1 expression was significant reduced in those $CD4^+CD25^-$ T cells transduced with the RV-miR-183/-96 or the RV-miR-183(mut)/-96 vector compared to control vector-transduced cells (Figure 14 D). Taken together, these results show that the overexpression of both miRNAs as well as miR-96 alone in $CD4^+$ effector T cells results in a decreased expression of the transcription factor EGR-1. To further investigate, if overexpression of miR-183 and miR-96 that decreases EGR-1 expression results in an altered PTEN expression, retroviral-transduced $CD4^+CD25^-$ T cells were also analyzed for PTEN expression by flow cytometry (Figure 15 A). Similar to the EGR-1 expression, the frequency of $PTEN^+GFP^+$ cells showed no differences comparing control vector-transduced with miRNA overexpressing $CD4^+CD25^-$ T cells (Figure 15 B). However, cells that overexpressed miR-96 and miR-183 as well as cells that only overexpressed miR-96 exhibited a significant lower MFI of PTEN compared to control vector-transduced cells (Figure 15 C). The decreased PTEN expression in miR-96 and miR-183 overexpressing cells suggests that miR-96 and miR-183 as well as miR-96 alone influencing the EGR-1-PTEN-PI3K/Akt axis and thereby alter cell proliferation.

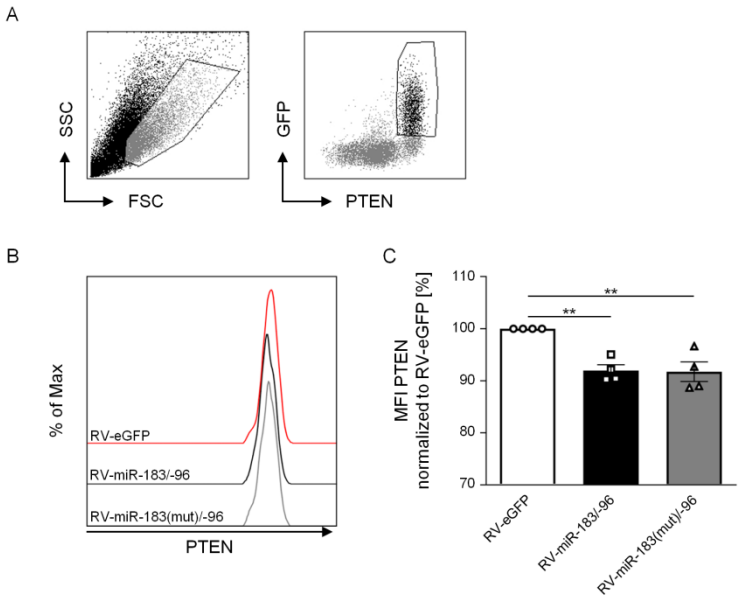

Figure 15: MiR-96 and miR-183 overexpression decreases PTEN expression. PTEN expression of miRNA and control vector transduced $CD4^+CD25^-$ T cells was analyzed by flow cytometry 48 hours post transduction. (**A**) $PTEN^+GFP^+$ cells were gated from lymphocytes. (**C**) Representative overlayed histograms, showing PTEN expression of gated GFP^+ cells from all three differently transduced samples. (**C**) Mean fluorescent intensity (MFI) of control vector-transduced cells was set to 100 percent and MFI of miRNA-transduced cells (GFP^+) was normalized to RV-eGFP. Data from four individual experiments were summarized as mean ± SEM. One-way ANOVA followed by Bonferroni's post-hoc comparisons test was used for statistical analysis. **$p < 0.01$

As a major negative regulator for the PI3K/Akt pathway, PTEN competes with PI3K for phosphorylation which by itself phosphorylates and thereby activates the

serine/threonine-specific protein kinase Akt (Myers et al., 1998). To analyze whether miR-96 and miR-183 affect $CD4^+$ effector T cell proliferation by the EGR-1-PTEN-PI3K/Akt axis, Akt expression and phosphorylation was determined in retroviral-transduced $CD4^+CD25^-$ T cells by flow cytometry. Two days after transduction with RV-eGFP, RV-miR-183/-96 or RV-miR-183(mut)/-96, $CD4^+CD25^-$ T cell were re-stimulated with 1 µg/mL anti-CD3 for 30 minutes. Thereafter, Akt expression and the two phosphorylation sites pAkt (Ser473) and pAkt (Thr308) were analyzed by intracellular flow cytometry (Figure 16 A). Cells that overexpressed the miRNAs showed the same frequencies of Akt^+GFP^+ as well as pAkt $(Ser473)^+GFP^+$ and pAkt $(Thr308)^+GFP^+$ cells compared to control vector-transduced cells (Figure 16 B). Comparing the MFI of Akt, pAkt (Ser473) and pAkt (Thr308) between all three cell populations revealed a significantly increased phosphorylation at position Ser473 of RV-miR-183/-96 and RV-miR-183(mut)/-96-transduced cells (Figure 16 C).

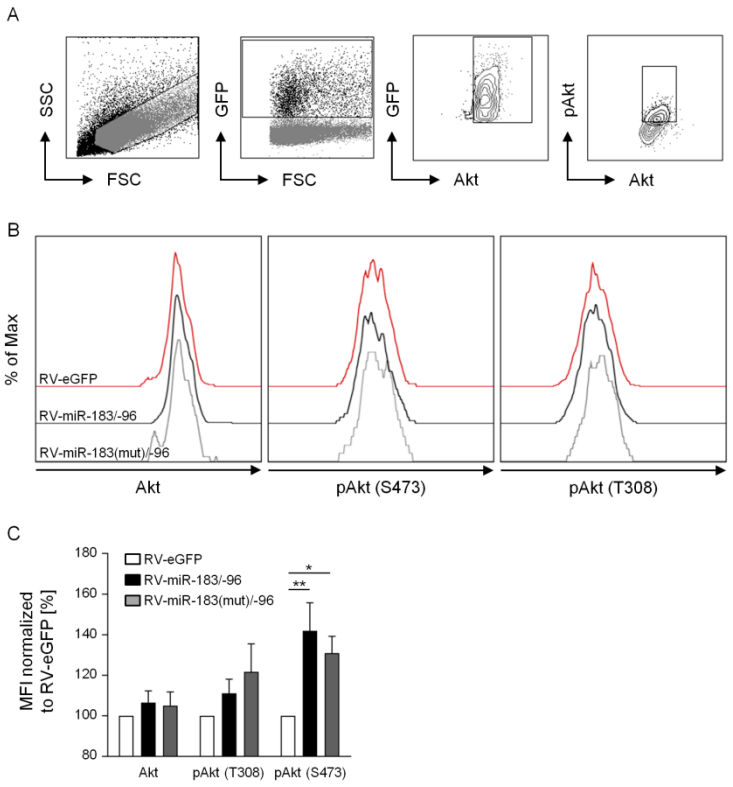

Figure 16: MiR-96 and miR-183 over-expression affects PI3K/Akt pathway. Akt expression and phosphorylation of miRNA and control vector-transduced $CD4^+CD25^-$ T cells were analyzed by flow cytometry 48 hours post transduction and after 30 minutes of re-stimulation with anti-CD3. (**A**) Akt^+GFP^+ and $phosphoAkt^+GFP^+$ cells were gated from lymphocytes (**B**) Representative overlayed histograms, showing Akt^+, pAkt $(S473)^+$ and pAkt $(T308)^+$ expression of gated GFP^+ cells from all three differently transduced samples. (**C**) Mean fluorescent intensity (MFI) of control vector-transduced cells was set to 100 percent and MFI of miRNA-transduced cells (GFP^+) was normalized to RV-eGFP. Data from eight individual experiments were summarized as mean ± SEM. One-way ANOVA followed by Bonferroni's post-hoc comparisons test was used for statistical analysis. *$p < 0.05$, **$p < 0.01$

Taken together, results obtained from analysis of miR-96 and miR-183 overexpressing cells strongly suggest that both miRNAs interfere with EGR-1 expression (Figure 14) and the PI3K/Akt pathway (Figure 16) resulting in increased proliferative activity (Figure 10). Furthermore, the data reveal a more dominant role of miR-96 since $CD4^+CD25^-$ T cells transduced with the retroviral vector RV-miR-183(mut)/-96 display the same cellular characteristics as RV-miR-183/-96-transduced cells. To get further details on the cellular function of each individual miRNA, miRNA knockdown experiments in $CD4^+CD25^-$ T cells were performed.

5.1.8 Specific knockdown of microRNA-96 and microRNA-183 in antagomir-transduced $CD4^+CD25^-$ T cells

MiRNA knockdown experiments were performed using antagomirs directed against miR-96 and miR-183.

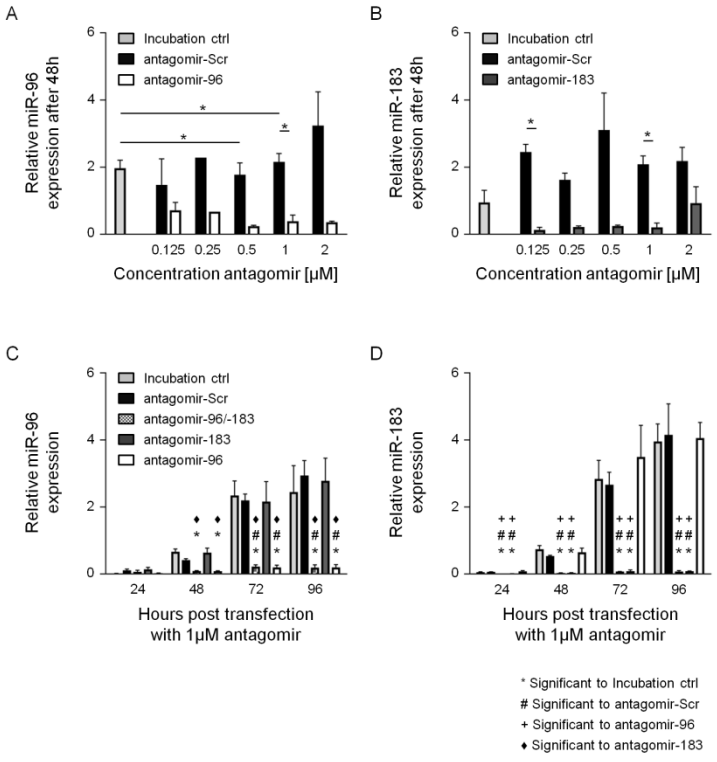

Figure 17: MiRNA expression profile of antagomir-96 and antagomir-183-transduced $CD4^+CD25^-$ T cells upon activation. $CD4^+CD25^-$ T cells were isolated from naïve BALB/c mice by magnetic-associated cell sorting and incubated in serum-free medium supplemented with antagomir-96, antagomir-183, antagomir-Scr or without antagomir (Incubation ctrl) for 90 minutes. Afterwards, cells were activated in the presence of anti-CD3 and anti-CD28. (**A, B**) Cells were treated with concentrations of 0.125 to 2 µM of antagomir-96, antagomir-183 and antagomir-Scr and activated for 48 hours. (**C, D**) Cells were treated with a concentration of 1 µM of antagomir-96, antagomir-183 and antagomir-Scr and activated for indicated time points in the presence of anti-CD3 and anti-CD28. MiRNAs were isolated, reverse transcribed and analyzed for (**A, C**) miR-96, (**B, D**) miR-183 and RNU6B (housekeeping control) expression by qRT-PCR. Data from two independent experiments are summarized as mean ± SEM. One-way ANOVA followed by Bonferroni's post-hoc comparisons test was used for statistical analysis. *p < 0.05, **p < 0.01, ***p < 0.001

Antagomirs are single stranded, chemically-enhanced RNA oligonucleotides designed to bind and sequester the complimentary, mature miRNA strand (Krutzfeldt et al., 2005). The antagomirs used in this study were purchased from Dharmacon, USA. MiRNA-specific antagomirs were used alone and in combination (antagomir-96/-183). Next to the miR-96 and miR-183-specific antagomir a scrambled antagomir (antagomir-Scr) was used as an internal control. Furthermore, untreated cells were always analyzed as incubation control to exclude a transfection dependent effect. $CD4^+CD25^-$ T cells were transfected with the different oligonucleotides as described by Haftmann et al. (Haftmann et al., 2015). First, it was necessary to determine an adequate antagomir concentration for effective miRNA knockdown in $CD4^+CD25^-$ T cells (Figure 17 A, B). Therefore, $CD4^+CD25^-$ T cells were treated with different antagomir concentrations ranging from 0.125 to 2 µM of antagomir-96, antagomir-183, antagomir-Scr or without antagomir (incubation ctrl) in serum-free medium for 90 minutes. 48 hours after activation in the presence of 0.75 µg/mL anti-CD3 and 1 µg/mL anti-CD28 cells were harvested and miRNA expression was determined by qRT-PCR. A concentration of 1 µM turned out as optimal concentration for miR-96 and miR-183 knockdown. At this concentration miR-96 and miR-183 expression was significantly reduced compared to antagomir-Scr and untreated cells (Figure 17 A, B). To determine the specificity of both antagomirs and how long the miRNA knockdown persists after antagomir transfection, time kinetic experiments were performed. 1 µM antagomir-treated cells were activated for up to four days and miR-96 and miR-183 expression levels were analyzed via qRT-PCR every day. The treatment with antagomir-96 and the combination of antagomir-96/-183 led to a significant decreased miR-96 expression in $CD4^+CD25^-$ T cells after 48 hours. This miRNA knockdown lasted for up to 96 hours post activation (Figure 17 C). 24 hours after activation, miR-183 expression was already significant lower in antagomir-183 and antagomir-96/-183-treated cells compared to antagomir-96, antgomir-Scr-treated or untreated cells. Even 96 hours post activation, the miR-183 expression was still significantly decreased in antagomir-183-treated $CD4^+CD25^-$ T cells (Figure 17 D, for detailed statistics see supplemental Table 16 and Table 17). These results show that antagomirs are a suitable tool to efficiently knockdown specific miRNAs in activated $CD4^+$ effector T cells.

5.1.9 Decreased proliferation of microRNA-96 and microRNA-183 antagomir-treated $CD4^+CD25^-$ T cells *in vitro*

Antagomir-treated $CD4^+CD25^-$ T cells were analyzed for their proliferative capacity. Here, $CD4^+CD25^-$ T cells were labeled with the cell proliferation dye eFluor®670 72 hours after antagomir treatment and initial activation. The labeled cells were re-

stimulated with 1 µg/mL anti-CD3 in the presence of $CD4^+$-depleted irradiated splenocytes for another 72 hours. The proliferation was assessed as loss of eFluor®670 dye by flow cytometry. Compared to the antagomir untreated incubation control, miR-96 and miR-183 knockdown cells displayed a significantly decreased proliferation. Nevertheless, there seemed to be no synergistic effect by the knockdown of both miRNAs on proliferation (Figure 18). MiR-96 and miR-183 knockdown shows an opposing effect on proliferation of T cells compared to miRNA overexpressing experiments (Figure 10) and strengthen the assumption that both miRNAs play an important role in $CD4^+$ T cell activation.

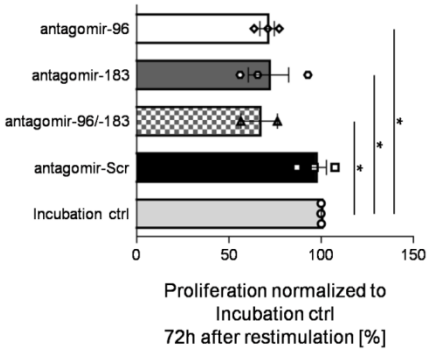

Figure 18: Proliferative capacity of antagomir-96 and antagomir-183-transfected $CD4^+CD25^-$ T cells. $CD4^+CD25^-$ T cells were isolated from naïve BALB/c mice by magnetic-associated cell sorting and incubated in serum-free medium supplemented with 1 µM antagomir-96, antagomir-183, antagomir-Scr or without antagomir (incubation ctrl) for 90 minutes. Afterwards, cells were activated in the presence of anti-CD3 and anti-CD28 for 72 hours. Antagomir-transduced cells were labeled with cell proliferation dye eFlour®670 and stimulated with anti-CD3 in the presence of $CD4^+$-depleted irradiated splenocytes for another 72 hours. Proliferation was assessed as loss of eFluor®670 dye by flow cytometry. Proliferation of antagomir-transduced T cells was normalized to Incubation ctrl cells (set as 100%). Data from three independent experiments are summarized as mean ± SEM. One-way ANOVA followed by Dunnett's post-hoc comparisons test was used for statistical analysis. *$p < 0.05$

5.1.10 Knockdown of microRNA-96 and microRNA-183 results in elevated EGR-1 and PTEN expression

To evaluate how the EGR-1 and PTEN expression was influenced by the miRNA knockdown, $CD4^+CD25^-$ T cells were treated with 1 µM antagomir and analyzed 72 hours after initial activation by flow cytometry. The normalized EGR-1 MFI was not altered between the incubation control and the antagomir-Scr-treated T cells. Furthermore, the single treatment with either the miR-96 or miR-183 specific antagomir did not alter the EGR-1 expression compared to the incubation control. Interestingly, the combined transfection of antagomir-96 and antagomir-183 led to a significant increase of EGR-1 expression in activated $CD4^+CD25^-$ T cells (Figure 19 A). Downstream of the transcription factor EGR-1, PTEN was not differentially expressed in untreated cells compared to antagomir-Scr- and antagomir-183-treated cells. Again

the combination of antagomir-96 and -183 resulted in a significant increased expression of PTEN compared to the incubation control. Furthermore, PTEN expression was also significantly increased in miR-96 knockdown T cells (Figure 19 B). Results from miRNA knockdown experiments confirm EGR-1 as target protein of miR-96 and miR-183 *in vitro*. Moreover, it underlines the mode of action of both miRNAs influencing the EGR-1-PTEN signaling pathway.

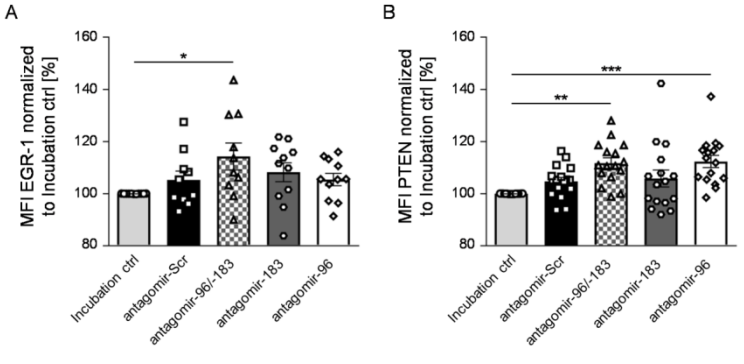

Figure 19: EGR-1 and PTEN expression in antagomir-96 and antagomir-183-transfected CD4$^+$CD25$^-$ T cells. CD4$^+$CD25$^-$ T cells were isolated form naïve BALB/c mice by magnetic-associated cell sorting and incubated in serum-free medium supplemented with 1 µM antagomir-96, antagomir-183, antagomir-Scr or without antagomir (Incubation ctrl) for 90 minutes. Afterwards, cells were activated in the presence of anti-CD3 and anti-CD28 for 72 hours. (**A**) EGR-1 and (**B**) PTEN expression of antagomir-treated cells was analyzed by flow cytometry. The expression of EGR-1 and PTEN of untreated cells (Incubation ctrl) was set to 100 percent and used to normalize the mean fluorescent intensity (MFI) of antagomir-treated cells. Results from five (**A**) and six (**B**) independent experiments are summarized as mean ± SEM. One-way ANOVA followed by Bonferroni's post-hoc comparisons test was used for statistical analysis. *$p < 0.05$, **$p < 0.01$, ***$p < 0.001$

5.1.11 Decreased Akt expression and phosphorylation in microRNA-96 and -183 as well as microRNA-96 antagomir-treated CD4$^+$CD25$^-$ T cells

Since the miR-96 and miR-183 knockdown in activated CD4$^+$CD25$^-$ T cells led to a decreased proliferation accompanied by elevated EGR-1 and PTEN expression, the role of Akt as a crucial downstream factor was examined. CD4$^+$CD25$^-$ T cells were treated with the different antagomirs or left untreated and activated with 0.75 µg/mL anti-CD3 and 1 µg/mL anti-CD28 for 72 hours. Afterwards one half of each sample was re-stimulated with 1 µg/mL anti-CD3 for 30 minutes. Cells were harvested and subsequently processed for SDS Page and Western Blot analysis. Figure 20 A shows a representative Western Blot of unstimulated and re-stimulated samples for all five differently transfected T cells (Original Western Blots are depicted in supplementary Figure 31 - Figure 33). By Western Blot whole Akt, phosphoAkt (Ser473) and phosphoAkt (Thr308) were detected together with the house keeping protein GAPDH. Detectable bands with a size of 60 kDa representing the Akt proteins and bands with a size of 37 kDa for GAPDH were densitometrically quantified with ImageJ (open

source). Density of bands from Akt proteins were normalized to the density of corresponding GAPDH bands and re-stimulated samples were normalized to unstimulated controls. In accordance with results obtained from miRNA overexpression experiments (Figure 16), knockdown of miR-96 and miR-183 as well as knockdown of miR-96 alone led to a significant decreased phosphorylation of Akt at the position Ser473 in $CD4^+CD25^-$ T cells (Figure 20 B). The data suggests that the reduction of miR-96 and miR-183 expression in $CD4^+$ effector T cells results in a more inactive PI3K/Akt pathway *in vitro*.

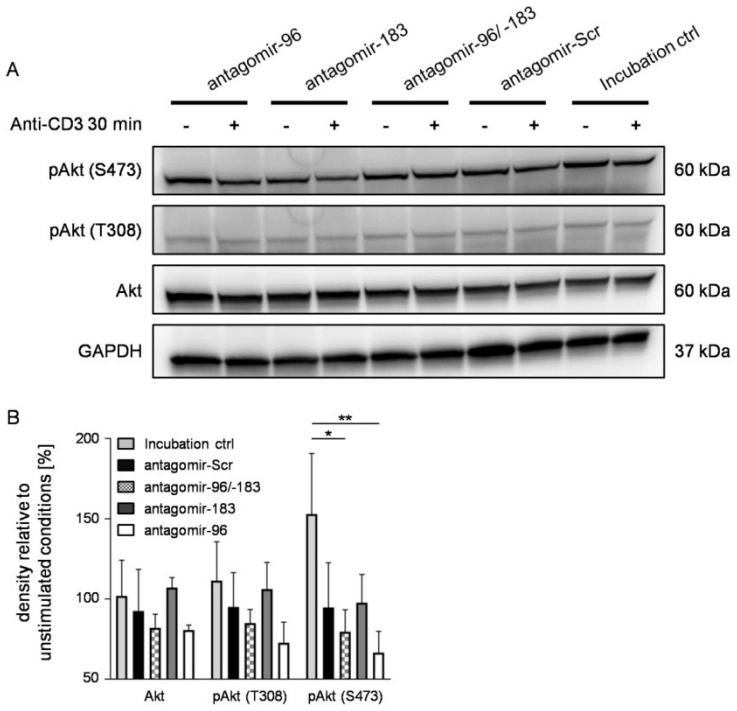

Figure 20: Akt expression and phosphorylation in antagomir-96 and antagomir-183-transfected $CD4^+CD25^-$ T cells. $CD4^+CD25^-$ T cells were isolated from naïve BALB/c mice by magnetic-associated cell sorting and incubated in serum-free medium supplemented with 1 µM antagomir-96, antagomir-183, antagomir-Scr or without antagomir (Incubation ctrl) for 90 minutes. Afterwards, cells were activated in the presence of anti-CD3 and anti-CD28 for 72 hours. On day three, half of the cells were stimulated with 1 µg/mL anti-CD3 for 30 minutes. (**A**) One representative Western Blot stained with antibodies against Akt, pAkt (S473), pAkt (T308) and GAPDH. Western Blots were densitometrically quantified with ImageJ. (**B**) Density of Akt, pAkt (T308) and pAkt (S473) bands were normalized to the density of GAPDH bands and to unstimulated conditions. Results from three independent experiments are summarized as mean ± SEM. One-way ANOVA followed by Dunnett's post-hoc comparisons test was used for statistical analysis. *p < 0.05, **p < 0.01

5.1.12 Increased apoptosis of stimulated $CD4^+CD25^-$ T cells upon microRNA-96 and microRNA-183 knockdown

EGR-1 and PTEN were also described as key players of apoptosis. The upregulation of PTEN by EGR-1 could trigger the initial steps of apoptosis after irradiation or represents a mechanism for phosphatase inhibitor induced apoptosis (Okamura et al.,

2005; Virolle et al., 2001). To investigate, if miRNA knockdown induced upregulation of EGR-1 and PTEN (Figure 19) was able to increase apoptosis, Annexin-V staining was performed on antagomir-treated $CD4^+CD25^-$ T cells 72 hours after initial activation. Indeed, the number of Annexin-V^+ cells among the $CD4^+CD25^-$ T cells significantly increased in those cells that were transfected with the combination of antagomir-96 and -183 compared to untreated or antagomir-Scr-treated cells. The transfection with only one antagomir either directed against miR-96 or miR-183 did not enhance the number of Annexin-V^+ apoptotic cells (Figure 21). The knockdown of miR-96 and miR-183 seems not only to reduce the proliferative capacity (Figure 18) of $CD4^+$ effector T cells but also leads to a concurrent induction of apoptosis by affecting the EGR-1 and PTEN expression and Akt phosphorylation *in vitro*.

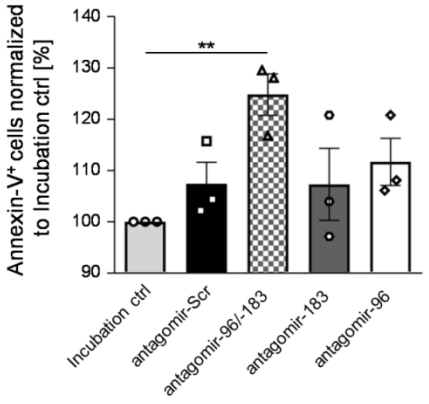

Figure 21: Frequency of Annexin-V^+ expressing antagomir-96 and antagomir-183-transfected $CD4^+CD25^-$ T cells. $CD4^+CD25^-$ T cells were isolated from naïve BALB/c mice by magnetic-associated cell sorting and incubated in serum-free medium supplemented with 1 µM antagomir-96, antagomir-183, antagomir-Scr or without antagomir (Incubation ctrl) for 90 minutes. Thereafter, cells were activated in the presence of anti-CD3 and anti-CD28 for 72 hours. Annexin-V expression of antagomir-treated cells was analyzed by flow cytometry. The frequency of Annexin-V^+ untreated cells (Incubation ctrl) was set to 100 percent and used to normalize the frequncy of antagomir-treated cells. Results from three independent experiments are summarized as mean ± SEM. One-way ANOVA followed by Bonferroni's post-hoc comparisons test was used for statistical analysis. **$p < 0.01$

5.1.13 Knockdown of microRNA-96 and microRNA-183 in effector T cells prolongs development of autoimmune diabetes *in vivo*

The INS-HA x Rag2-KO mouse model was applied to investigate the effect of miR-96 and miR-183 knockdown on $CD4^+$ T cell proliferation in a more complex *in vivo* situation. HA-specific (6.5^+) $CD4^+CD25^-$ T cells from TCR-HA x Thy1.1 mice were sorted and transduced with 1 µM fluorescein-coupled antagomir-96/-183, antagomir-Scr or left untreated (incubation ctrl). 72 hours after transduction, the amount of Fluorescein$^+$ T cells was determined by flow cytometry and 1 x 10^5 Fluorescein$^+$ T cells were adoptively transferred to INS-HA x Rag2-KO mice. Fluorescein-coupled

antagomirs were used to determine the transfection efficiency prior cell transfer, and therefore injection of exactly the same number of successfully antagomir-treated donor $CD4^+CD25^-$ T cells. Based on the *in vitro* data that showed the strongest impact on EGR-1, PTEN expression and Akt phosphorylation with a combined knockdown of miR-96 and miR-183, *in vivo* experiments were performed with HA-specific $CD4^+$ T cells either transfected with antagomir-96/-183 and antagomir-Scr or left untreated as control. By measuring the blood glucose level at indicated time points the onset of diabetes (blood glucose level ≥ 200 mg/dL) was monitored (Figure 22 A).

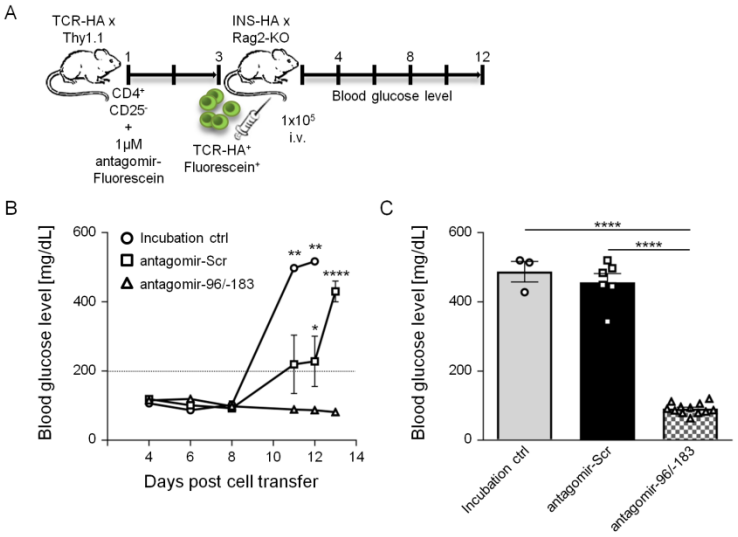

Figure 22: Adoptive transfer of antagomir-96/-183, antagomir-Scr or untreated HA-specific T cells to INS-HA x Rag2-KO mice. (**A**) HA-specific (6.5^+) $CD4^+CD25^-$ T cells from TCR-HA x Thy1.1 mice were sorted and transduced with 1 µM Fluorescein-coupled antagomir-96/-183, antagomir-Scr or left untreated (Incubation ctrl). 72 hours after transduction, the amount of $Fluorescein^+$ T cells was determined by flow cytometry and 1 x 10^5 $Fluorescein^+$ T cells were adoptively transferred to INS-HA x Rag2-KO mice. (**B**) The development of diabetes was monitored by blood glucose level at indicated time points. Mice with a blood glucose level > 200 mg/dL were considered as diabetic. (**C**) Endpoint blood glucose level. Data from n = 3 – 12 mice analyzed in three independent experiments are summarized as mean ± SEM. Each data point represents one animal. One-way ANOVA followed by Bonferroni's post-hoc comparisons test was used for statistical analysis. *p < 0.05, **p < 0.01, ****p < 0.0001

Eleven days after cell transfer the blood glucose level of INS-HA x Rag2-KO mice that received the untreated (incubation control) or the antagomir-Scr-treated HA-specific T cells was higher than 200 mg/dL, while mice which received antagomir-96/-183-transfected HA-specific T cells were still healthy. The blood glucose level of mice, which received untreated HA-specific $CD4^+$ T cells, increased clearly faster compared with antagomir-treated mice. In INS-HA x Rag2-KO mice adoptively transferred with antagomir-Scr-treated donor cells, the increase in blood glucose level was more moderate, but at day 13 it almost reached the levels of the mice that received incubation control cells. Nevertheless, antagomir-96/-138-treated HA-specific $CD4^+$ T

cells did not induce diabetes in INS-HA x Rag2-KO mice in the same time frame (Figure 22 B).

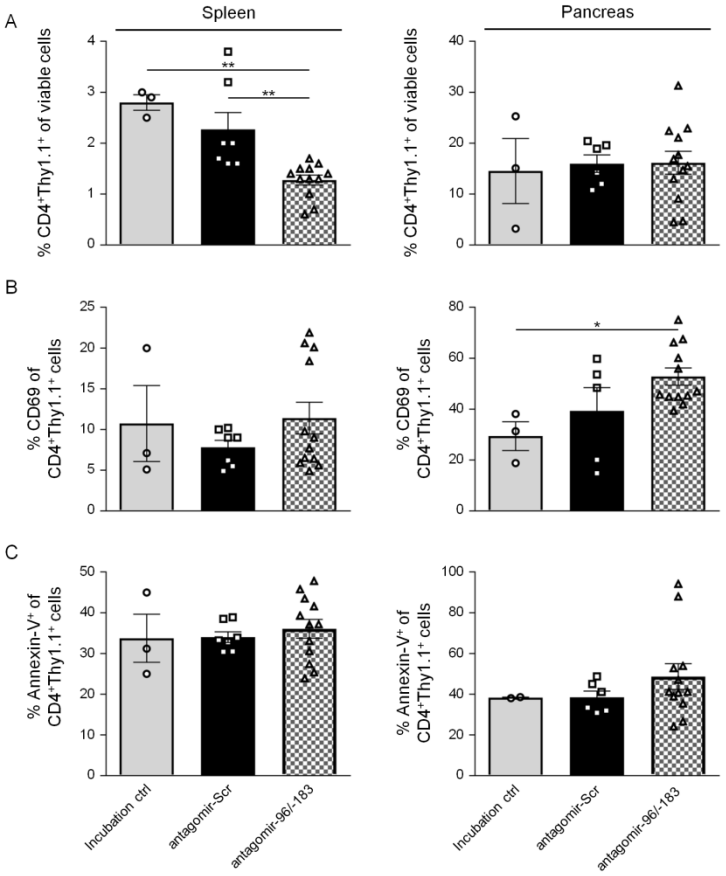

Figure 23: Analysis of transferred antagomir-96/-183, antagomir-Scr or untreated HA-specific T cells in INS-HA x Rag2-KO mice. After the adoptive transfer of antagomir-treated HA-specific T cells in INS-HA x Rag2-KO mice, blood glucose level was monitored up to 13 days. Diabetic and non-diabetic control mice were sacrificed and cells from spleen and pancreas of INS-HA x Rag2-KO mice were analyzed by flow cytometry. (**A**) Percentage of transferred $CD4^+Thy1.1^+$ T cells, (**B**) frequency of CD69 and (**C**) Annexin-V expressing $CD4^+Thy1.1^+$ T cells from spleen and pancreas of INS-HA x Rag2-KO mice analyzed by flow cytometry. Data from n = 3 – 12 mice analyzed in three independent experiments are summarized as mean ± SEM. Each data point represents one animal. One-way ANOVA followed by Bonferroni's post-hoc comparisons test was used for statistical analysis. *p < 0.05, **p < 0.01

Comparing glycaemia at the day of analysis, it was significantly decreased in mice that received the miR-96 and miR-183 knockdown HA-specific $CD4^+$ T cells compared to controls (Figure 22 C). Cellular analysis of spleen and pancreas revealed a significantly decreased frequency of $CD4^+Thy1.1^+$ effector T cells in the spleen of mice adoptively transferred with antagomir-96/-183-treated T cells (Figure 23 A). Interestingly, the expression of CD69 among the $CD4^+Thy1.1^+$ T cells within the pancreas was significantly elevated in INS-HA x Rag2-KO mice transferred with antagomir-96/-183-treated HA-specific T cells compared to mice that received untreated control cells (Figure 23 B).No alteration in the number of Annexin-V^+ apoptotic cells within the transferred T cells, neither in the spleen nor in the pancreas, was detected between the

three different groups *in vivo* (Figure 23 C). Since the development of diabetes in this *in vivo* experiment was significantly prolonged accompanied with significant decreased frequencies of $CD4^+Thy1.1^+$ effector T cells in mice transferred with antagomir-96/-183-treated T cells, the data further emphasize that miR-96 and miR-183 have an impact on $CD4^+$ T cell proliferation.

5.1.14 Enhanced microRNA-96 and microRNA-183 expression in human $CD4^+$ and $CD8^+$ T cells after activation

To further investigate, if miR-96 and miR-183 also play a role in the human system the expression profiles of both miRNAs were assessed in activated human $CD4^+$ and $CD8^+$ T cells. $CD4^+$ and $CD8^+$ T cells were isolated by magnetic activated cell sorting from PBMCs of healthy donors. The cells were activated in the presence of 0.75 µg/mL anti-CD3 and 1 µg/mL anti-CD28 for 96 hours. At indicated time points, cells were harvested and miR-96 and miR-183 expression were analyzed by qRT-PCR. Similar to the expression pattern in activated murine $CD4^+CD25^-$ and $CD8^+$ T cells, miR-96 and miR-183 expression significantly increased in both human T cell subsets 96 hours post activation compared to unstimulated (day 0) cells (Figure 24).

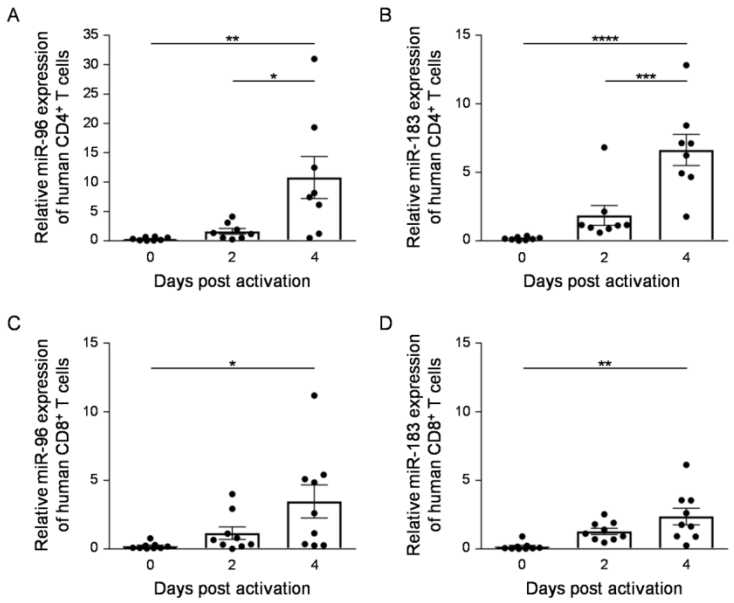

Figure 24: MiR-96 and miR-183 expression profile in naïve and activated human $CD4^+$ and $CD8^+$ T cells. (**A, B**) $CD4^+$ and (**C, D**) $CD8^+$ T cells were isolated from human PBMCs by magnetic-associated cell sorting, left unstimulated or activated for indicated time points in the presence of anti-CD3 and anti-CD28. MiRNAs were isolated, reverse transcribed and analyzed for (**A**, **C**) miR-96, (**B, D**) miR-183 and RNU6B expression, as housekeeping control, by qRT-PCR. Results from three independent experiments with n = 8 – 9 were summarized as mean ± SEM. One-way ANOVA followed by Bonferroni's post-hoc comparisons test was used for statistical analysis. *p < 0.05, **p < 0.01, ***p < 0.001, ****p < 0.0001

5.1.15 Elevated microRNA-96 and microRNA-183 expression in CD4$^+$ T cells of patients suffering from severe endocrine orbitopathy

Autoimmunity is characterized by autoreactive T cells with impaired activity (Theofilopoulos et al., 2017). MiR-96 and miR-183 were highly upregulated upon T cell activation in the murine (Figure 7) as well as in the human system (Figure 24) and the modulation of these two miRNA affected the development of diabetes in the autoimmune mouse model (Figure 11, Figure 22). To address the question, whether both miRNAs are differentially regulated in T cells from patients and thereby display a potential biomarker or therapeutic target for the development of autoimmune diseases, the expression of miR-96 and miR-183 were compared between CD4$^+$ T cells of patients suffering from severe EO and age- and sex-matched healthy controls. Figure 25 demonstrates that the expression of miR-96 and miR-183 were significantly increased in CD4$^+$ T cells from patients suffering from the autoimmune disease compared to CD4$^+$ T cells of healthy donors. Taken together, the results suggest a potential role of miR-96 and miR-183 resulting in the more activated T cell phenotype of patients suffering from EO and therefore may represent a potential therapeutic target for the treatment of autoimmune disease.

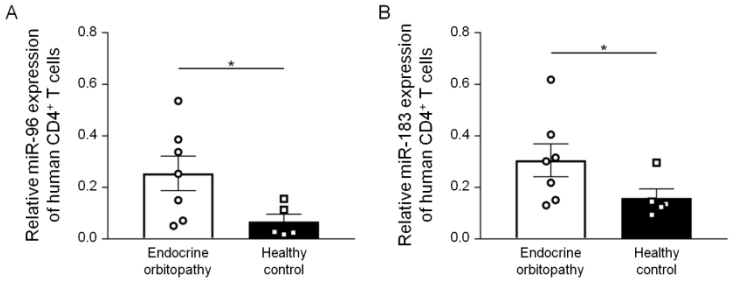

Figure 25: MiR-96 and miR-183 expression in human CD4$^+$ T cells from patients suffering from severe endocrine orbitopathy compared to healthy control. CD4$^+$ T cells were isolated from human PBMCs by magnetic-associated cell sorting. MiRNAs were isolated, reverse transcribed and analyzed for (**A**) miR-96, (**B**) miR-183 and RNU6B expression, as housekeeping control, by qRT-PCR. Data from n = 7 (Endocrine orbitopathy) and n = 5 (Healthy control) were analyzed in one experiment and summarized as mean ± SEM. Mann-Whitney test was used for statistical analysis. *p < 0.05

5.2 Part II

5.2.1 T cell-specific Nrp-1-deficient mice show an earlier onset of diabetes compared to INS-HA x TCR-HA mice with Nrp-1 expressing T cells

Nrp-1 represents a co-receptor for VEGF and was found to be highly expressed in CD4$^+$CD25$^+$FoxP3$^+$ Tregs (Bruder et al., 2004). In 2012, Hansen et al. demonstrated Nrp-1 dependent infiltration of Tregs into tumorous tissue along a VEGF gradient

(Hansen et al., 2012). The second part of this thesis investigates, if T cell-specific Nrp-1 expression has also an impact on other inflammatory immune responses *in vivo*. Here, the influence of Nrp-1 expression on T cells was analyzed in an autoimmune diabetes model. Nrp-$1^{fl/fl}$ x CD4cre x TCR-HA x INS-HA mice were generated by crossing INS-HA x TCR-HA mice with Nrp-$1^{fl/fl}$ x CD4cre mice. INS-HA x TCR-HA double transgenic mice harbor $CD4^+$ T cells expressing a α:β T cell receptor which recognizes the MHC class II $H2E^d$:$HA_{110-120}$-restricting epitope of the influenza HA accompanied by the expression of the model antigen HA under control of the rat insulin-promotor on pancreatic beta cells. Spontaneously, around 40% of those mice develop diabetes (Bruder et al., 2005).

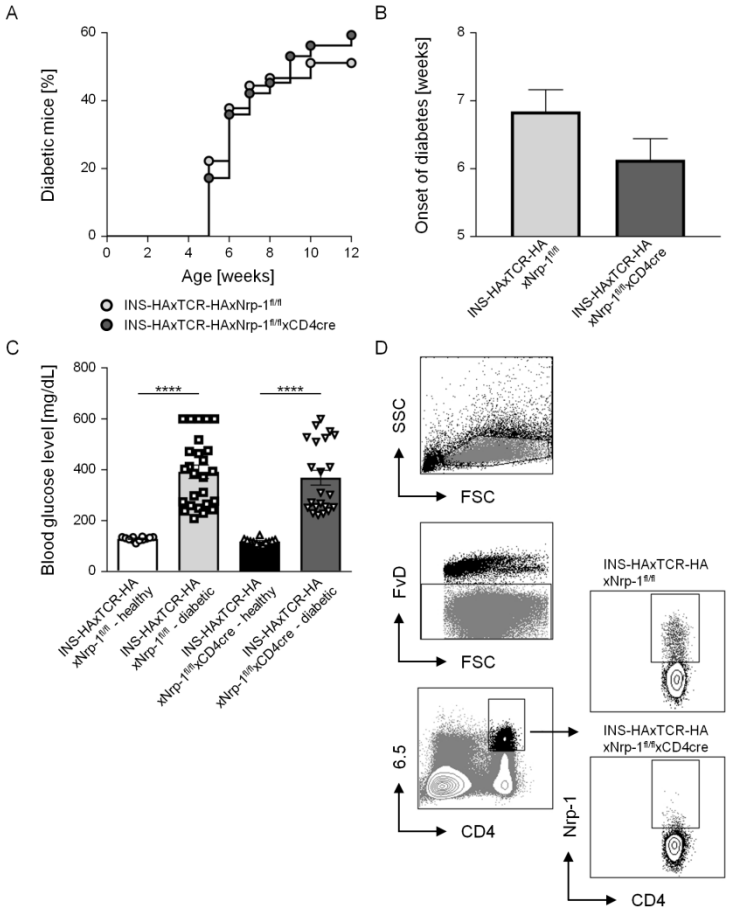

Figure 26: Diabetes onset of INS-HA x TCR-HA x Nrp-$1^{fl/fl}$ and INS-HA x TCR-HA x Nrp-$1^{fl/fl}$ x CD4cre mice. Nrp$1^{fl/fl}$ x CD4cre x TCR-HA x INS-HA mice were generated to analyze the influence of T cell-specific Nrp-1 expression on the development of autoimmune diabetes. Starting five weeks after birth, blood glucose level was measured every week until the onset of diabetes (blood glucose level ≥ 200 mg/dL) or in terms of non-diabetic mice until week 12. (**A**) Percentage of diabetic mice, n = 45 - 64 mice. (**B**) Time point of diabetes onset (blood glucose levels ≥ 200 mg/dL): (**C**) Endpoint blood glucose level: Data from n = 12 - 26 mice are summarized as mean ± SEM. Each data point represents one animal. One-way ANOVA followed by Bonferroni's post-hoc comparisons test was used for statistical analysis. ****$p < 0.0001$ (**D**) Gating strategy: Nrp-1 expression of 6.5^+CD4^+ T cells gated from living (FvD^-) lymphocytes.

The Nrp-1$^{fl/fl}$ x CD4cre x TCR-HA x INS-HA mice also express the HA-antigen within the pancreas and concurrently harbor HA-specific T cells deficient for Nrp-1. The blood glucose level of T cell-specific Nrp-1 wild type and knockout INS-HA x TCR-HA double transgenic mice were monitored over a period of eight weeks, starting from week five after birth. During the eight weeks of analysis, similar percentages of T cell-specific Nrp-1 wild type (INS-HAxTCR-HAxNrp-1$^{fl/fl}$) and knockout INS-HA x TCR-HA mice (INS-HAxTCR-HAxNrp-1$^{fl/fl}$xCD4cre) developed diabetes (Figure 26 A).

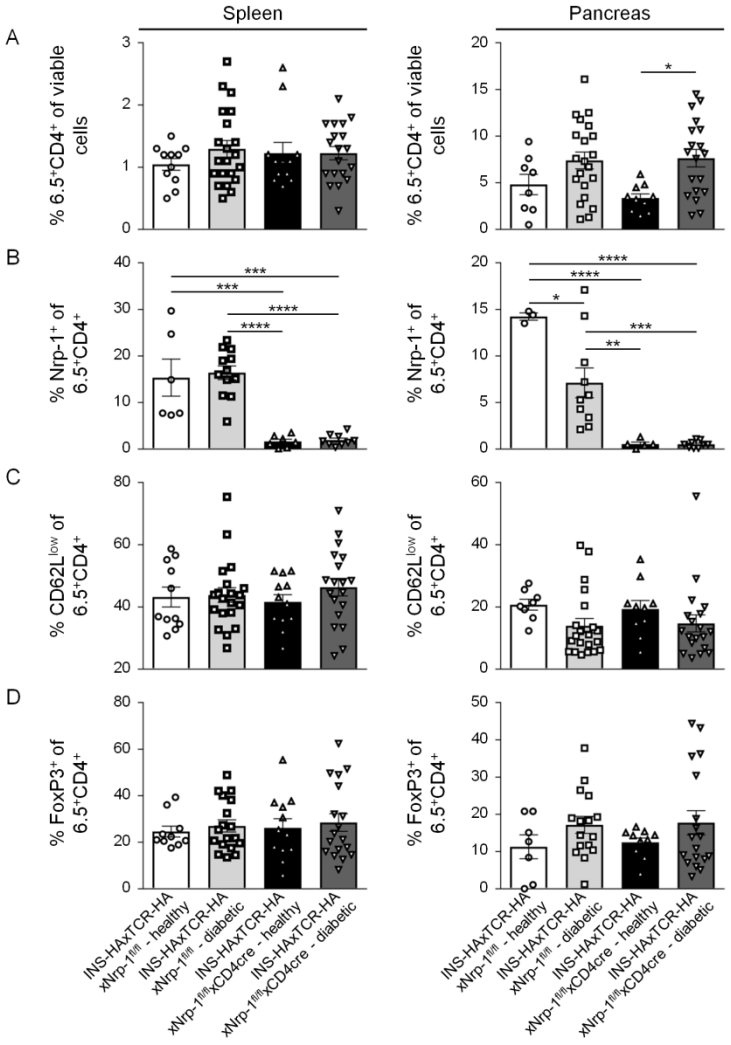

Figure 27: Analysis of HA-specific 6.5$^+$CD4$^+$ T cells from INS-HA x TCR-HA x Nrp-1$^{fl/fl}$ and INS-HA x TCR-HA x Nrp-1$^{fl/fl}$ x CD4cre mice. INS-HA x TCR-HA x Nrp-1$^{fl/fl}$ and INS-HA x TCR-HA x Nrp-1$^{fl/fl}$ x CD4cre mice, that developed diabetes within the measuring period of 8 weeks, were sacrificed at the day of disease onset and non-diabetic controls were sacrificed with 12 weeks of age. HA-specific T cells from spleen and pancreas were analyzed by flow cytometry. (**A**) The frequencies of 6.5$^+$CD4$^+$ cells, as well as the expression of (**B**) Nrp-1, (**C**) of the activation marker CD62L and (**D**) the transcription factor FoxP3 was determined. Data from n = 3 – 21 mice are summarized as mean ± SEM. Each data point represents one animal. One-way ANOVA followed by Bonferroni's post-hoc comparisons test was used for statistical analysis. *p < 0.05, **p < 0.01, ***p < 0.001, ****p < 0.0001

Nevertheless, INS-HA x TCR-HA mice harboring Nrp-1-deficient T cells (mean = 6) developed diabetes almost one week earlier than INS-HA x TCR-HA with Nrp-1 wild

type T cells (mean = 6.7, Figure 26 B). At the day of analysis, no differences in glycaemia were detected between T cell-specific Nrp-1 wild type and knockout INS-HA x TCR-HA mice (Figure 26 C). HA-specific $6.5^{+}CD4^{+}$ T cells from spleen and pancreas of diabetic and healthy control mice were analyzed by flow cytometry (Figure 26 D). Within the spleen no differences in the frequency of HA-specific $6.5^{+}CD4^{+}$ T cells were detected within the four different groups. However, there was a significant increase of HA-specific $6.5^{+}CD4^{+}$ T cells in the pancreas of diabetic INS-HA x TCR-HA mice harboring Nrp-1-deficient T cells compared to their healthy counterparts (Figure 27 A). As expected, HA-specific $6.5^{+}CD4^{+}$ T cells deficient for Nrp-1 expressed almost no Nrp-1 either in spleen or in pancreas. Comparing healthy and diabetic INS-HA x TCR-HA mice harboring Nrp-1 expressing T cells, diabetic mice had a significantly reduced Nrp-1 expression (Figure 27 B). For the activation marker CD62L and the transcription factor FoxP3 no differential expression in HA-specific $6.5^{+}CD4^{+}$ T cells in both organs were found between the four different groups (Figure 27 C, D).

Since T cell-specific Nrp-1 deficiency in the whole $CD4^{+}$ T cell compartment, consisting of $FoxP3^{-}$ effector T cells and $FoxP3^{+}$ Tregs, led to an accelerated development of autoimmune diabetes accompanied with more HA-specific $6.5^{+}CD4^{+}$ T cells within the pancreas, the next step was to analyze the impact of Nrp-1 deficiency on Tregs in autoimmune diabetes.

5.2.2 Nrp-1-deficient regulatory T cells are not able to control the onset of diabetes as efficient as Nrp-1 expressing regulatory T cells

To analyze the impact of Nrp-1 deficiency especially in Tregs on the onset of autoimmune diabetes, the INS-HA x Rag2-KO mouse model for antigen-specific induction of diabetes was used. Therefore, HA-specific $6.5^{+}CD4^{+}CD25^{-}$ effector T cells from TCR-HA x Thy1.1 mice were co-transferred with $6.5^{+}CD4^{+}CD25^{+}$ Tregs from either T cell-specific Nrp-1 knockout ($Nrp\text{-}1^{fl/fl}$ x CD4cre x TCR-HA) or wild type ($Nrp\text{-}1^{fl/fl}$ x TCR-HA) mice into INS-HA x Rag2-KO mice. The interaction of the HA-specific donor cells with the HA-expressing pancreatic beta cells of the recipient led to an antigen specific induction of diabetes which was monitored by an increase in blood glucose level over 200 mg/dL (Figure 28 A). Eight days post cell transfer the blood glucose level in mice of all three groups increased above 200 mg/dL. Nevertheless, blood glucose levels were significantly higher in those mice that received only effector T cells compared to mice that were transferred additionally with the Nrp-1 expressing Tregs nine days after transfer (Figure 28 B).

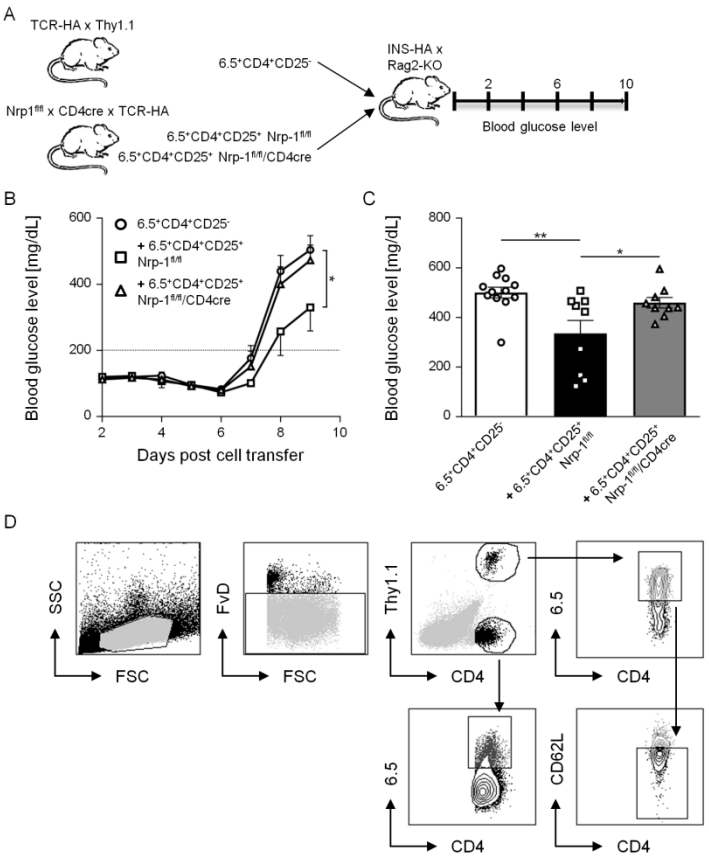

Figure 28: Adoptive transfer of HA-specific T effector cells alone or together with either Nrp-1 wild type or knockout regulatory T cells to INS-HA x Rag2-KO mice. (**A**) 10^5 $6.5^+CD4^+CD25^-$ effector T cells from TCR-HA x Thy1.1 mice and 10^5 $6.5^+CD4^+CD25^+$ regulatory T cells from either Nrp-1 wild type (Nrp-$1^{fl/fl}$ x TCR-HA) or T cell-specific Nrp-1 knockout (Nrp-$1^{fl/fl}$ x CD4cre x TCR-HA) mice were transferred i.v. into the recipient INS-HA x Rag2-KO mice. The control group only received 10^5 $6.5^+CD4^+CD25^-$ effector T cells. (**B**) The development of diabetes was monitored by blood glucose level at indicated time points. Mice with a blood glucose level > 200 mg/dL were considered as diabetic. (**C**) Endpoint blood glucose level. Data from n = 9 - 12 mice analyzed in four independent experiments are summarized as mean ± SEM One-way ANOVA followed by Bonferroni's post-hoc comparisons test was used for statistical analysis. *p < 0.05, **p < 0.01 (**D**) Gating strategy: $6.5^+CD4^+Thy1.1^+$ effector and $6.5^+CD4^+Thy1.1^-$ regulatory T cells were gated from living (FvD^-) lymphocytes for further analyis.

Comparing glycaemia at the day of analysis between all three different groups, mice that received the effector T cells in combination with the Nrp-1 wild type Tregs showed a significant lower blood glucose level compared to both other groups of mice. The blood glucose level of mice that additionally received Nrp-1-deficient Tregs did not differ from mice transferred only with effector T cells (Figure 28 C). $6.5^+CD4^+Thy1.1^+$ effector and $6.5^+CD4^+Thy1.1^-$ Tregs were isolated from spleen and pancreas and analyzed by flow cytometry (Figure 28 D). In the pancreas of INS-HA x Rag2-KO mice the frequency of HA-specific $6.5^+CD4^+Thy1.1^+$ effector T cells was significantly decreased in mice that were co-transferred with Nrp-1 expressing Tregs compared to those that received the Nrp-1-deficient Tregs (Figure 29 A).

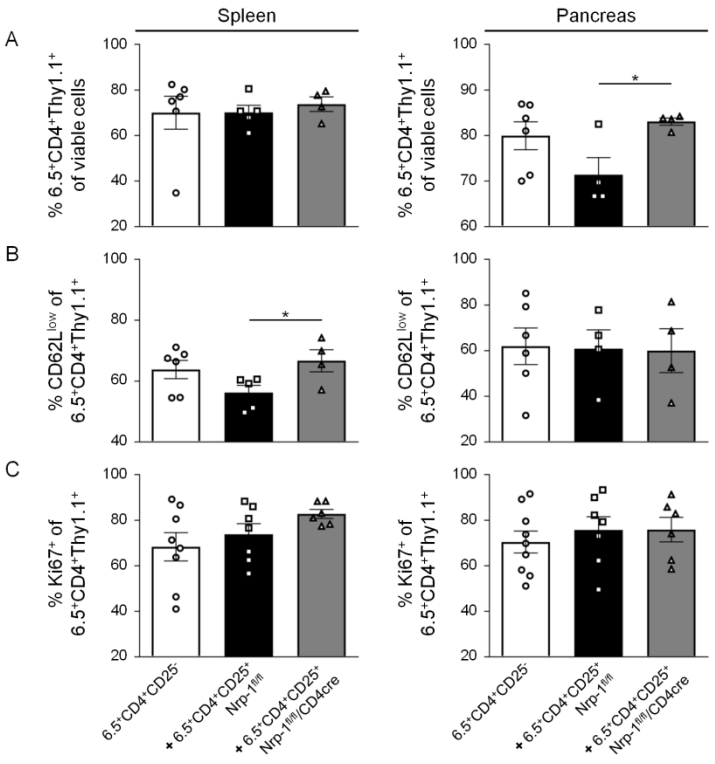

Figure 29: Analysis of transferred HA-specific 6.5$^+$CD4$^+$Thy1.1$^+$ effector T cells in INS-HA x Rag2-KO mice. Nine days post T cell transfer, cells from spleen and pancreas of INS-HA x Rag2-KO mice were analyzed for the (**A**) frequency of HA-specific 6.5$^+$CD4$^+$Thy1.1$^+$ effector T cells, (**B**) the expression of the activation marker CD62L and (**C**) their proliferative capacity by measuring the expression of Ki67. Data from n = 4 – 9 mice analyzed in four independent experiments are summarized as mean ± SEM One-way ANOVA followed by Bonferroni's post-hoc comparisons test was used for statistical analysis. *p < 0.05

This was accompanied by significantly decreased CD62L expression of splenic 6.5$^+$CD4$^+$Thy1.1$^+$ effector T cells of INS-HA x Rag2-KO mice transferred with Nrp-1 wild type Tregs (Figure 29 B). The expression of the proliferation marker Ki67 in 6.5$^+$CD4$^+$Thy1.1$^+$ T cells did not differ between the three different groups (Figure 29 C). As expected, within the pancreas of INS-HA x Rag2-KO mice which received either the Nrp-1 wild type or deficient Tregs a significant higher frequency of 6.5$^+$CD4$^+$Thy1.1$^-$ T cells were detected compared to mice transferred with effector T cell only (Figure 30 A). Interestingly, the frequency of 6.5$^+$CD4$^+$Thy1.1$^-$ Tregs and the expression of the transcription factor FoxP3 did not differ between mice transferred with Nrp-1 wild type or knockout Tregs (Figure 30 B). Furthermore, the expression of the proliferation marker Ki67 was comparable in both types of 6.5$^+$CD4$^+$Thy1.1$^-$ Tregs (Figure 30 C).

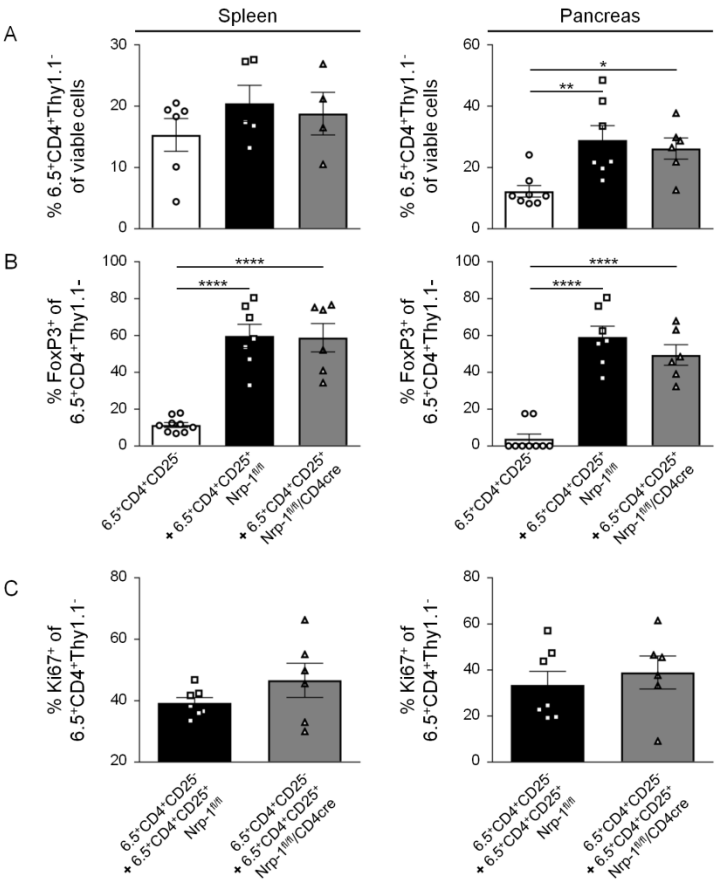

Figure 30: Analysis of transferred HA-specific 6.5$^+$CD4$^+$Thy1.1$^-$ Tregs in INS-HA x Rag2-KO mice. Nine days post T cell transfer, cells from spleen and pancreas of INS-HA x Rag2-KO mice were analyzed for the (**A**) frequency of HA-specific 6.5$^+$CD4$^+$Thy1.1$^-$ Tregs, (**B**) the expression of the transcription marker FoxP3 and (**C**) their proliferative capacity by measuring the expression of Ki67. Data from n = 4 – 9 mice analyzed in four independent experiments are summarized as mean ± SEM One-way ANOVA followed by Bonferroni's post-hoc comparisons test was used for statistical analysis. *p < 0.05, **p < 0.01, ****p < 0.0001

In summary, Nrp-1 expressing Tregs were more efficient in controlling the onset of diabetes as Nrp-1-deficient Tregs. Due to the decreased HA-specific effector T cells in the pancreas of mice transferred with Nrp-1 wild type Tregs, these data suggest that Nrp-1 expression is crucial for the suppressive capacity of Tregs during autoimmune diseases.

6 Discussion

6.1 MicroRNA-96 and microRNA-183 in T cell-mediated autoimmunity

Autoimmune disorders have a prevalence of around 7-9 % in the population. They are caused by autoantigen-induced inflammation that results in a breakdown of peripheral tolerance by reactivation of autoreactive T and B cells. Depending on the site and tissues which are involved, autoimmunity is separated into organ-specific or systemic diseases (Theofilopoulos et al., 2017). Since miRNAs are reported to be involved in a variety of immunological processes, including central and peripheral tolerance, they are shown to be important in the modulation of autoimmunity. Dicer-deficient $CD4^+$ T cells failed to discriminate between activating and anergy-inducing stimuli. They produced IL-2 in the absence of co-stimulation leading to autocrine proliferation (Marcais et al., 2014) Furthermore, mice with a conditional knockout of Dicer in $FoxP3^+$ Tregs spontaneously developed lethal autoimmune inflammatory disease due to impaired development and function of those Tregs (Liston et al., 2008; Zhou et al., 2008). In addition, aberrant expression of miR-155, miR-21, miR-146a and the miR-17~92 cluster in immune cells is involved in the pathogenesis of multiple autoimmune diseases like MS, RA, inflammatory bowel disease (IBD), and T1D (Garo and Murugaiyan, 2016). Moreover, miRNAs emerge more and more as potential therapeutic targets in the treatment and prevention of autoimmune diseases. For example, silencing of miR-326 and miR-155 resulted in less severe experimental autoimmune encephalomyelitis (EAE) by affecting Th1 and Th17 cells and miR-146a silencing could ameliorate experimental autoimmune myasthenia gravis (Garo and Murugaiyan, 2016). This demonstrates the importance of proper miRNA expression to prevent T cell-mediated autoimmunity.

EO is a thyroid-associated orbitopathy which is closely related to the organ-specific autoimmune disorder GD (Bahn, 2010). The pathogenesis of EO is driven by autoreactive T cells that infiltrate the orbit of the eye (Feldon et al., 2005). Dysregulated miRNA expression contributing to the pathogenesis is also described for GD (Chen et al., 2015; Jang et al., 2016). Two independent studies indicated the miR-183 cluster to be associated in this specific autoimmune disease. Compared to healthy controls, miR-183 expression is upregulated in thyroid tissue from GD patients and its predicted targets A kinase anchor protein 12 and zinc finger protein multitype 2 were decreased (Qin et al., 2015). Moreover, in the serum of GD patients' highly increased miR-96

expression correlates with a more severe outcome of the disease (Martinez-Hernandez et al., 2018). In our study, miR-96 and miR-183 expression was found to be highly upregulated in $CD4^+$ T cells from patients suffering from severe EO compared to healthy controls. Furthermore, *in vitro* stimulated human as well as murine $CD4^+CD25^-$ and $CD8^+$ T cells showed a significant elevated miR-96 and miR-183 expression upon activation. These results support the aforementioned studies and implicate an important role for both miRNAs in T cell-mediated autoimmunity. To investigate, if the aberrant regulation of miR-96 and miR-183 expression is a general mechanism in T cell-mediated autoimmunity, it would be interesting to analyze the miRNA expression pattern in $CD4^+$ T cells of patients suffering from T1D or other T cell-induced autoimmune diseases.

To further characterize the impact of miR-96 and miR-183 expression on murine $CD4^+CD25^-$ T cell phenotype and function, we used gain- and loss-of-function experiments. By using retroviral gene transfer, both miR-96 and miR-183 as well as miR-96 alone were successfully overexpressed in activated $CD4^+CD25^-$ T cells after 48 hours. MiRNA knockdown was obtained by transfecting $CD4^+CD25^-$ T cells with 1 µM of miRNA-specific antagomirs. The antagomirs used here are single stranded, chemically-enhanced RNA oligonucleotides that bind and sequester the complimentary mature miR-96 or miR-183 strand (Krutzfeldt et al., 2005). Successful knockdown of specific miRNAs by antagomirs was demonstrated before *in vitro* and *in vivo* (Ishida and Selaru, 2013). Here, significant and specific knockdown of miR-96 as well as miR-183 was achieved 48 hours after initial activation and lasted at least 96 hours *in vitro*. As described previously (Haftmann et al., 2015), our results confirm antagomirs as suitable tools for specific miRNA knockdown in T cells.

Elevated miR-96 and miR-183 expression was reported for different cancer types including breast, ovary, prostate, colorectal cancer and HCC. In all these cancers, upregulation of miR-96 and miR-183 was related to increased proliferation (Baik et al., 2016; Cheng et al., 2016; Fendler et al., 2013; Haflidadottir et al., 2013; Larne et al., 2015; Li et al., 2014; Lin et al., 2010; Zhang et al., 2015a; Zhang et al., 2015b). In T cells, miR-182, the third member of the miR-183 cluster, was identified to promote clonal expansion of activated Th cells and overexpression of this specific miRNA led to enhanced proliferation (Stittrich et al., 2010). Furthermore, the miR-183 cluster was found to play a crucial role for pathogenic cytokine production in Th17 cells in EAE *in vivo* (Ichiyama et al., 2016). Our results promote the connection between miR-96 and miR-183 expression and the proliferative capacity also in $CD4^+CD25^-$ T cells *in vitro* and *in vivo*. Overexpressing both miRNAs as well as only miR-96 resulted in elevated

proliferation of $CD4^+CD25^-$ T cells compared to control vector-transduced cells. In line with this result, we observed reduced proliferative capacity in miR-96, miR-183 as well as miR-96 and miR-183 knockdown $CD4^+CD25^-$ T cells. Thus, in $CD4^+$ T cells, miR-96 and miR-183 seem to regulate signaling pathways which control activation and proliferation.

In autoimmune diseases, hyperproliferative T cells are a major course of pathology (Theofilopoulos et al., 2001). Therefore, we investigated how the impaired proliferation of miR-96 and miR-183 overexpressing and knockdown $CD4^+CD25^-$ T cells affect the development of autoimmune response in an antigen-specific diabetes mouse model. Overexpression of both miRNAs as well as miR-96 alone in transferred effector T cells led to an earlier onset of diabetes in recipient mice accompanied by higher frequencies of transferred $CD4^+Thy1.1^+$ effector T cells in spleen and pancreas. The combined knockdown of miR-96 and miR-183 in adoptively transferred effector T cells prolonged the development of autoimmune diabetes compared to mice which received antagomir-Scr or untreated control T cells. In contrast with the gain-of-function experiment, mice adoptively transferred with miRNA knockdown T cells showed reduced frequency of $CD4^+Thy1.1^+$ T cells within the spleen. Hence, our results provide evidence that differential expression of miR-96 and miR-183 in $CD4^+CD25^-$ T cells modulates the induction of antigen-specific autoimmune diabetes *in vivo*, most probably by interfering with proliferation.

The surface receptor CD69 is described as an early activation marker for T cells, since its expression is rapidly induced after T cell stimulation. In addition, it was described to be expressed on infiltrating lymphocytes in a variety of human chronic inflammatory conditions (Cibrian and Sanchez-Madrid, 2017). CD69 expression was also shown to be important for lymphocyte migration as well as retention in lymphoid organs, by the interaction and internalization of S1P1 receptor (Shiow et al., 2006). Moreover, high CD69 expression was reported for peripheral tissue-resident memory T cells, mainly due to its retention properties (Mackay et al., 2015). Knowing that CD69 is an activation and a tissue-resident marker on T cells, one might expect that the adoptively transferred $CD4^+CD25^-$ T cells from diabetic mice that had already encountered their antigen, express higher levels of CD69 than $CD4^+CD25^-$ T cells from non-diabetic mice. In contrast to the literature, adoptively transferred miRNA overexpressing $CD4^+Thy1.1^+$ T cells of diabetic mice showed a decreased expression of CD69 while miR-96 and miR-183 knockdown $CD4^+Thy1.1^+$ T cells from healthy mice displayed an increased CD69 expression within the pancreas. In both experiments, $CD4^+CD25^-$ T cells were pre-activated prior transfer and analyzed 10 to 13 days post transfer. Since

CD69 is a marker for very early activation, here it might not be an adequate marker to detect differences in the activation status of T cells. To further characterize miRNA overexpressing and knockdown $CD4^+CD25^-$ T cells *in vivo*, the expression of other activation marker like co-stimulatory, adhesion, MHC class II molecules or chemokine receptors need to be analyzed (Shipkova and Wieland, 2012). Nevertheless, we observed differences in the expression of CD69 between diabetic and non-diabetic mice that do not fit to the role of CD69 as a tissue-resident marker. To explain the differences one might speculate that they are a result of the impaired miRNA expression. CD69 was also described as a negative regulator of Th17-mediated immune response (Martin et al., 2010) which plays an important role in tissue inflammation during autoimmune diseases (Ichiyama et al., 2016). CD69 signaling increases STAT5 phosphorylation which enables the protein to compete with STAT3 leading to impaired Th17 response. The downregulation of CD69 in the presence of IL-6 favors STAT3 to induce IL-17 production (Martin et al., 2010). Furthermore, the IL-6-STAT3 pathway was shown to induce the expression of the miR-183 cluster by STAT3 binding to proximal conserved non-coding sequences (CNS) of the cluster in Th17 cells leading to decreased FoxO1 expression and increased IL-17A production (Ichiyama et al., 2016). Possibly, miR-96 and miR-183 are able to control CD69 expression by a so far unknown mechanism to further promote STAT3-mediated IL17 production. Moreover, the effect of decreased CD69 expression in diabetic mice can result from the highly glucose environment as CD69 was also described as a metabolic gatekeeper. Anti-CD69 antibody enhanced the glucose uptake in activated T cells (Conde et al., 1996). Thus, apart from a miRNA-specific effect, one might assume that T cells in a highly glucose environment decrease their CD69 expression to regulate glycolysis and prevent glucose induced damages. However, further analyses are necessary to better understand the role of CD69 expression on T cells in diabetic mice.

As the modulation of miR-96 and miR-183 expression in $CD4^+CD25^-$ T cells resulted in an impaired proliferative capacity *in vitro* and *in vivo*, we investigated the underlying signaling mechanism. From different cancer cell lines a variety of miR-183 cluster target molecules are known that play a role in proliferation. For example, miR-96 targets FoxO1 (Fendler et al., 2013) and FoxO3 (Lin et al., 2010), while miR-183 inhibits PDCD6 (Wang et al., 2017b) or mTOR (Kye et al., 2014).

In 2010, Saver et al. described the miR-183-mediated suppression of the transcription factor EGR-1 in different synovial sarcoma and colon cancer cell lines (Sarver et al., 2010). Here, we demonstrate that upon activation EGR-1 expression increased in $CD4^+CD25^-$ T cells in the first two days followed by a decline by day three. This

expression pattern negatively correlates with the expression of miR-96 and miR-183. Luciferase reporter gene assay confirmed EGR-1 as a direct target of miR-183 in $CD4^+$ T cells. Moreover, we could demonstrate for the first time, that miR-96 also targets this specific transcription factor. Overexpression of miR-96 and miR-183 as well as miR-96 alone, led to decreased EGR-1 protein levels in transduced $CD4^+CD25^-$ T cells. In line with these results, the combined knockdown of miR-96 and miR-183 in $CD4^+CD25^-$ T cells increased EGR-1 expression. Our results indicate that members of the miR-183 cluster target EGR-1 not only in cancer cells but also in $CD4^+$ T cells.

EGR-1 is able to regulate the expression of the tumor suppressor gene PTEN, a major negative regulator of the PI3K/Akt pathway (Sukhatme et al., 1988; Wu et al., 1998). In activated $CD4^+CD25^-$ T cells, PTEN expression is increased until day three post stimulation. As described for EGR-1, PTEN expression negatively correlates with miR-96 expression. Although there was a clear trend, the expression of miR-183 and PTEN did not reach a significant correlation. Nevertheless, overexpression of miR-96 and miR-183 as well as miR-96 alone led to decreased PTEN protein levels in $CD4^+CD25^-$ T cells. Moreover, PTEN expression increased in miR-96 and miR-183 as well as only miR-96 knockdown $CD4^+CD25^-$ T cells. These results demonstrate a miR-96 and miR-183-mediated decrease of EGR-1 and thereby reduced PTEN expression in $CD4^+$ T cells upon activation.

PTEN-deficient mature T cells were reported to become resistant against FAS-induced programmed cell death leading to multiorgan autoimmunity (Liu et al., 2010). Here, we demonstrate that knockdown of miR-96 and miR-183 led to elevated PTEN expression *in vitro* that might explain the decelerated development of autoimmune diabetes after transfer of miRNA knockdown cells *in vivo*. Furthermore, increased expression of EGR-1 and thereby PTEN was described to be a key player in apoptosis (Okamura et al., 2005; Virolle et al., 2001). Indeed, our results confirm an impact of EGR-1-PTEN axis on apoptosis of $CD4^+$ T cell *in vitro*. MiR-96 and miR-183 knockdown $CD4^+CD25^-$ T cells which showed an increase in EGR-1 and PTEN expression also displayed elevated binding of Annexin-V demonstrating increased apoptosis. Nevertheless, this observation was not confirmed *in vivo*, since no difference in the viability was detected in transferred miRNA knockdown cells. These results support the assumption that the prolonged onset of diabetes and the decreased frequencies of transferred miRNA knockdown cell are a direct effect of impaired proliferation *in vivo* at least in our experimental setting.

EGR-1-dependent upregulation of PTEN impairs the PI3K/Akt pathway resulting in impaired proliferation, migration and apoptosis in several cell types (Tsugawa et al.,

2003; Virolle et al., 2001). PTEN opposes PI3K resulting in decreased Akt phosphorylation and activity (Wu et al., 1998). Akt needs to be phosphorylated at both the T308 and S473 residue to be fully activated (Alessi et al., 1996). Nevertheless, the dual phosphorylation of Akt is not necessarily required for all functions. Absence of S473 phosphorylation for example affects the interaction with FoxO1 and 3a (Jacinto et al., 2006). Furthermore, the ratio between T308 and S473 phosphorylation was described to be crucial for Akt substrate specificity (Yung et al., 2011). Recently, Wang et al. reported that miR-182 regulates axon outgrowth and dendrite maturation through the regulation of the PTEN-Akt pathway (Wang et al., 2017a). Besides decreased EGR-1 and PTEN expression, we demonstrated increased Akt phosphorylation at the Serine residue S473 in miR-96 and miR-183 as well as only miR-96 overexpressing $CD4^+CD25^-$ T cells. Furthermore, knockdown of both miRNAs as well as only miR-96 resulted in decreased Akt phosphorylation at S473. Taken together, our study identifies miR-96 and miR-183 to be involved in $CD4^+CD25^-$ T cell activation and proliferation by targeting EGR-1 and thereby interfering with the PTEN-Akt signaling pathway.

Our results demonstrate that the combined overexpression or knockdown of miR-96 and miR-183 are able to affect the EGR-1-PTEN-Akt signaling pathway and thereby proliferation of $CD4^+$ T cells. However, overexpression of miR-96 alone was sufficient to cause the same effects, suggesting that miR-96 is the most potent member of the cluster facilitating the observed effect. This observation was made before in mice suffering from EAE. MiR-96 overexpression was more potent to induce pathogenic cytokine production in Th17 cells *in vitro* and those cells led to more severe EAE although miR-96 was not able to rescue Th17 cytokine production in miR-183 cluster-deficient mice (Ichiyama et al., 2016). Our *in vitro* data indicated stronger effects on EGR-1 and PTEN expression when both miRNAs were downregulated simultaneously. On this account, only T cells with a combined knockdown were used in the *in vivo* transfer model of antigen-specific autoimmune diabetes. Further *in vivo* experiments with overexpression or knockdown of one specific miRNA are necessary to better distinguish between their specific potential to induce autoimmune disease. Nevertheless, it cannot be excluded that only the modulation of all cluster members together has a beneficial effect, since miRNAs of polycistronic clusters have the capacity to compensate for each other (Mehta and Baltimore, 2016).

Since miR-96 and miR-183 expression was demonstrated to play a crucial role in Th17 pathogenicity in EAE (Ichiyama et al., 2016), it would be interesting to analyze the expression pattern of both miRNAs in different Th cell subtypes under polarizing

conditions *in vitro* as well as investigating Th cell-specific cytokines in the autoimmune diabetes mouse model *in vivo*.

Although our data clearly show that the miR-96 and miR-183-mediated effect on $CD4^+CD25^-$ T cell proliferation is driven by the EGR-1-PTEN-Akt pathway, we cannot exclude other additional mechanisms. Single miRNAs are known to interact with multiple targets and members of one cluster target different proteins within one specific cellular pathway (Mehta and Baltimore, 2016). Besides a variety of targets in cancer cell lines, members of the miR-183 cluster were described to target the transcription factor FoxO1 in $CD4^+$ T cells. FoxO1 was shown to be essential for T cell homeostasis and tolerance (Ouyang et al., 2010) and homing of human T cells (Fabre et al., 2008). Furthermore, FoxO1 was demonstrated to be pivotal for Treg function (Ouyang et al., 2012) and to negatively regulate Th17 response by RORγt inhibition (Laine et al., 2015). Moreover, maintenance of memory-effector T cells was described to be dependent on FoxO1 expression (Utzschneider et al., 2018). In Th17 cells, miR-183 cluster was described to target FoxO1 promoting Th17 pathogenicity (Ichiyama et al., 2016). In addition, miR-182-mediated suppression of FoxO1 was shown in activated Th cells (Stittrich et al., 2010). Hawse et al. demonstrated that the PTEN transcription is regulated by FoxO1. FoxO1 was able to interact with a binding site 5 kb upstream of the PTEN promoter in resting $CD4^+$ T cells and Tregs. The PI3K/Akt pathway is upstream of FoxO1 and Akt-mediated FoxO1 phosphorylation leads to a nuclear exclusion of the transcription factor. Through the regulation of FoxO1, Akt was also able to regulate PTEN expression (Hawse et al., 2015). Based on this data, the here presented regulation of the PTEN-Akt pathway, could not only rely on miR-96 and miR-183-mediated EGR-1 targeting but also on miR-96 and miR-183-associated FoxO1 modulation. Therefore, FoxO1 expression and phosphorylation should be investigated under gain- and loss-of-function conditions, to show if the transcription factor is also a target in $CD4^+CD25^-$ T cells used to induce autoimmune diabetes.

Nevertheless, our data clearly indicates that miR-96 and miR-183 regulate the activation of $CD4^+$ T cells *in vitro* and *in vivo* and might represent a potential therapeutic target for the treatment of T cell-mediated autoimmune disorders.

6.2 Nrp-1 in T cell-mediated autoimmune diabetes

The organ-specific autoimmune disorder T1D is caused by autoreactive T cells which promote the destruction of the pancreatic beta cells (Wang et al., 2017c). Under normal conditions, autoreactive T cells are regulated by different mechanisms of the peripheral tolerance. One mechanism is the suppression of effector T cells by Tregs. Among other

mechanisms, Tregs secret inhibitory cytokines, granzymes or modulate DC maturation to facilitate suppression (Vignali et al., 2008). The loss of suppressive capacity by Tregs promotes the development of autoimmune diseases (Theofilopoulos et al., 2017). The non-tyrosine kinase receptor Nrp-1 is a specific surface marker for murine $CD4^+CD25^+$ Tregs and correlates with their suppressive phenotype (Bruder et al., 2004). Furthermore, Nrp-1 on Tregs prolongs the interaction with immature DCs (Sarris et al., 2008). In the inflammatory microenvironment of tumors, Nrp-1 expression mediates the migration of Tregs along a VEGF gradient into the tumorous tissue (Hansen et al., 2012). This indicates the pivotal role for Nrp-1 expression on Tregs during inflammation which might also affect the development of T cell-mediated autoimmunity.

Spontaneous autoimmune diabetes is driven by antigen-specific $CD4^+$ T cells which recognize antigens presented in an organ-specific manner (Sarukhan et al., 1998). Here, we could demonstrate a trend towards an earlier onset of spontaneous autoimmune diabetes in mice which harbor a T cell-specific deletion of Nrp-1 expression, although similar percentages of mice with Nrp-1 expressing (INS-HAxTCR-HAxNrp-$1^{fl/fl}$) or Nrp-1-deficient T cells (INS-HAxTCR-HAxNrp-$1^{fl/fl}$xCD4cre) developed diabetes. Comparing non-diabetic and diabetic mice with Nrp-1-deficient T cells, diabetic mice had significantly more HA-specific T cells within the pancreas, explaining the pathology. Nrp-1 is a co-receptor for VEGF and Nrp-1-mediated migration towards a VEGF gradient was described to facilitate Treg infiltration into tumor microenvironment (Hansen et al., 2012). Since we did not found differences in the frequency of HA-specific $CD4^+$ T cells in mice harboring a T cell-specific deletion of Nrp-1 compared to mice with Nrp-1 expressing T cells, our results exclude migration along a VEGF gradient into pancreatic tissue. Nevertheless, further experiments are necessary to analyze the expression and secretion of VEGF or other Nrp-1 ligands by pancreatic tissue. In addition, we did not detect differences in the expression of the activation marker CD62L and the Treg-specific transcription factor FoxP3 between mice with Nrp-1-deficient or Nrp-1 wild type T cells. Tregs as well as T effector cells are affected by the Nrp-1 deletion in our mouse model of spontaneous autoimmune diabetes. Since Nrp-1 expression on Tregs is associated with their suppressive capacity (Bruder et al., 2004), we performed further experiments to analyze, if the Treg-specific Nrp-1 expression has an impact on the development of autoimmunity.

Tregs were demonstrated to play a pivotal part in the development of autoimmune diabetes. Within the pancreas, Tregs prevent a rapid progression of the disease (Sarukhan et al., 1998). To analyze the impact of Nrp-1 deficiency in Tregs on the

development of autoimmune diabetes in more detail, we used a co-transfer model to induce antigen-specific autoimmune diabetes in INS-HA x Rag2-KO mice. INS-HA x Rag2-KO mice transferred only with HA-specific effector T cells as well as mice which received a co-transfer of Nrp-1-deficient Tregs had a higher blood glucose level compared to mice which were additionally transferred with Nrp-1 wild type Tregs. Furthermore, in comparison to mice which received Nrp-1 wild type Tregs, mice co-transferred with Nrp-1-deficient Tregs had higher frequencies of HA-specific effector T cells in the pancreas and those cells were more activated within the spleen.

Our results indicate that Nrp-1-deficient Tregs were not able to suppress HA-specific effector T cells and thereby were not able to control the onset of diabetes as properly as Nrp-1 wild type Tregs. However, no difference in FoxP3 expression was detected between Nrp-1-deficient and Nrp-1 expressing Tregs. Similar expression of FoxP3 by Nrp-1-deficient and wild type $CD4^+CD25^+$ Tregs was described before in mouse melanoma models indicating no direct impact of Nrp-1 expression on their suppressive capacity (Hansen et al., 2012). Our results might be explained by the Nrp-1-dependent interaction of DCs and Tregs (Sarris et al., 2008). The deletion of Nrp-1 on Tregs might favor the interaction between DCs and effector T cells leading to increased activation. Furthermore, loss of Nrp-1 expression was described to result in IFNγ-driven Treg fragility and loss of suppressive activity without alterations in FoxP3 expression in the tumor microenvironment (Overacre-Delgoffe et al., 2017). Moreover, it was demonstrated that the infiltration of the pancreas during diabetes led to elevated IFNγ production (Sarukhan et al., 1998). To further define the functional abnormalities of Nrp-1-deficient Tregs which might lead to the observed phenotype, the expression of other Treg markers like PD-1, CD103 or CTLA-4 should be investigated. All three markers have been described to be essential for the suppressive capacity of Tregs and were upregulated on $CD4^+Nrp\text{-}1^{high}$ cells compared to $Nrp\text{-}1^{low}$ cells (Bruder et al., 2004). In addition, further experiments are necessary to analyze the pancreatic cytokine milieu and show whether Nrp-1-deficient Tregs are also influenced by IFNγ-mediated fragility during the development of antigen-specific autoimmune diabetes.

Furthermore, we detected no differences in the frequencies of HA-specific Tregs or in their proliferation between the two groups. These results might be due to homeostatic proliferation of T cells. The adoptive transfer of small populations of T cells into immune-deficient hosts like Rag-KO mice was demonstrated to induce spontaneous extensive proliferation (Rocha et al., 1989; Surh and Sprent, 2000). However, it was also reported that Treg numbers are not uniformly reduced in patients with autoimmune disorders and that the ratio of Tregs to effector T cells is one mechanism promoting

pathogenesis (Lu et al., 2017). Since Nrp-1^{+}FoxP3^{-} effector T cells were demonstrated to have an impaired proliferative capacity compared to Nrp-1^{-}FoxP3^{-} effector T cells (Tatura et al., 2015), it would also be interesting to analyze the influence of Nrp-1 expression on CD4^{+}CD25^{-} effector T cells on the development of antigen-specific autoimmune diabetes. Therefore, HA-specific Nrp-1-deficient and wild type effector T cells could be transferred into INS-HA x Rag2-KO mice and analyzed for their capacity to induce diabetes.

Our results on the impact of Nrp-1 expression on CD4^{+} T cell-mediated autoimmune disease provide first evidence that Nrp-1 expression on Tregs modulates inflammatory immune responses also in autoimmunity.

7 Abstract

Autoimmune diseases are caused by tissue damage in the presence of autoantibodies and self-reactive lymphocytes. The identification of target molecules that have an impact on the development of T cell-dependent autoimmunity is of special therapeutic interest.

Aberrant microRNA (miRNA) expression patterns in immune cells were described in many autoimmune disorders. MiRNAs are small non-coding transcripts that posttranscriptionally regulate gene expression by binding to complementary sites mostly in the 3`UTR of target mRNAs resulting in translational inhibition or degradation. However, the role of specific miRNAs in the regulation of T cell-mediated autoimmunity is still under investigation. Here, we identified miRNA-96 and miRNA-183 to be highly expressed in $CD4^+$ T cells of patients suffering from the severe autoimmune disease Graves' orbitopathy as well as in murine and human $CD4^+$ T cells upon activation *in vitro*. Therefore, we aimed to analyze the impact of both miRNAs on $CD4^+$ T cell function. By luciferase reporter gene assay EGR-1 was identified as a direct target of miR-96 and miR-183 in T cells. Retroviral overexpression of both miRNAs in $CD4^+CD25^-$ T cells resulted in decreased EGR-1 and PTEN expression accompanied by increased phosphorylation of Akt at S473 and enhanced proliferative capacity *in vitro*. The knockdown of both miRNAs in $CD4^+CD25^-$ T cells with specific antagomirs led to an increase in EGR-1 and PTEN expression, decreased Akt phosphorylation and proliferation *in vitro*. Adoptive transfer of antigen-specific miRNA-96/183 transduced T cells elicited a more severe autoimmune response in a murine diabetes model while the transfer of antagomir-treated T cells prolonged the onset of diabetes *in vivo.* Our results indicate that miRNA-96 and miR-183 modulate intracellular signaling in activated T cells and thereby are involved in regulation of T cell-mediated autoimmunity.

Neuropilin-1 (Nrp-1) is a specific cell surface marker for murine Tregs and was demonstrated to facilitate the VEGF-dependent migration of Tregs into tumor microenvironment. If this mechanism is specific for tumorous tissue or can be applied in general to other inflamed settings like autoimmunity is still elusive. Here, we showed that T cell-specific Nrp-1 deletion led to an earlier onset of spontaneous autoimmune diabetes *in vivo*. Furthermore, our results demonstrate that Nrp-1-deficient Tregs fail to control the onset of diabetes as properly as Nrp-1 expressing Tregs in a transfer model of antigen-specific autoimmune diabetes *in vivo*. Thus, our date provide first evidence that Nrp-1 expression on Tregs modulates inflammatory immune responses also in autoimmunity.

8 Zusammenfassung

Autoimmunkrankheiten entstehen durch Gewebeschäden in Folge von Autoantikörpern und selbstreaktiven Lymphozyten. Zum besseren Verständnis der Krankheitsbilder und zur Entwicklung möglicher Therapien, ist es von großem Interesse Moleküle zu identifizieren, die an der Entstehung von T-Zell-vermittelter Autoimmunität beteiligt sind. Die Veränderung von microRNA (miRNAs) Expressionsmustern in Immunzellen steht im Zusammenhang mit einigen Autoimmunerkrankungen. Bei miRNAs handelt es sich um kurze, nicht-proteinkodierende Transkripte, die an der posttranskriptionalen Regulierung von Genen beteiligt sind. MiRNAs binden meist an komplementäre Bereiche in der 3'UTR ihrer Ziel-mRNA. Als Folge dieser Bindung kommt es entweder zur Inhibierung der Translation oder zum Abbau der mRNA.

Die hier präsentierten Ergebnisse zeigen, dass $CD4^+$ T-Zellen von Patienten mit schwerer endokrine Orbitopathie eine erhöhte Expression von miR-96 und miR-183 aufweisen. Zu diesem Anstieg kam es auch in murinen und humanen $CD4^+CD25^-$ T-Zellen nach Aktivierung *in vitro*. Um den Einfluss beider miRNAs auf die Funktion von $CD4^+$ T-Zellen zu untersuchen, wurden die miRNAs zum einen mittels retroviralem Gentransfer überexprimiert und zum anderen durch Antagomirs herunterreguliert. In einem Luciferase Reporter Gen Assay konnten wir EGR-1 als Ziel-mRNA von miR-96 und miR-183 identifizieren. T-Zellen, welche die beiden miRNAs überexprimieren wiesen eine verringerte Expression von EGR-1 und PTEN, sowie eine erhöhte Phosphorylierung von Akt und gesteigerte proliferative Aktivität auf. Umgekehrt konnten wir zeigen, dass die verringerte Expression von miR-96 und miR-183 zur erhöhten Expression von EGR-1 und PTEN, gefolgt von verringerter Akt Phosphorylierung und geringerer Proliferation in $CD4^+CD25^-$ T Zellen führte. In einem Mausmodel für Antigen-spezifischen Autoimmun-Diabetes führte der Transfer von miRNA-überexprimierenden Effektorzellen zur Beschleunigung des Krankheitsverlaufes während der Transfer von T-Zellen mit verringerter miRNA Expression den Beginn der Krankheit hinauszögerte. Unsere Ergebnisse zeigen, dass miR-96 und miR-183 an der Regulation der T-Zell Aktivierung beteiligt sind und somit auch bei der T-Zell-vermittelten Autoimmunität eine entscheidende Rolle spielen.

Neuropillin-1 (Nrp-1) ist ein spezifischer Marker für murine regulatorische T-Zellen (Tregs) und vermittelt die Migration entlang eines VEGF-Gradienten ins Tumorgewebe. Ob es sich hierbei um einen Tumor-spezifischen oder generellen Mechanismus handelt, der auch auf andere Entzündungsreaktionen übertragbar ist, ist noch nicht beschrieben. Unsere Ergebnisse weisen darauf hin, dass die Deletion von Nrp-1 in der gesamten T-Zell Population die Entstehung von Autoimmun-Diabetes beschleunigt.

Des Weiteren, scheinen Nrp-1-defiziente Tregs, die Entstehung von Autoimmun-Diabetes schlechter zu kontrollieren. Diese Ergebnisse geben erste Hinweise, dass die Expression von Nrp-1 auf Tregs wichtig für die generelle Kontrolle von Immunreaktionen ist.

9 References

Alessi, D.R., Andjelkovic, M., Caudwell, B., Cron, P., Morrice, N., Cohen, P., and Hemmings, B.A. (1996). Mechanism of activation of protein kinase B by insulin and IGF-1. EMBO J *15*, 6541-6551.

Bahn, R.S. (2010). Graves' ophthalmopathy. N Engl J Med *362*, 726-738.

Baik, S.H., Lee, J., Lee, Y.S., Jang, J.Y., and Kim, C.W. (2016). ANT2 shRNA downregulates miR-19a and miR-96 through the PI3K/Akt pathway and suppresses tumor growth in hepatocellular carcinoma cells. Exp Mol Med *48*, e222.

Battaglia, A., Buzzonetti, A., Monego, G., Peri, L., Ferrandina, G., Fanfani, F., Scambia, G., and Fattorossi, A. (2008). Neuropilin-1 expression identifies a subset of regulatory T cells in human lymph nodes that is modulated by preoperative chemoradiation therapy in cervical cancer. Immunology *123*, 129-138.

Blevins, R., Bruno, L., Carroll, T., Elliott, J., Marcais, A., Loh, C., Hertweck, A., Krek, A., Rajewsky, N., Chen, C.Z.*, et al.* (2015). microRNAs regulate cell-to-cell variability of endogenous target gene expression in developing mouse thymocytes. PLoS Genet *11*, e1005020.

Bopp, T., Becker, C., Klein, M., Klein-Hessling, S., Palmetshofer, A., Serfling, E., Heib, V., Becker, M., Kubach, J., Schmitt, S.*, et al.* (2007). Cyclic adenosine monophosphate is a key component of regulatory T cell-mediated suppression. J Exp Med *204*, 1303-1310.

Bruder, D., Probst-Kepper, M., Westendorf, A.M., Geffers, R., Beissert, S., Loser, K., von Boehmer, H., Buer, J., and Hansen, W. (2004). Neuropilin-1: a surface marker of regulatory T cells. Eur J Immunol *34*, 623-630.

Bruder, D., Westendorf, A.M., Hansen, W., Prettin, S., Gruber, A.D., Qian, Y., von Boehmer, H., Mahnke, K., and Buer, J. (2005). On the edge of autoimmunity: T-cell stimulation by steady-state dendritic cells prevents autoimmune diabetes. Diabetes *54*, 3395-3401.

Campos-Mora, M., Morales, R.A., Perez, F., Gajardo, T., Campos, J., Catalan, D., Aguillon, J.C., and Pino-Lagos, K. (2015). Neuropilin-1+ regulatory T cells promote skin allograft survival and modulate effector CD4+ T cells phenotypic signature. Immunol Cell Biol *93*, 113-119.

Cao, L.L., Xie, J.W., Lin, Y., Zheng, C.H., Li, P., Wang, J.B., Lin, J.X., Lu, J., Chen, Q.Y., and Huang, C.M. (2014). miR-183 inhibits invasion of gastric cancer by targeting Ezrin. Int J Clin Exp Pathol *7*, 5582-5594.

Chaudhary, B., and Elkord, E. (2015). Novel expression of Neuropilin 1 on human tumor-infiltrating lymphocytes in colorectal cancer liver metastases. Expert Opin Ther Targets *19*, 147-161.

Chen, J., Tian, J., Tang, X., Rui, K., Ma, J., Mao, C., Liu, Y., Lu, L., Xu, H., and Wang, S. (2015). MiR-346 regulates CD4(+)CXCR5(+) T cells in the pathogenesis of Graves' disease. Endocrine *49*, 752-760.

Chen, Z., and O'Shea, J.J. (2008). Th17 cells: a new fate for differentiating helper T cells. Immunol Res *41*, 87-102.

Cheng, Y., Xiang, G., Meng, Y., and Dong, R. (2016). MiRNA-183-5p promotes cell proliferation and inhibits apoptosis in human breast cancer by targeting the PDCD4. Reprod Biol *16*, 225-233.

Cibrian, D., and Sanchez-Madrid, F. (2017). CD69: from activation marker to metabolic gatekeeper. Eur J Immunol *47*, 946-953.

Cobb, B.S., Nesterova, T.B., Thompson, E., Hertweck, A., O'Connor, E., Godwin, J., Wilson, C.B., Brockdorff, N., Fisher, A.G., Smale, S.T.*, et al.* (2005). T cell lineage choice and differentiation in the absence of the RNase III enzyme Dicer. J Exp Med *201*, 1367-1373.

Conde, M., Montano, R., Moreno-Aurioles, V.R., Ramirez, R., Sanchez-Mateos, P., Sanchez-Madrid, F., and Sobrino, F. (1996). Anti-CD69 antibodies enhance phorbol-dependent glucose metabolism and Ca2+ levels in human thymocytes. Antagonist effect of cyclosporin A. J Leukoc Biol *60*, 278-284.

Corbel, C., Lemarchandel, V., Thomas-Vaslin, V., Pelus, A.S., Agboton, C., and Romeo, P.H. (2007). Neuropilin 1 and CD25 co-regulation during early murine thymic differentiation. Dev Comp Immunol *31*, 1082-1094.

Curtale, G., Citarella, F., Carissimi, C., Goldoni, M., Carucci, N., Fulci, V., Franceschini, D., Meloni, F., Barnaba, V., and Macino, G. (2010). An emerging player in the adaptive immune response: microRNA-146a is a modulator of IL-2 expression and activation-induced cell death in T lymphocytes. Blood *115*, 265-273.

Dai, R., McReynolds, S., Leroith, T., Heid, B., Liang, Z., and Ahmed, S.A. (2013). Sex differences in the expression of lupus-associated miRNAs in splenocytes from lupus-prone NZB/WF1 mice. Biol Sex Differ *4*, 19.

Dai, R., Zhang, Y., Khan, D., Heid, B., Caudell, D., Crasta, O., and Ahmed, S.A. (2010). Identification of a common lupus disease-associated microRNA expression pattern in three different murine models of lupus. PLoS One *5*, e14302.

Dambal, S., Shah, M., Mihelich, B., and Nonn, L. (2015). The microRNA-183 cluster: the family that plays together stays together. Nucleic Acids Res *43*, 7173-7188.

Delgoffe, G.M., Woo, S.R., Turnis, M.E., Gravano, D.M., Guy, C., Overacre, A.E., Bettini, M.L., Vogel, P., Finkelstein, D., Bonnevier, J.*, et al.* (2013). Stability and function of regulatory T cells is maintained by a neuropilin-1-semaphorin-4a axis. Nature *501*, 252-256.

Donatelli, S.S., Zhou, J.M., Gilvary, D.L., Eksioglu, E.A., Chen, X., Cress, W.D., Haura, E.B., Schabath, M.B., Coppola, D., Wei, S.*, et al.* (2014). TGF-beta-inducible microRNA-183 silences tumor-associated natural killer cells. Proc Natl Acad Sci U S A *111*, 4203-4208.

Dudda, J.C., Salaun, B., Ji, Y., Palmer, D.C., Monnot, G.C., Merck, E., Boudousquie, C., Utzschneider, D.T., Escobar, T.M., Perret, R.*, et al.* (2013). MicroRNA-155 is required for effector CD8+ T cell responses to virus infection and cancer. Immunity *38*, 742-753.

Ellis, L.M. (2006). The role of neuropilins in cancer. Mol Cancer Ther *5*, 1099-1107.

Fabre, S., Carrette, F., Chen, J., Lang, V., Semichon, M., Denoyelle, C., Lazar, V., Cagnard, N., Dubart-Kupperschmitt, A., Mangeney, M.*, et al.* (2008). FOXO1 regulates

L-Selectin and a network of human T cell homing molecules downstream of phosphatidylinositol 3-kinase. J Immunol *181*, 2980-2989.

Feldon, S.E., Park, D.J., O'Loughlin, C.W., Nguyen, V.T., Landskroner-Eiger, S., Chang, D., Thatcher, T.H., and Phipps, R.P. (2005). Autologous T-lymphocytes stimulate proliferation of orbital fibroblasts derived from patients with Graves' ophthalmopathy. Invest Ophthalmol Vis Sci *46*, 3913-3921.

Fendler, A., Jung, M., Stephan, C., Erbersdobler, A., Jung, K., and Yousef, G.M. (2013). The antiapoptotic function of miR-96 in prostate cancer by inhibition of FOXO1. PLoS One *8*, e80807.

Ferraro, B., Bepler, G., Sharma, S., Cantor, A., and Haura, E.B. (2005). EGR1 predicts PTEN and survival in patients with non-small-cell lung cancer. J Clin Oncol *23*, 1921-1926.

Finetti, F., and Baldari, C.T. (2018). The immunological synapse as a pharmacological target. Pharmacol Res *134*, 118-133.

Fontenot, J.D., Gavin, M.A., and Rudensky, A.Y. (2003). Foxp3 programs the development and function of CD4+CD25+ regulatory T cells. Nat Immunol *4*, 330-336.

Garo, L.P., and Murugaiyan, G. (2016). Contribution of MicroRNAs to autoimmune diseases. Cell Mol Life Sci *73*, 2041-2051.

Ghisi, M., Corradin, A., Basso, K., Frasson, C., Serafin, V., Mukherjee, S., Mussolin, L., Ruggero, K., Bonanno, L., Guffanti, A.*, et al.* (2011). Modulation of microRNA expression in human T-cell development: targeting of NOTCH3 by miR-150. Blood *117*, 7053-7062.

Glinka, Y., and Prud'homme, G.J. (2008). Neuropilin-1 is a receptor for transforming growth factor beta-1, activates its latent form, and promotes regulatory T cell activity. J Leukoc Biol *84*, 302-310.

Gotot, J., Dhana, E., Yagita, H., Kaiser, R., Ludwig-Portugall, I., and Kurts, C. (2018). Antigen-specific Helios(-) , Neuropilin-1(-) Tregs induce apoptosis of autoreactive B cells via PD-L1. Immunol Cell Biol.

Gregory, S.H., and Wing, E.J. (1993). IFN-gamma inhibits the replication of Listeria monocytogenes in hepatocytes. J Immunol *151*, 1401-1409.

Gu, C., Rodriguez, E.R., Reimert, D.V., Shu, T., Fritzsch, B., Richards, L.J., Kolodkin, A.L., and Ginty, D.D. (2003). Neuropilin-1 conveys semaphorin and VEGF signaling during neural and cardiovascular development. Dev Cell *5*, 45-57.

Haflidadottir, B.S., Larne, O., Martin, M., Persson, M., Edsjo, A., Bjartell, A., and Ceder, Y. (2013). Upregulation of miR-96 enhances cellular proliferation of prostate cancer cells through FOXO1. PLoS One *8*, e72400.

Haftmann, C., Riedel, R., Porstner, M., Wittmann, J., Chang, H.D., Radbruch, A., and Mashreghi, M.F. (2015). Direct uptake of Antagomirs and efficient knockdown of miRNA in primary B and T lymphocytes. J Immunol Methods *426*, 128-133.

Hammond, S.M., Boettcher, S., Caudy, A.A., Kobayashi, R., and Hannon, G.J. (2001). Argonaute2, a link between genetic and biochemical analyses of RNAi. Science *293*, 1146-1150.

Hansen, W., Hutzler, M., Abel, S., Alter, C., Stockmann, C., Kliche, S., Albert, J., Sparwasser, T., Sakaguchi, S., Westendorf, A.M.*, et al.* (2012). Neuropilin 1 deficiency on CD4+Foxp3+ regulatory T cells impairs mouse melanoma growth. J Exp Med *209*, 2001-2016.

Hardin, J.A., and Mimori, T. (1985). Autoantibodies to ribonucleoproteins. Clin Rheum Dis *11*, 485-505.

Hawse, W.F., Sheehan, R.P., Miskov-Zivanov, N., Menk, A.V., Kane, L.P., Faeder, J.R., and Morel, P.A. (2015). Cutting Edge: Differential Regulation of PTEN by TCR, Akt, and FoxO1 Controls CD4+ T Cell Fate Decisions. J Immunol *194*, 4615-4619.

Hou, T., Liao, J., Zhang, C., Sun, C., Li, X., and Wang, G. (2018). Elevated expression of miR-146, miR-139 and miR-340 involved in regulating Th1/Th2 balance with acute exposure of fine particulate matter in mice. Int Immunopharmacol *54*, 68-77.

Hu, R., Huffaker, T.B., Kagele, D.A., Runtsch, M.C., Bake, E., Chaudhuri, A.A., Round, J.L., and O'Connell, R.M. (2013). MicroRNA-155 confers encephalogenic potential to Th17 cells by promoting effector gene expression. J Immunol *190*, 5972-5980.

Huangfu, L., Liang, H., Wang, G., Su, X., Li, L., Du, Z., Hu, M., Dong, Y., Bai, X., Liu, T.*, et al.* (2016). miR-183 regulates autophagy and apoptosis in colorectal cancer through targeting of UVRAG. Oncotarget *7*, 4735-4745.

Ichiyama, K., Gonzalez-Martin, A., Kim, B.S., Jin, H.Y., Jin, W., Xu, W., Sabouri-Ghomi, M., Xu, S., Zheng, P., Xiao, C.*, et al.* (2016). The MicroRNA-183-96-182 Cluster Promotes T Helper 17 Cell Pathogenicity by Negatively Regulating Transcription Factor Foxo1 Expression. Immunity *44*, 1284-1298.

Ishida, M., and Selaru, F.M. (2013). miRNA-Based Therapeutic Strategies. Curr Anesthesiol Rep *1*, 63-70.

Iwasaki, A., and Medzhitov, R. (2015). Control of adaptive immunity by the innate immune system. Nat Immunol *16*, 343-353.

Jacinto, E., Facchinetti, V., Liu, D., Soto, N., Wei, S., Jung, S.Y., Huang, Q., Qin, J., and Su, B. (2006). SIN1/MIP1 maintains rictor-mTOR complex integrity and regulates Akt phosphorylation and substrate specificity. Cell *127*, 125-137.

Jang, S.Y., Chae, M.K., Lee, J.H., Lee, E.J., and Yoon, J.S. (2016). Role of miR-146a in the Regulation of Inflammation in an In Vitro Model of Graves' Orbitopathy. Invest Ophthalmol Vis Sci *57*, 4027-4034.

Jia, L., Luo, S., Ren, X., Li, Y., Hu, J., Liu, B., Zhao, L., Shan, Y., and Zhou, H. (2017). miR-182 and miR-135b Mediate the Tumorigenesis and Invasiveness of Colorectal Cancer Cells via Targeting ST6GALNAC2 and PI3K/AKT Pathway. Dig Dis Sci *62*, 3447-3459.

Jiang, S., Li, C., Olive, V., Lykken, E., Feng, F., Sevilla, J., Wan, Y., He, L., and Li, Q.J. (2011). Molecular dissection of the miR-17-92 cluster's critical dual roles in promoting Th1 responses and preventing inducible Treg differentiation. Blood *118*, 5487-5497.

Jin, Z.B., Hirokawa, G., Gui, L., Takahashi, R., Osakada, F., Hiura, Y., Takahashi, M., Yasuhara, O., and Iwai, N. (2009). Targeted deletion of miR-182, an abundant retinal microRNA. Mol Vis *15*, 523-533.

Jindra, P.T., Bagley, J., Godwin, J.G., and Iacomini, J. (2010). Costimulation-dependent expression of microRNA-214 increases the ability of T cells to proliferate by targeting Pten. J Immunol *185*, 990-997.

Keene, J.A., and Forman, J. (1982). Helper activity is required for the in vivo generation of cytotoxic T lymphocytes. J Exp Med *155*, 768-782.

Khvorova, A., Reynolds, A., and Jayasena, S.D. (2003). Functional siRNAs and miRNAs exhibit strand bias. Cell *115*, 209-216.

Kirberg, J., Baron, A., Jakob, S., Rolink, A., Karjalainen, K., and von Boehmer, H. (1994). Thymic selection of CD8+ single positive cells with a class II major histocompatibility complex-restricted receptor. J Exp Med *180*, 25-34.

Krutzfeldt, J., Rajewsky, N., Braich, R., Rajeev, K.G., Tuschl, T., Manoharan, M., and Stoffel, M. (2005). Silencing of microRNAs in vivo with 'antagomirs'. Nature *438*, 685-689.

Kumar, B.V., Connors, T.J., and Farber, D.L. (2018). Human T Cell Development, Localization, and Function throughout Life. Immunity *48*, 202-213.

Kurosaki, T., Kometani, K., and Ise, W. (2015). Memory B cells. Nat Rev Immunol *15*, 149-159.

Kye, M.J., Niederst, E.D., Wertz, M.H., Goncalves Ido, C., Akten, B., Dover, K.Z., Peters, M., Riessland, M., Neveu, P., Wirth, B.*, et al.* (2014). SMN regulates axonal local translation via miR-183/mTOR pathway. Hum Mol Genet *23*, 6318-6331.

Lagos-Quintana, M., Rauhut, R., Yalcin, A., Meyer, J., Lendeckel, W., and Tuschl, T. (2002). Identification of tissue-specific microRNAs from mouse. Curr Biol *12*, 735-739.

Laine, A., Martin, B., Luka, M., Mir, L., Auffray, C., Lucas, B., Bismuth, G., and Charvet, C. (2015). Foxo1 Is a T Cell-Intrinsic Inhibitor of the RORgammat-Th17 Program. J Immunol *195*, 1791-1803.

Larne, O., Ostling, P., Haflidadottir, B.S., Hagman, Z., Aakula, A., Kohonen, P., Kallioniemi, O., Edsjo, A., Bjartell, A., Lilja, H.*, et al.* (2015). miR-183 in prostate cancer cells positively regulates synthesis and serum levels of prostate-specific antigen. Eur Urol *68*, 581-588.

Lee, P.P., Fitzpatrick, D.R., Beard, C., Jessup, H.K., Lehar, S., Makar, K.W., Perez-Melgosa, M., Sweetser, M.T., Schlissel, M.S., Nguyen, S.*, et al.* (2001). A critical role for Dnmt1 and DNA methylation in T cell development, function, and survival. Immunity *15*, 763-774.

Lee, R.C., Feinbaum, R.L., and Ambros, V. (1993). The C. elegans heterochronic gene lin-4 encodes small RNAs with antisense complementarity to lin-14. Cell *75*, 843-854.

Lee, Y., Ahn, C., Han, J., Choi, H., Kim, J., Yim, J., Lee, J., Provost, P., Radmark, O., Kim, S.*, et al.* (2003). The nuclear RNase III Drosha initiates microRNA processing. Nature *425*, 415-419.

Lepelletier, Y., Moura, I.C., Hadj-Slimane, R., Renand, A., Fiorentino, S., Baude, C., Shirvan, A., Barzilai, A., and Hermine, O. (2006). Immunosuppressive role of semaphorin-3A on T cell proliferation is mediated by inhibition of actin cytoskeleton reorganization. Eur J Immunol *36*, 1782-1793.

Leung, W.K., He, M., Chan, A.W., Law, P.T., and Wong, N. (2015). Wnt/beta-Catenin activates MiR-183/96/182 expression in hepatocellular carcinoma that promotes cell invasion. Cancer Lett *362*, 97-105.

Li, B., Wang, X., Choi, I.Y., Wang, Y.C., Liu, S., Pham, A.T., Moon, H., Smith, D.J., Rao, D.S., Boldin, M.P.*, et al.* (2017). miR-146a modulates autoreactive Th17 cell differentiation and regulates organ-specific autoimmunity. J Clin Invest *127*, 3702-3716.

Li, P., Sheng, C., Huang, L., Zhang, H., Huang, L., Cheng, Z., and Zhu, Q. (2014). MiR-183/-96/-182 cluster is up-regulated in most breast cancers and increases cell proliferation and migration. Breast Cancer Res *16*, 473.

Li, Q.J., Chau, J., Ebert, P.J., Sylvester, G., Min, H., Liu, G., Braich, R., Manoharan, M., Soutschek, J., Skare, P.*, et al.* (2007). miR-181a is an intrinsic modulator of T cell sensitivity and selection. Cell *129*, 147-161.

Lin, H., Dai, T., Xiong, H., Zhao, X., Chen, X., Yu, C., Li, J., Wang, X., and Song, L. (2010). Unregulated miR-96 induces cell proliferation in human breast cancer by downregulating transcriptional factor FOXO3a. PLoS One *5*, e15797.

Linette, G.P., Grusby, M.J., Hedrick, S.M., Hansen, T.H., Glimcher, L.H., and Korsmeyer, S.J. (1994). Bcl-2 is upregulated at the CD4+ CD8+ stage during positive selection and promotes thymocyte differentiation at several control points. Immunity *1*, 197-205.

Liston, A., Lu, L.F., O'Carroll, D., Tarakhovsky, A., and Rudensky, A.Y. (2008). Dicer-dependent microRNA pathway safeguards regulatory T cell function. J Exp Med *205*, 1993-2004.

Liu, S.Q., Jiang, S., Li, C., Zhang, B., and Li, Q.J. (2014). miR-17-92 cluster targets phosphatase and tensin homology and Ikaros Family Zinc Finger 4 to promote TH17-mediated inflammation. J Biol Chem *289*, 12446-12456.

Liu, X., Karnell, J.L., Yin, B., Zhang, R., Zhang, J., Li, P., Choi, Y., Maltzman, J.S., Pear, W.S., Bassing, C.H.*, et al.* (2010). Distinct roles for PTEN in prevention of T cell lymphoma and autoimmunity in mice. J Clin Invest *120*, 2497-2507.

Lo, D., Freedman, J., Hesse, S., Palmiter, R.D., Brinster, R.L., and Sherman, L.A. (1992). Peripheral tolerance to an islet cell-specific hemagglutinin transgene affects both CD4+ and CD8+ T cells. Eur J Immunol *22*, 1013-1022.

Lu, L., Barbi, J., and Pan, F. (2017). The regulation of immune tolerance by FOXP3. Nat Rev Immunol *17*, 703-717.

Lu, L.F., Boldin, M.P., Chaudhry, A., Lin, L.L., Taganov, K.D., Hanada, T., Yoshimura, A., Baltimore, D., and Rudensky, A.Y. (2010). Function of miR-146a in controlling Treg cell-mediated regulation of Th1 responses. Cell *142*, 914-929.

Macian, F., Im, S.H., Garcia-Cozar, F.J., and Rao, A. (2004). T-cell anergy. Curr Opin Immunol *16*, 209-216.

Mackay, L.K., Braun, A., Macleod, B.L., Collins, N., Tebartz, C., Bedoui, S., Carbone, F.R., and Gebhardt, T. (2015). Cutting edge: CD69 interference with sphingosine-1-phosphate receptor function regulates peripheral T cell retention. J Immunol *194*, 2059-2063.

Marcais, A., Blevins, R., Graumann, J., Feytout, A., Dharmalingam, G., Carroll, T., Amado, I.F., Bruno, L., Lee, K., Walzer, T.*, et al.* (2014). microRNA-mediated regulation of mTOR complex components facilitates discrimination between activation and anergy in CD4 T cells. J Exp Med *211*, 2281-2295.

Marie-Cardine, A., and Schraven, B. (1999). Coupling the TCR to downstream signalling pathways: the role of cytoplasmic and transmembrane adaptor proteins. Cell Signal *11*, 705-712.

Markowitz, D., Hesdorffer, C., Ward, M., Goff, S., and Bank, A. (1990). Retroviral gene transfer using safe and efficient packaging cell lines. Ann N Y Acad Sci *612*, 407-414.

Martin, P., Gomez, M., Lamana, A., Cruz-Adalia, A., Ramirez-Huesca, M., Ursa, M.A., Yanez-Mo, M., and Sanchez-Madrid, F. (2010). CD69 association with Jak3/Stat5 proteins regulates Th17 cell differentiation. Mol Cell Biol *30*, 4877-4889.

Martinez-Hernandez, R., Sampedro-Nunez, M., Serrano-Somavilla, A., Ramos-Levi, A.M., de la Fuente, H., Trivino, J.C., Sanz-Garcia, A., Sanchez-Madrid, F., and Marazuela, M. (2018). A MicroRNA Signature for Evaluation of Risk and Severity of Autoimmune Thyroid Diseases. J Clin Endocrinol Metab *103*, 1139-1150.

McComb, S., Thiriot, A., Krishnan, L., and Stark, F. (2013). Introduction to the immune system. Methods Mol Biol *1061*, 1-20.

Mehta, A., and Baltimore, D. (2016). MicroRNAs as regulatory elements in immune system logic. Nat Rev Immunol *16*, 279-294.

Meister, G., Landthaler, M., Patkaniowska, A., Dorsett, Y., Teng, G., and Tuschl, T. (2004). Human Argonaute2 mediates RNA cleavage targeted by miRNAs and siRNAs. Mol Cell *15*, 185-197.

Mihelich, B.L., Khramtsova, E.A., Arva, N., Vaishnav, A., Johnson, D.N., Giangreco, A.A., Martens-Uzunova, E., Bagasra, O., Kajdacsy-Balla, A., and Nonn, L. (2011). miR-183-96-182 cluster is overexpressed in prostate tissue and regulates zinc homeostasis in prostate cells. J Biol Chem *286*, 44503-44511.

Milpied, P., Renand, A., Bruneau, J., Mendes-da-Cruz, D.A., Jacquelin, S., Asnafi, V., Rubio, M.T., MacIntyre, E., Lepelletier, Y., and Hermine, O. (2009). Neuropilin-1 is not a marker of human Foxp3+ Treg. Eur J Immunol *39*, 1466-1471.

Montoya, M.C., Sancho, D., Vicente-Manzanares, M., and Sanchez-Madrid, F. (2002). Cell adhesion and polarity during immune interactions. Immunol Rev *186*, 68-82.

Muljo, S.A., Ansel, K.M., Kanellopoulou, C., Livingston, D.M., Rao, A., and Rajewsky, K. (2005). Aberrant T cell differentiation in the absence of Dicer. J Exp Med *202*, 261-269.

Murphy, K., Travers, P., Walport, M., and Janeway, C. (2012). Janeway's immunobiology, 8th edn (New York: Garland Science).

Myers, M.P., Pass, I., Batty, I.H., Van der Kaay, J., Stolarov, J.P., Hemmings, B.A., Wigler, M.H., Downes, C.P., and Tonks, N.K. (1998). The lipid phosphatase activity of PTEN is critical for its tumor supressor function. Proc Natl Acad Sci U S A *95*, 13513-13518.

Nagata, S. (1996). Fas-mediated apoptosis. Adv Exp Med Biol *406*, 119-124.

Nauciel, C. (1995). [Defense mechanisms against bacteria of intracellular development]. Presse Med *24*, 129-132.

Nitta, T., and Suzuki, H. (2016). Thymic stromal cell subsets for T cell development. Cell Mol Life Sci *73*, 1021-1037.

Nutt, S.L., Hodgkin, P.D., Tarlinton, D.M., and Corcoran, L.M. (2015). The generation of antibody-secreting plasma cells. Nat Rev Immunol *15*, 160-171.

Okamura, H., Yoshida, K., Morimoto, H., and Haneji, T. (2005). PTEN expression elicited by EGR-1 transcription factor in calyculin A-induced apoptotic cells. J Cell Biochem *94*, 117-125.

Ouyang, W., Beckett, O., Ma, Q., Paik, J.H., DePinho, R.A., and Li, M.O. (2010). Foxo proteins cooperatively control the differentiation of Foxp3+ regulatory T cells. Nat Immunol *11*, 618-627.

Ouyang, W., Liao, W., Luo, C.T., Yin, N., Huse, M., Kim, M.V., Peng, M., Chan, P., Ma, Q., Mo, Y.*, et al.* (2012). Novel Foxo1-dependent transcriptional programs control T(reg) cell function. Nature *491*, 554-559.

Overacre-Delgoffe, A.E., Chikina, M., Dadey, R.E., Yano, H., Brunazzi, E.A., Shayan, G., Horne, W., Moskovitz, J.M., Kolls, J.K., Sander, C.*, et al.* (2017). Interferon-gamma Drives Treg Fragility to Promote Anti-tumor Immunity. Cell *169*, 1130-1141 e1111.

Prud'homme, G.J., and Glinka, Y. (2012). Neuropilins are multifunctional coreceptors involved in tumor initiation, growth, metastasis and immunity. Oncotarget *3*, 921-939.

Pucella, J.N., Yen, W.F., Kim, M.V., van der Veeken, J., Luo, C.T., Socci, N.D., Naito, Y., Li, M.O., Iwai, N., and Chaudhuri, J. (2015). miR-182 is largely dispensable for adaptive immunity: lack of correlation between expression and function. J Immunol *194*, 2635-2642.

Qin, Q., Wang, X., Yan, N., Song, R.H., Cai, T.T., Zhang, W., Guan, L.J., Muhali, F.S., and Zhang, J.A. (2015). Aberrant expression of miRNA and mRNAs in lesioned tissues of Graves' disease. Cell Physiol Biochem *35*, 1934-1942.

Rocha, B., Dautigny, N., and Pereira, P. (1989). Peripheral T lymphocytes: expansion potential and homeostatic regulation of pool sizes and CD4/CD8 ratios in vivo. Eur J Immunol *19*, 905-911.

Rodriguez, A., Vigorito, E., Clare, S., Warren, M.V., Couttet, P., Soond, D.R., van Dongen, S., Grocock, R.J., Das, P.P., Miska, E.A.*, et al.* (2007). Requirement of bic/microRNA-155 for normal immune function. Science *316*, 608-611.

Roy, S., Bag, A.K., Singh, R.K., Talmadge, J.E., Batra, S.K., and Datta, K. (2017). Multifaceted Role of Neuropilins in the Immune System: Potential Targets for Immunotherapy. Front Immunol *8*, 1228.

Russell, J.H., and Ley, T.J. (2002). Lymphocyte-mediated cytotoxicity. Annu Rev Immunol *20*, 323-370.

Sarris, M., Andersen, K.G., Randow, F., Mayr, L., and Betz, A.G. (2008). Neuropilin-1 expression on regulatory T cells enhances their interactions with dendritic cells during antigen recognition. Immunity *28*, 402-413.

Sarukhan, A., Lanoue, A., Franzke, A., Brousse, N., Buer, J., and von Boehmer, H. (1998). Changes in function of antigen-specific lymphocytes correlating with progression towards diabetes in a transgenic model. EMBO J *17*, 71-80.

Sarver, A.L., Li, L., and Subramanian, S. (2010). MicroRNA miR-183 functions as an oncogene by targeting the transcription factor EGR1 and promoting tumor cell migration. Cancer Res *70*, 9570-9580.

Shinkai, Y., Rathbun, G., Lam, K.P., Oltz, E.M., Stewart, V., Mendelsohn, M., Charron, J., Datta, M., Young, F., Stall, A.M*., et al.* (1992). RAG-2-deficient mice lack mature lymphocytes owing to inability to initiate V(D)J rearrangement. Cell *68*, 855-867.

Shiow, L.R., Rosen, D.B., Brdickova, N., Xu, Y., An, J., Lanier, L.L., Cyster, J.G., and Matloubian, M. (2006). CD69 acts downstream of interferon-alpha/beta to inhibit S1P1 and lymphocyte egress from lymphoid organs. Nature *440*, 540-544.

Shipkova, M., and Wieland, E. (2012). Surface markers of lymphocyte activation and markers of cell proliferation. Clin Chim Acta *413*, 1338-1349.

Shrestha, S., Yang, K., Guy, C., Vogel, P., Neale, G., and Chi, H. (2015). Treg cells require the phosphatase PTEN to restrain TH1 and TFH cell responses. Nat Immunol *16*, 178-187.

Silverman, E.S., and Collins, T. (1999). Pathways of Egr-1-mediated gene transcription in vascular biology. Am J Pathol *154*, 665-670.

Singer, A., Adoro, S., and Park, J.H. (2008). Lineage fate and intense debate: myths, models and mechanisms of CD4- versus CD8-lineage choice. Nat Rev Immunol *8*, 788-801.

Siu, M.K., Tsai, Y.C., Chang, Y.S., Yin, J.J., Suau, F., Chen, W.Y., and Liu, Y.N. (2015). Transforming growth factor-beta promotes prostate bone metastasis through induction of microRNA-96 and activation of the mTOR pathway. Oncogene *34*, 4767-4776.

Smigielska-Czepiel, K., van den Berg, A., Jellema, P., Slezak-Prochazka, I., Maat, H., van den Bos, H., van der Lei, R.J., Kluiver, J., Brouwer, E., Boots, A.M*., et al.* (2013). Dual role of miR-21 in CD4+ T-cells: activation-induced miR-21 supports survival of memory T-cells and regulates CCR7 expression in naive T-cells. PLoS One *8*, e76217.

So, T., and Croft, M. (2013). Regulation of PI-3-Kinase and Akt Signaling in T Lymphocytes and Other Cells by TNFR Family Molecules. Front Immunol *4*, 139.

Sonkoly, E., Janson, P., Majuri, M.L., Savinko, T., Fyhrquist, N., Eidsmo, L., Xu, N., Meisgen, F., Wei, T., Bradley, M*., et al.* (2010). MiR-155 is overexpressed in patients with atopic dermatitis and modulates T-cell proliferative responses by targeting cytotoxic T lymphocyte-associated antigen 4. J Allergy Clin Immunol *126*, 581-589 e581-520.

Steck, P.A., Pershouse, M.A., Jasser, S.A., Yung, W.K., Lin, H., Ligon, A.H., Langford, L.A., Baumgard, M.L., Hattier, T., Davis, T*., et al.* (1997). Identification of a candidate tumour suppressor gene, MMAC1, at chromosome 10q23.3 that is mutated in multiple advanced cancers. Nat Genet *15*, 356-362.

Stittrich, A.B., Haftmann, C., Sgouroudis, E., Kuhl, A.A., Hegazy, A.N., Panse, I., Riedel, R., Flossdorf, M., Dong, J., Fuhrmann, F*., et al.* (2010). The microRNA miR-182

is induced by IL-2 and promotes clonal expansion of activated helper T lymphocytes. Nat Immunol *11*, 1057-1062.

Sukhatme, V.P., Cao, X.M., Chang, L.C., Tsai-Morris, C.H., Stamenkovich, D., Ferreira, P.C., Cohen, D.R., Edwards, S.A., Shows, T.B., Curran, T.*, et al.* (1988). A zinc finger-encoding gene coregulated with c-fos during growth and differentiation, and after cellular depolarization. Cell *53*, 37-43.

Sun, X., and Zhang, C. (2015). MicroRNA-96 promotes myocardial hypertrophy by targeting mTOR. Int J Clin Exp Pathol *8*, 14500-14506.

Surh, C.D., and Sprent, J. (2000). Homeostatic T cell proliferation: how far can T cells be activated to self-ligands? J Exp Med *192*, F9-F14.

Tatura, R., Zeschnigk, M., Hansen, W., Steinmann, J., Vidigal, P.G., Hutzler, M., Pastille, E., Westendorf, A.M., Buer, J., and Kehrmann, J. (2015). Relevance of Foxp3(+) regulatory T cells for early and late phases of murine sepsis. Immunology *146*, 144-156.

Theofilopoulos, A.N., Dummer, W., and Kono, D.H. (2001). T cell homeostasis and systemic autoimmunity. J Clin Invest *108*, 335-340.

Theofilopoulos, A.N., Kono, D.H., and Baccala, R. (2017). The multiple pathways to autoimmunity. Nat Immunol *18*, 716-724.

Tordjman, R., Lepelletier, Y., Lemarchandel, V., Cambot, M., Gaulard, P., Hermine, O., and Romeo, P.H. (2002). A neuronal receptor, neuropilin-1, is essential for the initiation of the primary immune response. Nat Immunol *3*, 477-482.

Trifari, S., Pipkin, M.E., Bandukwala, H.S., Aijo, T., Bassein, J., Chen, R., Martinez, G.J., and Rao, A. (2013). MicroRNA-directed program of cytotoxic CD8+ T-cell differentiation. Proc Natl Acad Sci U S A *110*, 18608-18613.

Tsugawa, K., Jones, M.K., Akahoshi, T., Moon, W.S., Maehara, Y., Hashizume, M., Sarfeh, I.J., and Tarnawski, A.S. (2003). Abnormal PTEN expression in portal hypertensive gastric mucosa: a key to impaired PI 3-kinase/Akt activation and delayed injury healing? FASEB J *17*, 2316-2318.

Turvey, S.E., and Broide, D.H. (2010). Innate immunity. J Allergy Clin Immunol *125*, S24-32.

Utzschneider, D.T., Delpoux, A., Wieland, D., Huang, X., Lai, C.Y., Hofmann, M., Thimme, R., and Hedrick, S.M. (2018). Active Maintenance of T Cell Memory in Acute and Chronic Viral Infection Depends on Continuous Expression of FOXO1. Cell Rep *22*, 3454-3467.

Valencia-Sanchez, M.A., Liu, J., Hannon, G.J., and Parker, R. (2006). Control of translation and mRNA degradation by miRNAs and siRNAs. Genes Dev *20*, 515-524.

Vignali, D.A., Collison, L.W., and Workman, C.J. (2008). How regulatory T cells work. Nat Rev Immunol *8*, 523-532.

Virolle, T., Adamson, E.D., Baron, V., Birle, D., Mercola, D., Mustelin, T., and de Belle, I. (2001). The Egr-1 transcription factor directly activates PTEN during irradiation-induced signalling. Nat Cell Biol *3*, 1124-1128.

Vishwamitra, D., Li, Y., Wilson, D., Manshouri, R., Curry, C.V., Shi, B., Tang, X.M., Sheehan, A.M., Wistuba, II, Shi, P.*, et al.* (2012). MicroRNA 96 is a post-transcriptional suppressor of anaplastic lymphoma kinase expression. Am J Pathol *180*, 1772-1780.

Wang, T.H., Yeh, C.T., Ho, J.Y., Ng, K.F., and Chen, T.C. (2016). OncomiR miR-96 and miR-182 promote cell proliferation and invasion through targeting ephrinA5 in hepatocellular carcinoma. Mol Carcinog *55*, 366-375.

Wang, W.M., Lu, G., Su, X.W., Lyu, H., and Poon, W.S. (2017a). MicroRNA-182 Regulates Neurite Outgrowth Involving the PTEN/AKT Pathway. Front Cell Neurosci *11*, 96.

Wang, X., Zuo, D., Yuan, Y., Yang, X., Hong, Z., and Zhang, R. (2017b). MicroRNA-183 promotes cell proliferation via regulating programmed cell death 6 in pediatric acute myeloid leukemia. J Cancer Res Clin Oncol *143*, 169-180.

Wang, Z., Xie, Z., Lu, Q., Chang, C., and Zhou, Z. (2017c). Beyond Genetics: What Causes Type 1 Diabetes. Clin Rev Allergy Immunol *52*, 273-286.

Weaver, C.T., Harrington, L.E., Mangan, P.R., Gavrieli, M., and Murphy, K.M. (2006). Th17: an effector CD4 T cell lineage with regulatory T cell ties. Immunity *24*, 677-688.

Weetman, A.P. (2000). Graves' disease. N Engl J Med *343*, 1236-1248.

Weiss, J.M., Bilate, A.M., Gobert, M., Ding, Y., Curotto de Lafaille, M.A., Parkhurst, C.N., Xiong, H., Dolpady, J., Frey, A.B., Ruocco, M.G.*, et al.* (2012). Neuropilin 1 is expressed on thymus-derived natural regulatory T cells, but not mucosa-generated induced Foxp3+ T reg cells. J Exp Med *209*, 1723-1742, S1721.

Winter, J., Jung, S., Keller, S., Gregory, R.I., and Diederichs, S. (2009). Many roads to maturity: microRNA biogenesis pathways and their regulation. Nat Cell Biol *11*, 228-234.

Wu, T., Wieland, A., Araki, K., Davis, C.W., Ye, L., Hale, J.S., and Ahmed, R. (2012). Temporal expression of microRNA cluster miR-17-92 regulates effector and memory CD8+ T-cell differentiation. Proc Natl Acad Sci U S A *109*, 9965-9970.

Wu, X., Senechal, K., Neshat, M.S., Whang, Y.E., and Sawyers, C.L. (1998). The PTEN/MMAC1 tumor suppressor phosphatase functions as a negative regulator of the phosphoinositide 3-kinase/Akt pathway. Proc Natl Acad Sci U S A *95*, 15587-15591.

Xiang, L., Chen, X.J., Wu, K.C., Zhang, C.J., Zhou, G.H., Lv, J.N., Sun, L.F., Cheng, F.F., Cai, X.B., and Jin, Z.B. (2017). miR-183/96 plays a pivotal regulatory role in mouse photoreceptor maturation and maintenance. Proc Natl Acad Sci U S A *114*, 6376-6381.

Xu, L., Li, Y., Yan, D., He, J., and Liu, D. (2014). MicroRNA-183 inhibits gastric cancer proliferation and invasion via directly targeting Bmi-1. Oncol Lett *8*, 2345-2351.

Xu, S., Witmer, P.D., Lumayag, S., Kovacs, B., and Valle, D. (2007). MicroRNA (miRNA) transcriptome of mouse retina and identification of a sensory organ-specific miRNA cluster. J Biol Chem *282*, 25053-25066.

Xu, X., Dong, Z., Li, Y., Yang, Y., Yuan, Z., Qu, X., and Kong, B. (2013). The upregulation of signal transducer and activator of transcription 5-dependent microRNA-

182 and microRNA-96 promotes ovarian cancer cell proliferation by targeting forkhead box O3 upon leptin stimulation. Int J Biochem Cell Biol *45*, 536-545.

Xue, Q., Guo, Z.Y., Li, W., Wen, W.H., Meng, Y.L., Jia, L.T., Wang, J., Yao, L.B., Jin, B.Q., Wang, T.*, et al.* (2011). Human activated CD4(+) T lymphocytes increase IL-2 expression by downregulating microRNA-181c. Mol Immunol *48*, 592-599.

Yadav, M., Louvet, C., Davini, D., Gardner, J.M., Martinez-Llordella, M., Bailey-Bucktrout, S., Anthony, B.A., Sverdrup, F.M., Head, R., Kuster, D.J.*, et al.* (2012). Neuropilin-1 distinguishes natural and inducible regulatory T cells among regulatory T cell subsets in vivo. J Exp Med *209*, 1713-1722, S1711-1719.

Yamamoto, M., Kondo, E., Takeuchi, M., Harashima, A., Otani, T., Tsuji-Takayama, K., Yamasaki, F., Kumon, H., Kibata, M., and Nakamura, S. (2011). miR-155, a Modulator of FOXO3a Protein Expression, Is Underexpressed and Cannot Be Upregulated by Stimulation of HOZOT, a Line of Multifunctional Treg. PLoS One *6*, e16841.

Yamamoto, M., Suzuki, K., Okuno, T., Ogata, T., Takegahara, N., Takamatsu, H., Mizui, M., Taniguchi, M., Chedotal, A., Suto, F.*, et al.* (2008). Plexin-A4 negatively regulates T lymphocyte responses. Int Immunol *20*, 413-420.

Yang, L., Boldin, M.P., Yu, Y., Liu, C.S., Ea, C.K., Ramakrishnan, P., Taganov, K.D., Zhao, J.L., and Baltimore, D. (2012). miR-146a controls the resolution of T cell responses in mice. J Exp Med *209*, 1655-1670.

Yang, M., Liu, R., Li, X., Liao, J., Pu, Y., Pan, E., Yin, L., and Wang, Y. (2014). miRNA-183 suppresses apoptosis and promotes proliferation in esophageal cancer by targeting PDCD4. Mol Cells *37*, 873-880.

Yao, R., Ma, Y.L., Liang, W., Li, H.H., Ma, Z.J., Yu, X., and Liao, Y.H. (2012). MicroRNA-155 modulates Treg and Th17 cells differentiation and Th17 cell function by targeting SOCS1. PLoS One *7*, e46082.

Yasutomo, K., Doyle, C., Miele, L., Fuchs, C., and Germain, R.N. (2000a). The duration of antigen receptor signalling determines CD4+ versus CD8+ T-cell lineage fate. Nature *404*, 506-510.

Yasutomo, K., Lucas, B., and Germain, R.N. (2000b). TCR signaling for initiation and completion of thymocyte positive selection has distinct requirements for ligand quality and presenting cell type. J Immunol *165*, 3015-3022.

Yi, R., Qin, Y., Macara, I.G., and Cullen, B.R. (2003). Exportin-5 mediates the nuclear export of pre-microRNAs and short hairpin RNAs. Genes Dev *17*, 3011-3016.

Yu, H., Liu, Y., Bai, L., Kijlstra, A., and Yang, P. (2014). Predisposition to Behcet's disease and VKH syndrome by genetic variants of miR-182. J Mol Med (Berl) *92*, 961-967.

Yu, X., Shen, N., Zhang, M.L., Pan, F.Y., Wang, C., Jia, W.P., Liu, C., Gao, Q., Gao, X., Xue, B.*, et al.* (2011). Egr-1 decreases adipocyte insulin sensitivity by tilting PI3K/Akt and MAPK signal balance in mice. EMBO J *30*, 3754-3765.

Yung, H.W., Charnock-Jones, D.S., and Burton, G.J. (2011). Regulation of AKT phosphorylation at Ser473 and Thr308 by endoplasmic reticulum stress modulates substrate specificity in a severity dependent manner. PLoS One *6*, e17894.

Zeng, Y., Yi, R., and Cullen, B.R. (2003). MicroRNAs and small interfering RNAs can inhibit mRNA expression by similar mechanisms. Proc Natl Acad Sci U S A *100*, 9779-9784.

Zhang, N., and Bevan, M.J. (2010). Dicer controls CD8+ T-cell activation, migration, and survival. Proc Natl Acad Sci U S A *107*, 21629-21634.

Zhang, Q., Ren, W., Huang, B., Yi, L., and Zhu, H. (2015a). MicroRNA-183/182/96 cooperatively regulates the proliferation of colon cancer cells. Mol Med Rep *12*, 668-674.

Zhang, W., Qian, P., Zhang, X., Zhang, M., Wang, H., Wu, M., Kong, X., Tan, S., Ding, K., Perry, J.K.*, et al.* (2015b). Autocrine/Paracrine Human Growth Hormone-stimulated MicroRNA 96-182-183 Cluster Promotes Epithelial-Mesenchymal Transition and Invasion in Breast Cancer. J Biol Chem *290*, 13812-13829.

Zhou, X., Jeker, L.T., Fife, B.T., Zhu, S., Anderson, M.S., McManus, M.T., and Bluestone, J.A. (2008). Selective miRNA disruption in T reg cells leads to uncontrolled autoimmunity. J Exp Med *205*, 1983-1991.

Zhu, E., Wang, X., Zheng, B., Wang, Q., Hao, J., Chen, S., Zhao, Q., Zhao, L., Wu, Z., and Yin, Z. (2014). miR-20b suppresses Th17 differentiation and the pathogenesis of experimental autoimmune encephalomyelitis by targeting RORgammat and STAT3. J Immunol *192*, 5599-5609.

Zhu, J., and Paul, W.E. (2010). Heterogeneity and plasticity of T helper cells. Cell Res *20*, 4-12.

Zhu, Q., Sun, W., Okano, K., Chen, Y., Zhang, N., Maeda, T., and Palczewski, K. (2011). Sponge transgenic mouse model reveals important roles for the microRNA-183 (miR-183)/96/182 cluster in postmitotic photoreceptors of the retina. J Biol Chem *286*, 31749-31760.

10 Supplemental material

Table 16 and Table 17 contain the detailed statistical significance of miR-96 and miR-183 expression in antagomir-treated $CD4^+CD25^-$ T cells upon activation (compare with Figure 17)

Table 16: Detailed statistical significance of miR-96 expression in antagomir-treated $CD4^+CD25^-$ T cells activated for up to 96 hours (see Figure 17 C).

MiR-96 expression	24h	48h	72h	96h
Incubation ctrl vs. antagomir-Scr	n.s.	n.s.	n.s.	n.s.
Incubation ctrl vs. antagomir-96/-183	n.s.	**	**	*
Incubation ctrl vs. antagomir-183	n.s.	n.s.	n.s.	n.s.
Incubation ctrl vs. antagomir-96	n.s.	**	**	*
antagomir-Scr vs. antagomir-96/-183	n.s.	n.s.	**	**
antagomir-Scr vs. antagomir-183	n.s.	n.s.	n.s.	n.s.
antagomir-Scr vs. antagomir-96	n.s.	n.s.	**	**
antagomir-96/-183 vs. antagomir-183	n.s.	**	**	*
antagomir-96/-183 vs. antagomir-96	n.s.	n.s.	n.s.	n.s.
antagomir-183 vs. antagomir-96	n.s.	**	**	*

Table 17: Detailed statistical significance of miR-183 expression in antagomir-treated $CD4^+CD25^-$ T cells activated for up to 96 hours (see Figure 17 D).

MiR-183 expression	24h	48h	72h	96h
Incubation ctrl vs. antagomir-Scr	n.s.	n.s.	n.s.	n.s.
Incubation ctrl vs. antagomir-96/-183	*	***	*	*
Incubation ctrl vs. antagomir-183	*	***	*	**
Incubation ctrl vs. antagomir-96	n.s.	n.s.	n.s.	n.s.
antagomir-Scr vs. antagomir-96/-183	*	**	*	*
antagomir-Scr vs. antagomir-183	*	**	*	**
antagomir-Scr vs. antagomir-96	n.s.	n.s.	n.s.	n.s.
antagomir-96/-183 vs. antagomir-183	n.s.	n.s.	n.s.	n.s.
antagomir-96/-183 vs. antagomir-96	**	**	**	*
antagomir-183 vs. antagomir-96	**	**	**	**

Figure 31, Figure 32 and Figure 33 are showing the original Western Blots. Rectangular areas are shown in Figure 20.

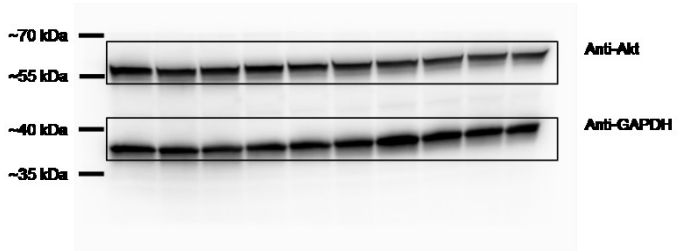

Figure 31: Original Western Blot stained with anti-Akt and anti-GAPDH antibodies.

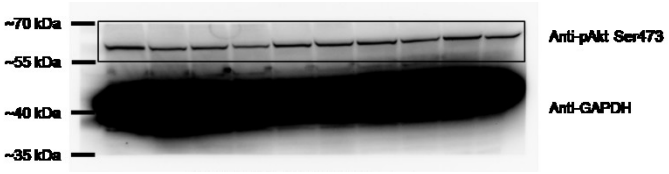

Figure 32: Original Western Blot stained with anti-phosphoAkt Ser473 and anti-GAPDH antibodies.

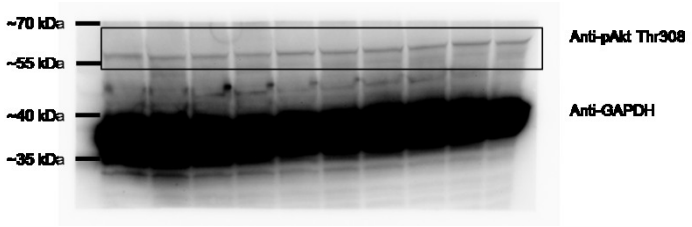

Figure 33: Original Western Blot stained with anti-phosphoAkt Thr308 and anti-GAPDH antibodies.

11 Directories

11.1 List of Abbreviations

°C	Grad Celsius
µ	Micro
3'UTR	3' untranslated region
Ago	Argonaute protein
Akt	Protein kinase B
AP-1	Activator protein-1
APCs	Antigen presenting cells
Bcl-2	B cell lymphoma 2
bp	Base pairs
cAMP	Cyclic adenosine monophosphate
cDNA	Complementary DNA
CNS	Conserved non-coding sequences
CO_2	Carbon dioxide
CREB1	cAMP-responsive element binding protein 1
CTLA-4	Cytotoxic T lymphocyte-associated protein 4
CTLs	Cytotoxic T lymphocytes
d	Deci
DAG	Diacylglycerol
DAMPs	Damage-associated molecular patterns
DCs	Dendritic cells
DGCR8	DiGeorge syndrome critical region gene 8
DN	Double negative
DP	Double-positive
EAE	Experimental autoimmune encephalomyelitis
EGR-1	Early growth response-1
EO	Endocrine orbitopathy
Exp-5	Exprotin-5
FACS	Fluorescence activated cell sorting
FADD	FAS-associated death domain
FAS	First apoptosis signaling
FoxO1 /3	Forkhead box O1/ 3
FoxP3	Forkhead box P3
g	Gramm
GAPDH	Glyceraldehyde 3-phosphate dehydrogenase
GD	Graves' disease
GFP	Green fluorescent protein
GO	Graves' orbitopathy
GRAP2	GRB2-related adaptor protein 2
HA	Hemagglutinin
HCC	Hepatocellular carcinoma
HGF	Hepatocyte growth factor
i.v.	Intravenously
IBD	Inflammatory bowel disease

ICAM	Intercellular adhesion molecule
IFNγ	Interferon γ
IgG	Immunoglobulin G
IKZF4	Ikaros family zinc finger 4
IL	Interleukin
IL2Rα	IL-2 receptor α
IP_3	Inositol trisphosphate
IRAK1	Interleukin-1 receptor-associated kinase 1
IRES	Internal ribosomal entry site
IS	Immunological synapse
ITAMs	Immunoreceptor tyrosine-based activation motifs
Itk	IL-2-inducible T cell kinase
iTregs	Induced Tregs
kb	Kilo base
kDa	Kilodalton
ko	Knockout
L	Liter
LAG-3	Lymphocyte-activation gene 3
LAT	Linker of activated T cells
Lck	Lymphocyte-specific protein tyrosine kinase
LCP2	Lymphocyte cytosolic protein 2
LFA-1	Lymphocyte function-associated antigen 1
m	Milli
M	Mole
MACS	Magnetic activated cell sorting
MHC	Major histocompatibility complex
miRNA	MicroRNA
MMLV	Moloney murine leukemia virus
mRNA	Messenger RNA
MS	Multiple sclerosis
mTOR	Mammalian target of rapamycin
mut	Mutated
NFAT	Nuclear factor of activated T cell
NFκB	Nuclear factor kappa-light-chain-enhancer of activated B cells
NK cells	Natural killer cells
Nrp-1	Neuropilin-1
nt	Nucleotides
nTregs	Thymic-derived natural Tregs
PAMPs	Pathogen associated molecular patterns
PBMCs	Peripheral blood mononuclear cells
P-bodies	Processing bodies
PCR	Polymerase chain reaction
PD-1	Programed cell death protein 1
PDCD4/ 6	Programmed cell death 4/ 6
PDGF	Platelet derived growth factor
PDK-1	Phosphoinositide-dependent protein kinase-1
PDZ binding motif	PSD-95/Dig/ZO-1 binding motif
PI3K	Phosphoinositide 3-kinase
PIP_2	Phosphatidylinositol(4,5)-bisphosphate

PIP_3	Phosphatidylinositol(3,4,5)-triphosphate
PLC-γ	Phospholipase C-γ
pre	Precursor
pri	Primary
PSA	Prostate-specific antigen
PTEN	Phosphatase and tensin homolog deleted on Chromosome ten
qRT-PCR	Quantitative real-time PCR
RA	Rheumatoid arthritis
Rag	Recombination activation gene
RISC	RNA-induced silencing complex
RNase	Ribonuclease
RPS9	Ribosomal protein S9
RV	Retrovirus
S1P	Sphingosine-1-phosphate
Sema	Class III semaphorin
Ser	Serin
SLE	Systemic lupus erythematosus
SMA	Spinal muscular atrophy
SOCS1	Suppressor of cytokine signaling 1
SP	Single positive
SPF	Specific pathogen-free
STAT	Signal transducer and activator of transcription
TCR	T cell receptor
TGFβ	Transforming growth factor β
TGFβ1	Transforming growth factor β1
Th cells	T helper cells
Thr	Threonin
T1D	Type I diabetes
TNFα	Tumor necrosis factor α
TRAF6	TNF receptor-associated factor 6
TRBP	Trans-activation response RNA-binding protein
Tregs	Regulatory T cells
TSHR	Thyroid-stimulating hormone receptor
U	Units
UVRAG	UV radiation resistance-associated gene
v/v	Volume per volume
VEGF	Vascular endothelial growth factor
VEGFR-2	VEGF receptor-2
wt	Wild type
x g	Gravity force
ZAP-70	Zeta-chain-associated protein kinase 70

11.2 List of Figures

11.3 List of Tables

Acknowledgment

Die Danksagung ist in der Online-Version aus Gründen des Datenschutzes nicht enthalten.

Curriculum vitae

Der Lebenslauf ist in der Online-Version aus Gründen des Datenschutzes nicht enthalten.

Affidavit

Erklärung

Hiermit erkläre ich, gem. § 6 Abs. 2, g der Promotionsordnung der Fakultät für Biologie zur Erlangung der Dr. rer. nat., dass ich das Arbeitsgebiet, dem das Thema „*The Impact of microRNAs 96/ 183 and Neuropilin-1 on T cell Activation and Autoimmunity*“ zuzuordnen ist, in Forschung und Lehre vertrete und den Antrag von Jacqueline Thiel befürworte.

Essen, den _____ _____

Wiebke Hansen

Erklärung

Hiermit erkläre ich, gem. § 7 Abs. 2, d und f der Promotionsordnung der Fakultät für Biologie zur Erlangung des Dr. rer. nat., dass ich die vorliegende Dissertation selbständig verfasst und mich keiner anderen als der angegebenen Hilfsmittel bedient habe und alle wörtlich oder inhaltlich übernommenen Stellen als solche gekennzeichnet habe.

Essen, den _____ _____

Jacqueline Thiel

Erklärung

Hiermit erkläre ich, gem. § 7 Abs. 2, e und g der Promotionsordnung der Fakultät für Biologie zur Erlangung des Dr. rer. nat., dass ich keine anderen Promotionen bzw. Promotionsversuche in der Vergangenheit durchgeführt habe, dass diese Arbeit von keiner anderen Fakultät abgelehnt worden ist, und dass ich die Dissertation nur in diesem Verfahren einreiche.

Essen, den _____ _____

Jacqueline Thiel